

**DRAFT**

**Most recent revision February 20, 2020**

**ICE, CLOUD, and Land Elevation Satellite-2  
(ICESat-2) Project**

**Algorithm Theoretical Basis Document (ATBD)  
for  
Land Ice Along-Track Height Product (ATL06)**

**Prepared By: Benjamin Smith, University of Washington Applied Physics  
Lab**

**With**

**David. Hancock, Kaitlin Harbeck, LeeAnne Roberts, Thomas Neumann,  
Kelly Brunt, Helen Fricker, Alex Gardner, Matthew Siegfried, Susheel  
Adusumilli, Beata Csathó, Nicholas Holschuh, Johan Nilsson, and Fernando  
Paolo.**



---

**Goddard Space Flight Center  
Greenbelt, Maryland**

---

***ICESat-2 Algorithm Theoretical Basis Document (ATBD) for Land Ice Along-Track Height  
(ATL06)***

***Release 003***

28

**Abstract**

29

30

## **CM Foreword**

31 This document is an Ice, Cloud, and Land Elevation Satellite-2 (ICESat-2) Project Science  
32 Office controlled document. Changes to this document require prior approval of the Science  
33 Development Team ATBD Lead or designee. Proposed changes shall be submitted in the  
34 ICESat-II Management Information System (MIS) via a Signature Controlled Request (SCoRe),  
35 along with supportive material justifying the proposed change.

36 In this document, a requirement is identified by “shall,” a good practice by “should,” permission  
37 by “may” or “can,” expectation by “will,” and descriptive material by “is.”

38 Questions or comments concerning this document should be addressed to:

39 ICESat-2 Project Science Office  
40 Mail Stop 615  
41 Goddard Space Flight Center  
42 Greenbelt, Maryland 20771

43

44

## **Preface**

45 This document is the Algorithm Theoretical Basis Document for the TBD processing to be  
46 implemented at the ICESat-2 Science Investigator-led Processing System (SIPS). The SIPS  
47 supports the ATLAS (Advance Topographic Laser Altimeter System) instrument on the ICESat-  
48 2 Spacecraft and encompasses the ATLAS Science Algorithm Software (ASAS) and the  
49 Scheduling and Data Management System (SDMS). The science algorithm software will produce  
50 Level 0 through Level 4 standard data products as well as the associated product quality  
51 assessments and metadata information.

52 The ICESat-2 Science Development Team, in support of the ICESat-2 Project Science Office  
53 (PSO), assumes responsibility for this document and updates it, as required, as algorithms are  
54 refined or to meet the needs of the ICESat-2 SIPS. Reviews of this document are performed  
55 when appropriate and as needed updates to this document are made. Changes to this document  
56 will be made by complete revision.

57 Changes to this document require prior approval of the Change Authority listed on the signature  
58 page. Proposed changes shall be submitted to the ICESat-2 PSO, along with supportive material  
59 justifying the proposed change.

60 Questions or comments concerning this document should be addressed to:

61 Thomas Neumann, ICESat-2 Project Scientist  
62 Mail Stop 615  
63 Goddard Space Flight Center  
64 Greenbelt, Maryland 20771

65

**Change History Log**

Revision Level	Description of Change	SCoRe No.	Date Approved
1.0	Initial Release		

67

**List of TBDs/TBRs**

Item No.	Location	Summary	Ind./Org.	Due Date

68

69	<b>Table of Contents</b>	
70	Abstract .....	ii
71	CM Foreword .....	iii
72	Prefaceiv	
73	Review/Approval Page .....	<b>Error! Bookmark not defined.</b>
74	Change History Log .....	v
75	List of TBDs/TBRs .....	vi
76	Table of Contents .....	vii
77	List of Figures .....	x
78	List of Tables.....	xi
79	1 INTRODUCTION.....	1
80	2 BACKGROUND INFORMATION and OVERVIEW .....	2
81	2.1 Background.....	2
82	2.2 Physical Basis of Measurements.....	4
83	2.2.1 Height retrieval over approximately planar surfaces.....	4
84	2.3 Potential Errors .....	6
85	2.4 Land-ice Level-3 products: ATL06: Land-Ice Height .....	7
86	3 ALGORITHM THEORY: Derivation of ATL 06/ Land Ice Height Parameters .....	9
87	1.1 Representation of the surface.....	9
88	3.1.1 Land-ice height definition .....	12
89	3.2 Outline of processing .....	12
90	3.3 PE selection.....	12
91	3.3.1 Along-track segments .....	12
92	3.3.2 Local Coordinate Systems .....	15
93	3.3.3 Parameters describing selected PEs .....	16
94	3.3.4 Handing of invalid segments.....	21
95	3.3.5 Surface-window refinement and least-squares height estimate .....	22
96	3.4 First-Photon Bias .....	24
97	3.4.1 Mathematical Description for the First-Photon Bias.....	25

*ICESat-2 Algorithm Theoretical Basis Document (ATBD) for Land Ice Along-Track Height  
(ATL06)*

*Release 003*

98	3.4.2	Correction Formulation for the First-Photon Bias .....	26
99	3.4.3	Statistics Derived from the First-Photon-Bias Correction .....	27
100	3.5	Transmit-pulse shape correction .....	32
101	3.6	Signal, Noise, and Error Estimates .....	35
102	3.6.1	Background PE rate .....	35
103	3.6.2	Signal PE count .....	35
104	3.6.3	Per-Photon Errors .....	36
105	3.6.4	Propagated Height Errors: .....	37
106	3.6.5	Uncorrected reflectance .....	37
107	3.7	Across-track slope calculation .....	37
108	3.8	Subsurface-Scattering Bias .....	38
109	3.9	Atmospheric-Scattering Bias .....	38
110	3.10	Segment geolocation .....	39
111	3.11	Noise-corrected robust estimators of spread .....	39
112	4	ATL06 Data product description .....	43
113	4.1	Data Granules .....	43
114	4.2	Segment_quality group .....	44
115	4.2.1	<i>Signal_selection_status</i> subgroup .....	45
116	4.3	<i>Land_ice_segments</i> group .....	45
117	4.3.1	geophysical subgroup .....	48
118	4.3.2	<i>ground_track</i> subgroup .....	52
119	4.3.3	<i>bias_correction</i> subgroup .....	54
120	4.3.4	<i>fit_statistics</i> subgroup .....	55
121	4.3.5	<i>DEM</i> subgroup .....	57
122	4.4	<i>residual_histogram</i> group .....	58
123	5	ALGORITHM IMPLEMENTATION: Land Ice Height (ATL 06/L3A) .....	61
124	5.1	Outline of Procedure .....	61
125	5.2	Input Parameters .....	61
126	5.3	Processing Procedure for Parameters .....	65

**ICESat-2 Algorithm Theoretical Basis Document (ATBD) for Land Ice Along-Track Height  
(ATL06)**

**Release 003**

127	5.4	Top-Level Fitting Routine.....	66
128	5.5	Signal selection based on ATL03 flags .....	71
129	5.6	Backup PE-selection routine. ....	73
130	5.7	Iterative Least-Squares Fitting Routine .....	75
131	5.8	Robust dispersion calculation from a collection of points, not including a background	
132		estimate .....	79
133	5.9	Robust dispersion calculation from a collection of points, including a background	
134		estimate .....	79
135	5.10	First- Photon Bias Correction .....	80
136	5.11	Gain-corrected median .....	82
137	5.12	Gain-corrected mean .....	83
138	5.13	Transmit-pulse-shape correction.....	84
139	5.14	Residual_histogram calculation .....	86
140	6	TEST DATA AND SOFTWARE REQUIREMENTS.....	90
141	6.1	ATL06 Test Data Setup .....	90
142	7	Browse Products at Q/A statistics .....	91
143	7.1	Browse Products .....	91
144	7.2	Q/A Statistics .....	91
145	8	Appendix A: Glossary .....	92
146		Glossary/Acronyms.....	98
147		References.....	100
148			

149 **List of Figures**

150

151 Figure Page

152 **Figure 2-1.** ICESat-2 repeat-track schematic..... 3

153 Figure 2-2. Schematic of returns from different surface types ..... 5

154 Figure 3-1. Surface return shape ..... 9

155 Figure 3-2. Mean and median height biases ..... 10

156 Figure 3-3. Reference point numbering schematic ..... 13

157 Figure 3-4. Example PE selection..... 14

158 Figure 3-5. RGT coordinates ..... 15

159 Figure 3-6 Segment fitting..... 17

160 Figure 3-7. First-photon bias correction ..... 24

161 Figure 3-8. Accuracy of first-photon bias correction elevation recovery ..... 29

162 Figure 3-9. Accuracy of first-photon-bias-correction signal strength recovery ..... 31

163 Figure 3-10. Transmit-pulse-shape correction..... 32

164 Figure 5-1. Flow chart for top-level ATL06 processing..... 65

165 Figure 5-2. Flow chart for iterative ground fit..... 75

166 Figure 8-1. Spots and tracks, forward flight ..... 96

167 Figure 8-2. Spots and tracks, forward flight ..... 96

168

169 **List of Tables**

170

171	<u>Table</u>	<u>Page</u>
172	Table 3-1 <i>signal_selection_source</i> values .....	19
173	Table 3-2 Status parameters for signal-selection algorithms .....	19
174	Table 4-1 <i>Segment_quality</i> group .....	44
175	Table 4-2 <i>land_ice_segments</i> group .....	45
176	Table 4-3 Segment characteristics for <i>ATL06_quality_summary</i> to be zero .....	48
177	Table 4-4 <i>geophysical</i> subgroup .....	49
178	Table 4-5 <i>ground_track</i> subgroup .....	53
179	Table 4-6 <i>bias_correction</i> subgroup .....	54
180	Table 4-7 <i>fit_statistics</i> subgroup .....	55
181	Table 4-8 <i>DEM</i> subgroup .....	57
182	Table 4-9 Parameters in the <i>residual_histogram</i> group .....	59
183	Table 5-1. Inputs for ATL06 .....	62
184		

185 **1 INTRODUCTION**

186 This document describes the theoretical basis and implementation of the level-3 land-ice  
187 processing algorithms. It currently includes ATL06, which provides geolocated land-ice surface  
188 heights, and ATL11, which provides time series of surface heights. The higher-level products,  
189 providing mapped height, and mapped height change will be described in supplements to this  
190 document available late 2016.

191 The ATL06 product provides the most basic derived values from the ATLAS instrument on  
192 ICESat-2: the surface height at a given point on Earth’s surface at a given time relative to the  
193 WGS-84 ellipsoid. ATL06 provides estimates of the ice-sheet surface height, and ancillary  
194 parameters needed to interpret and assess the quality of these height estimates. ATL06 heights  
195 represent the mean surface height averaged along 40-m segments of ground track, 20-m apart,  
196 for each of ATLAS’s six beams. Segments within adjacent beams are aligned to facilitate  
197 estimation of the across-track surface slope; they are also aligned from orbit to orbit so that  
198 subsequent repeat tracks give height estimates for nearly the same location on the surface,  
199 simplifying the estimation of height changes made through repeat-track analysis. Height  
200 estimates from ATL06 can also be compared with other geodetic data and used as inputs to  
201 higher-level ICESat-2 products, particularly ATL11, 14, and 15.

202 Higher-level products are based on the height estimates in ATL06. ATL11 provides heights  
203 corrected for displacements between the reference tracks and the location of the ATLAS  
204 measurements. ATL14 provides gridded height maps for selected epochs during the mission,  
205 based on the corrected heights in ATL11. ATL15 provides height-change maps based on the  
206 ATL14 height maps and height differences derived from ATL11.

207 In this document, section 2 provides an overview of land-ice products and gives a brief summary  
208 of the procedures used to derive products

209 Section 3 describes the algorithm used to generate the products.

210 Section 4 gives the processing steps and input data required to derive each parameter, and  
211 describes the products in detail.

212 Section 5 gives a detailed procedure for deriving selected parameters

213 Section 6 describes test data and specific tests that NASA’s implementation of the algorithm  
214 should pass.

215

216

## 217 **2 BACKGROUND INFORMATION AND OVERVIEW**

218 This section provides a conceptual description of ICESat-2's ice-sheet height measurements and  
219 gives a brief description of the derived products.

### 220 **2.1 Background**

221 ATLAS on ICESat-2 determines the range between the satellite and the Earth's surface by  
222 measuring the two-way time delay of short pulses of laser light that it transmits in six beams. It  
223 is different from previous operational ice-sheet altimeters in that uses a photon-counting  
224 detector. Previous altimeters (e.g. GLAS on ICESat-1, ATM, and LVIS) have used full-  
225 waveform digitizers that received millions or more photons for each transmitted pulse, allowing  
226 the receiver to generate a waveform, *i.e.* the return power as a function of time. ATLAS instead  
227 records a set of arrival times for individual photons, which are then analyzed to derive surface,  
228 vegetation, and cloud properties. Although ATLAS measures much weaker signals than full-  
229 waveform altimeters, it has three major design advantages over GLAS:

- 230 i) ATLAS has six beams arranged in three pairs (Figure 2-1), so that it samples each of  
231 three reference pair tracks with a pair of beams;
- 232 ii) ATLAS transmits pulses at 10 kHz, giving approximately one pulse every 0.7 m  
233 along track, more than two orders of magnitude finer than the 170-meter along-track  
234 of GLAS;
- 235 iii) ATLAS's expected pointing control will be better than 90 m RMS, better than the  
236 100-200 m achieved by ICESat-1.

237 ATLAS's six beams are spread over a small angle so that their projection onto the surface of the  
238 earth is a rectangular array with two rows and three columns, with about 3.3 km separation  
239 between each column and its neighbors, and 2.5 km between the rows. As ICESat-2 moves  
240 along its orbit, the ATLAS beams illuminate six tracks on the Earth's surface; the array is rotated  
241 slightly with respect to the satellite's flight direction so that tracks for the fore and aft beams in  
242 each column produce pairs of tracks, each pair separated by about 90 m (**Figure 2-1**). The  
243 separation between beams in each pair allows for measurement of the local surface slope in the  
244 across-track and along-track direction; this will allow ICESat-2 to make the most precise and  
245 detailed repeat estimates of ice-sheet height of any satellite to date.

246 ATLAS pulses are short, about 1.6 ns long (FWHM), and are transmitted every 0.1 ms (10 kHz);  
247 this fast repetition yields footprint centers separated by about 0.7 m in the along-track direction.  
248 Each pulse illuminates an approximately circular area on the ground ~17 m in diameter.  
249 ATLAS's strong beams detect at most 12 reflected photons from each transmitted pulse. Great  
250 care is taken to detect only photons with the same wavelength as the transmitted laser pulse and  
251 to limit the field of view of the detectors to a region slightly larger than the illuminated  
252 "footprint" of each beam; therefore, ground-return photon events (PEs, meaning photons that are  
253 detected) may readily be distinguished from solar background PEs because they are clustered in  
254 time, while background PEs are distributed evenly in time and arrive much less frequently.

255 The high (~45-meter RMS) accuracy of ICESat-2's pointing control means that pairs for  
256 consecutive repeats of each RPT (Reference Pair Track) are likely to overlap. The fine along-  
257 track sampling and the multi-beam capability allow height products to be defined for segments  
258 that are consistent in along-track position for repeated measurements along the same RPT.  
259

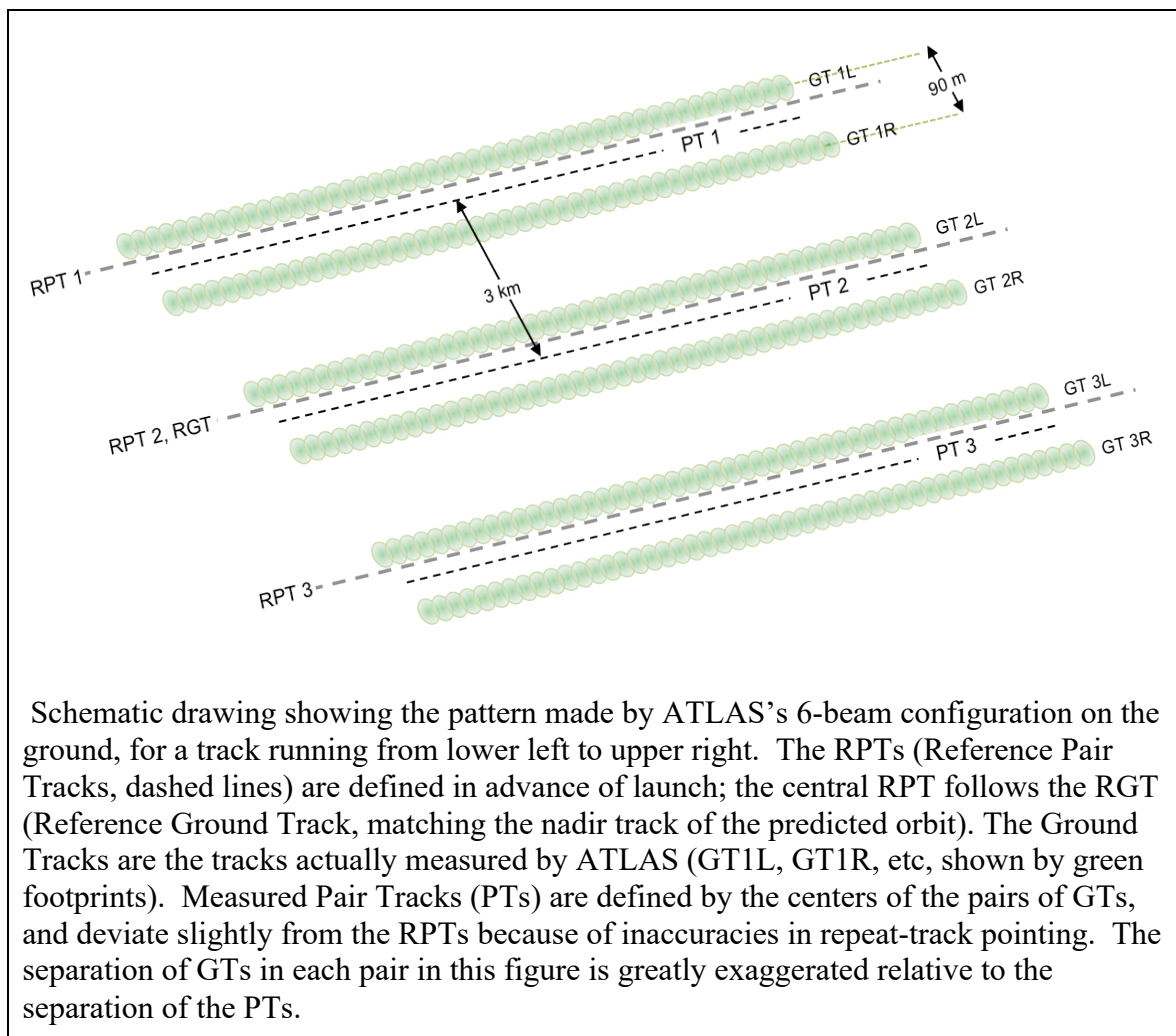


Figure 2-1. ICESat-2 repeat-track schematic

260  
261 Further processing of ATL06 heights will produce heights corrected for surface slope and  
262 curvature that give the estimated time-varying height for selected points on the RPTs and at  
263 track-to-track crossover points (ATL11). These shape-corrected heights will be processed further  
264 to give i) height maps for selected time intervals (semi-annual or annual, ATL14) and ii) annual  
265 height-change maps for the Antarctic and Greenland ice sheets (ATL15)

266

## 267 **2.2 Physical Basis of Measurements**

### 268 **2.2.1 Height retrieval over approximately planar surfaces**

269 Light from the ATLAS lasers reaches the earth's surface as flat disks of down-traveling photons,  
270 approximately 50 cm in vertical extent, and spread over about 17 m horizontally. On land ice,  
271 photons are scattered once, or many times, by snow and ice grains, into every direction,  
272 including towards the satellite; a tiny fraction return to the ATLAS telescope's focal plane, and a  
273 few of these are counted by the detector electronics and recorded as Photon Events (PEs). Over  
274 the vast majority of the earth's land ice, the surface is smooth, with small (single-degree)  
275 variations in surface slopes at scales less than a few hundred meters. This allows us to  
276 approximate the surface profiles measured by ATLAS with short linear segments. We aggregate  
277 PEs received by ATLAS into 50% overlapping along-track segments of a fixed length (40 m),  
278 whose centers are 20 m apart. We then fit these PEs with sloping line segments; for each  
279 segment, we estimate both the along-track slope and the height at the center of the segment.  
280 When both beams in a pair provide height measurements, we also calculate the across-track  
281 slope for the pair. Any height variation not captured by this fitting process will be treated as  
282 surface roughness.

283 The time variation in surface height is determined by fitting a simple spatial function to the  
284 heights from multiple repeat measurements, and using this function to correct the measurements  
285 for the height variations caused by spatial sampling of sloped and curving surfaces. This  
286 function is fit to the subset of the repeat measurements that we assess to be of the highest quality,  
287 but corrected height estimates are provided for all available repeats, and data-quality metrics are  
288 provided to allow users to decide which heights to use.

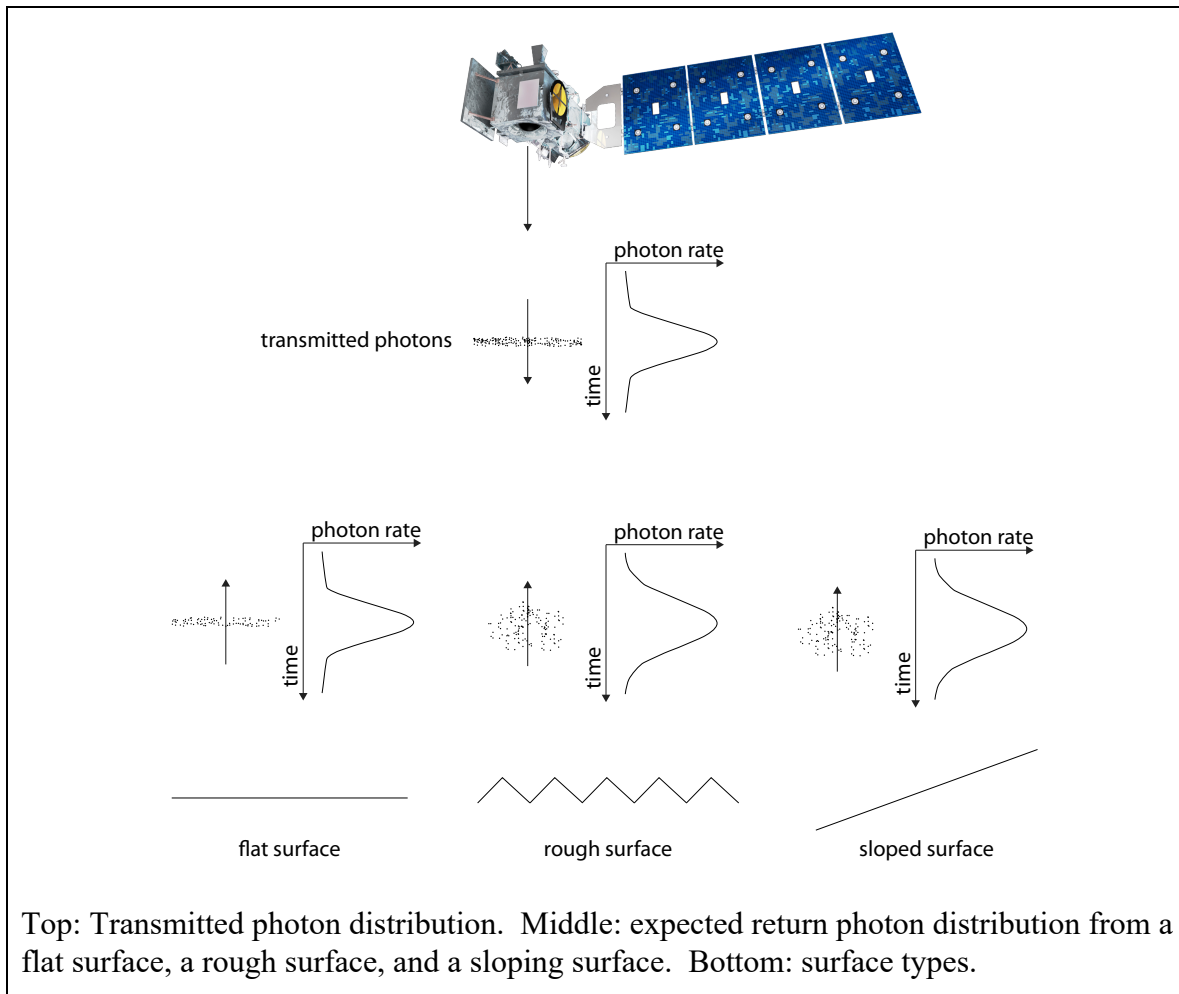
### 289 **2.2.2 Effects of surface slope and roughness**

290 Figure 2-2 shows how slope and roughness contribute to the shape of the return pulse. For many  
291 areas of glaciers, the ground may be treated as a rough planar surface, and the laser pulse as  
292 having a Gaussian distribution in space, with intensity falling to  $1/e^2$  of its peak value over a  
293 distance  $W/2$ . The laser pulses also have an approximate Gaussian distribution in time, with  
294 standard deviation  $\sigma_{tx}$ . If the incident beam is not parallel to the surface normal, photons from the  
295 edge of the footprint farthest from the satellite will be delayed relative to photons from the edge  
296 nearest the satellite. At the same time, a rough surface will yield early photons and late photons,  
297 further spreading the returned photons. If the angle between the beam and the surface normal is  
298  $\varphi$ , and the surface height within the footprint has a Gaussian distribution with RMS deviation  $R$   
299 relative to the plane of the surface, then the measured temporal distribution of the returned  
300 photons will be Gaussian as well (Yi & Bentley, 1999), with a temporal standard deviation equal  
301 to the quadratic sum of the spreads due to the transmitted pulse, the surface slope, and the  
302 roughness:

$$\sigma_R = \left[ \sigma_{tx}^2 + \left( \frac{2\sigma_{beam}}{c} \tan\varphi \right)^2 + \left( \frac{2R}{c} \right)^2 \right]^{1/2} \quad 1$$

303 For ATLAS,  $\sigma_{beam}$  is expected to be around 4.25 m (one quarter of W), and  $\sigma_{tx}$  around 0.68 ns,  
 304 corresponding to a FWHM (Full Width at Half Maximum) of 1.6 ns, so spreading due to sloping  
 305 surfaces will be smaller than the transmit-pulse duration for slopes up to approximately 1.3  
 306 degrees.

Figure 2-2. Schematic of returns from different surface types



307 Surface roughness on a 17-m scale is likely to be small except in heavily crevassed glacier  
 308 margins and in heavily channeled ablation zones. Although analysis of the return pulse shape  
 309 does not allow us to distinguish the effects of roughness from those of slope, the geometry of  
 310 ATLAS's tracks, with pairs of beams separated by 90 m, allows estimates of the across-track

311 slope at scales modestly larger than a single footprint, while the along-track component of the  
312 slope can be estimated from the along-track sequence of heights.

### 313 **2.2.3 Distinguishing return PEs and background PEs**

314 At the same time as signal photons are received by the ATLAS detector, background photons  
315 from sunlight are continually entering the telescope. Most of these are eliminated by filters that  
316 allow only photons with wavelengths close to the laser wavelengths through, but some pass these  
317 filters, and their timing is also recorded. The time distribution of the returned signal photons  
318 depends on the geometry and reflectance of the ice surface, and on scattering and attenuation in  
319 the atmosphere. We distinguish signal PEs from background PEs by their clustering in time.  
320 Sunlight scattered from bright (*i.e.* snow-covered) surfaces will produce detected PEs at rates up  
321 to around 12 MHz. For comparison, a return with as few as three PEs distributed over one half  
322 meter of range produces a brief return rate of 900 MHz. Signal returns are also distinct from the  
323 background because they are spatially contiguous, so that PEs will be clustered in time in a  
324 consistent way from one shot to the next.

## 325 **2.3 Potential Errors**

326 Errors in ATLAS land-ice products can come from a variety of sources:

- 327 1) Sampling error: ATLAS height estimates are based on a random sampling of the surface  
328 height distribution;
- 329 2) Background noise: Random-noise PEs are mixed with the signal PEs, so sampled PEs  
330 will include random outliers;
- 331 3) Complex topography: The along-track linear fit and across-track polynomial fit do not  
332 always resolve complex surface topography.
- 333 4) Misidentified PEs: The ATL03 product will not always identify the correct PEs as signal  
334 PEs;
- 335 5) First-photon bias: This is an error inherent to photon-counting detectors that results in a  
336 high bias in the mean detected PE height that depends on signal strength;
- 337 6) Atmospheric forward scattering: Photons traveling downward through a cloudy  
338 atmosphere may be scattered through small angles but still be reflected by the surface  
339 within the ATLAS field of view; these will be delayed, producing an apparently lower  
340 surface;
- 341 7) Subsurface scattering: Photons may be scattered many times within ice or snow before  
342 returning to the detector; these will be delayed, producing a surface estimate with a low  
343 bias.

344 These errors are each treated in a different way during the ATL06 processing:

345 1) and 2) are treated as random errors, and their effects are quantified in the error estimates  
346 associated with the products.

347 3) and 4) will produce relatively large errors, and will need to be addressed with consistency  
348 checks on the data during the generation of higher-level products.

349 5) will be corrected routinely during ATL06 processing (see Section 3.0).

350 6) and 7) require information about cloud structure and ice-surface conditions that will not be  
351 available at the time of processing of ATL06. Correcting for these errors remains an active  
352 avenue for research.

## 353 **2.4 Land-ice Level-3 products: ATL06: Land-Ice Height**

354 The ATL06 product provides surface height estimates organized by reference -pair track (RPT),  
355 in a format designed to facilitate comparison between different repeat measurements on the same  
356 RPT. It also combines information from the two beams in each PT to give across-track slope  
357 estimates. A variety of parameters are provided that indicate the quality of the surface-height  
358 estimates and the signal and noise levels associated with the measurement. Note that in cycles 1  
359 and 2 of the mission, ICESat-2 did not point at the RPTS, and ICESat2's pairs are offset by up to  
360 2 km from the RPT locations. The first cycle that was collected over the RPTS was the third.

361 We define ATL06 heights based on fits of a linear model to ATL03 height data from short  
362 (40 m) segments of the ground track, centered on reference points spaced at 20-m intervals  
363 along-track. We refer to height estimates for these short segments as "segment heights", and  
364 segment's horizontal location is that of the reference point, displaced in a direction perpendicular  
365 to the RGT to match the GT offset. The choice of 40 m for the segment length provides data  
366 from slightly more than two independent (non-overlapping) ATL03 heights (based on 17-m  
367 footprints) for the along-track slope estimate, so that this component of the slope can be  
368 eliminated as a cause of vertical scatter in the PE height distribution. The spacing between  
369 reference points is 20 m, so that each segment overlaps its neighbors by 50%. Defining  
370 overlapping segments in this way increases the chances that a segment will overlap a locally  
371 smooth area within a crevasse field, potentially improving elevation-rate recovery in these areas.

372 We use the same along-track sampling for both beams in each beam pair, and, for each cycle, use  
373 the same reference point each time we calculate a segment height. This allows for direct  
374 comparison between segment heights from the same RPT, without the need to interpolate in the  
375 along-track direction. The ATL03 PE used for each segment can be determined by associating  
376 the `/gtxx/land_ice_segments/segment_id` parameter in ATL06 with the  
377 `/gtxx/geolocation/segment_id` parameter in ATL03: segment  $m$  in ATL06 includes PEs from  
378 ATL03 segments  $m-1$  and  $m$  (here  $xx$  represents the ATLAS beam, with `gt1l` and `gt1r` providing  
379 the left and right beams for pair 1).

380 A minimal representation of the data is given in datasets in the ATL06 product in the  
381 `/gtxx/land_ice_segments` groups. In these groups, we give the latitude, longitude, height, slope,  
382 vertical error estimate, and a quality flag for each segment. This represents the minimum set of  
383 parameters needed by most users; a wide variety of parameters describing the segment fit, the

***ICESat-2 Algorithm Theoretical Basis Document (ATBD) for Land Ice Along-Track Height  
(ATL06)***

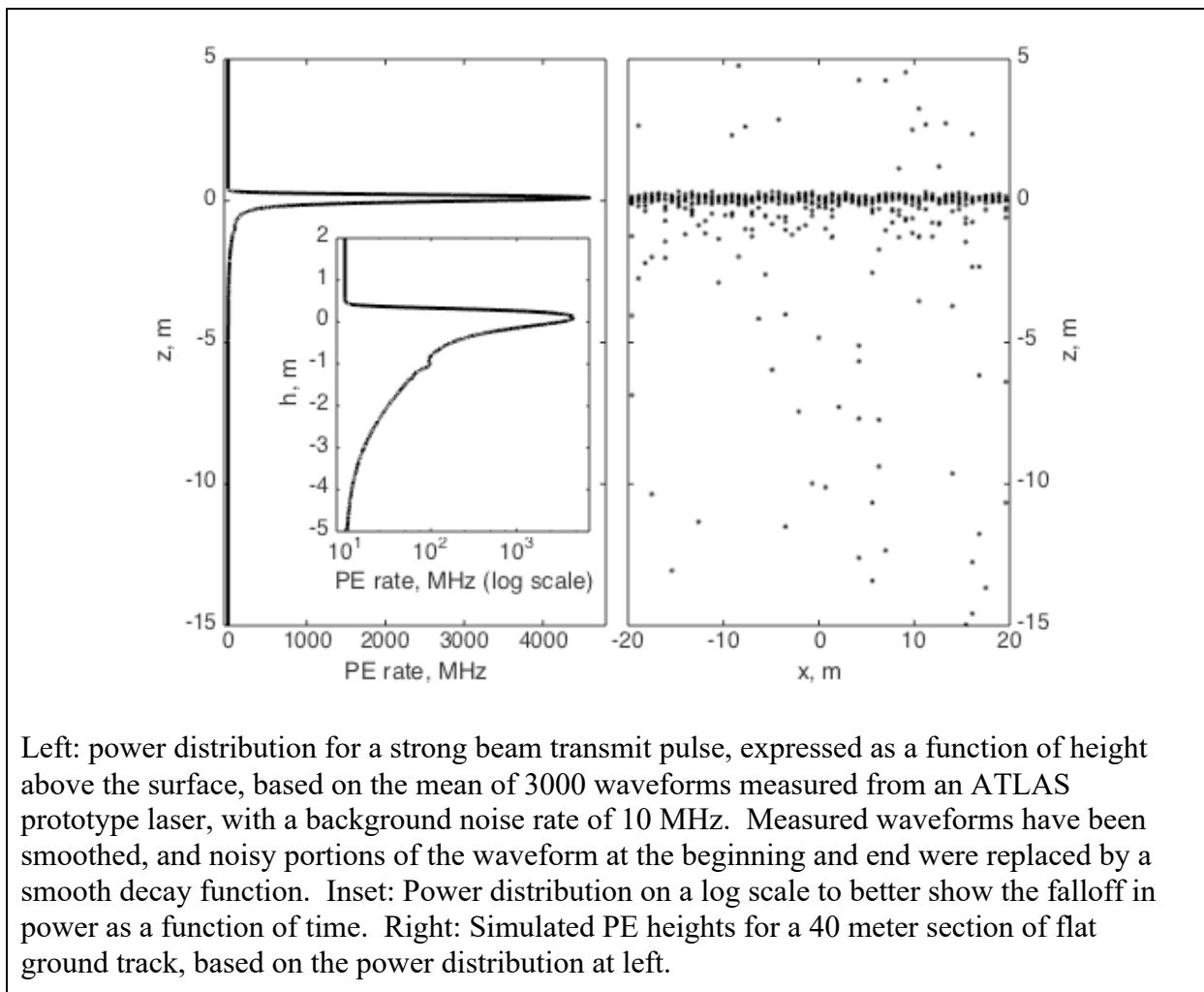
***Release 003***

384 input data, and the environmental conditions for the data are available in the subgroups within  
385 the *gtxx* groups.

386 **3 ALGORITHM THEORY: DERIVATION OF ATL 06/ LAND ICE HEIGHT**  
387 **PARAMETERS**

388 In this section, we describe the ATL06 height derivation from lower-level ATLAS data  
389 (primarily the PE heights, locations, and times provided by ATL03). This process provides  
390 height estimates and segment geolocations for a set of points (called reference points) spaced  
391 every 20 m along each of ATLAS's pair tracks. One height is calculated for each beam in each  
392 pair, for each reference point, for each cycle of ICESat-2's orbit.

Figure 3-1. Surface return shape

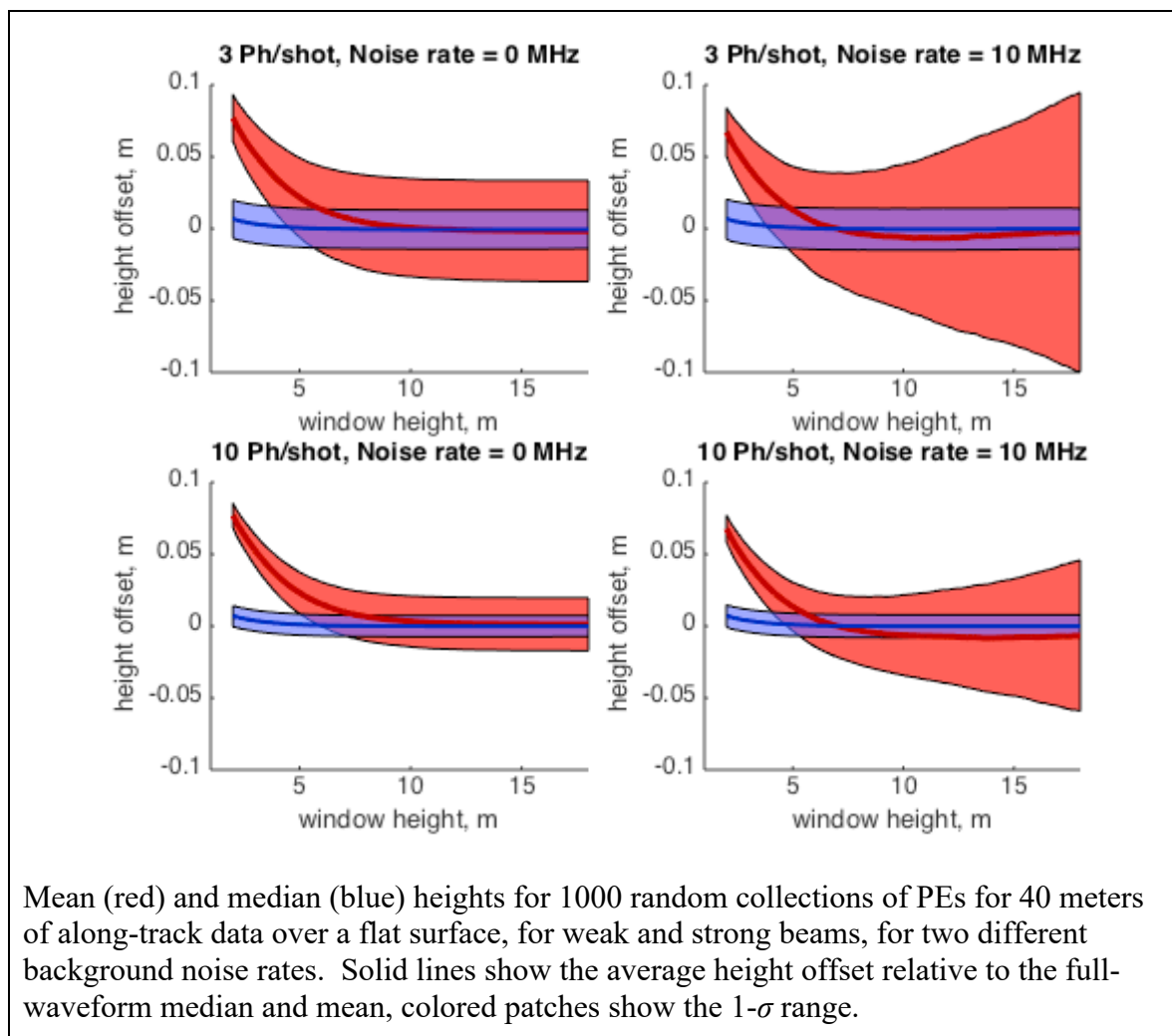


393 **1.1 Representation of the surface**

394

395 Figure 3-1 shows the expected surface-return power as a function of height above the surface,  
 396 based on waveforms measured from a prototype ATLAS laser, for sunlit ice-sheet conditions  
 397 with a background PE rate of 10 MHz, and a random set of photon heights generated based on  
 398 this waveform for a 40-meter along-track segment. The return has a sharp peak in power at the  
 399 ground, but it is asymmetric, with a leading edge (on the +z side) that is sharper than the trailing  
 400 edge (on the -z side), and with a long ‘tail’ of energy on the -z side caused by a slow decay in  
 401 laser power at the end of the pulse. This produces a dense collection of PEs at the surface height,  
 402 with scattered PEs above and below, some of which come from the sun and some of which come  
 403 from the tail of the waveform.

Figure 3-2. Mean and median height biases



404

405 One way to characterize the surface height for this segment would be to calculate the mean of all  
406 PE heights within a pre-determined height range (the ‘surface window’). For simplicity, one  
407 might choose a large surface window of 10-20 m to ensure the capture of all return PEs.  
408 However, this choice would lead to significant noise and potential bias in the estimated surface  
409 heights. The noise would come about because the mean of a distribution of heights is sensitive to  
410 the extreme values of the distribution, so the photons at the edge of the distribution would  
411 produce sampling errors in the recovered heights. The bias could come about if the shape of the  
412 transmit pulse were to change over time, because of temperature changes or because of aging of  
413 the lasers. If this were to happen, the mean recovered surface height could change even if the  
414 true surface height did not, again because the mean is sensitive to outlying data. Figure 3-2  
415 shows the expected bias and scatter magnitudes as a function of the width of the surface window  
416 for the means of 1000 random collections of PEs based on the waveform in Figure 3-1.  
417 Selecting a small surface window results in a narrow (2 cm or less) scatter of values around the  
418 mean, because the range of PE heights in the window is small. However, this leads to a 7-8 cm  
419 bias in the surface height, because the tail of the distribution is cut off. Selecting a large surface  
420 window leads to a small bias, but, particularly when background noise is large, it leads to scatter  
421 in the surface heights, potentially as large as  $\pm 10$  cm.

422 We ameliorate this problem in two ways: First, we use an iterative process to select a small  
423 surface window that includes the majority of the signal PEs but few background PEs. Second,  
424 we express the surface height as the median of the PE heights within the surface window. We  
425 select the median instead of the mean because it is less sensitive to sampling error for  
426 distributions containing a uniform, ‘background’ component. Median height offsets shown in  
427 Figure 3-1 have a spread of less than 2 cm, have maximum biases less than 7 mm, and are nearly  
428 independent of the surface-window height. This represents a large improvement in accuracy and  
429 precision over the mean, and further processing (discussed in 3.5) can correct for the remaining  
430 bias in the median heights.

431 In the course of processing photon-counting data, we frequently need to estimate the spread of a  
432 distribution of PE heights. For other types of data, we might choose to make this estimate based  
433 on the standard deviation of the sample of heights, but because our measurements contain a  
434 mixture of signal and noise PEs, the standard deviation often overestimates the spread of the  
435 data. Instead, we generally use the RDE (Robust Dispersion Estimator), which is equal to half  
436 the difference between the 16<sup>th</sup> and the 84<sup>th</sup> percentiles of a distribution. For Gaussian-  
437 distributed data, this statistic is approximately equal to the standard deviation, and for data  
438 containing a mixture of a large fraction of signal and a small fraction of noise, it can give an  
439 estimate of the spread of the signal that is relatively insensitive to the noise. In some cases, we  
440 use a version of this statistic that estimates the spread of the signal component of a distribution  
441 that contains a mixture signal (Gaussian- or near-Gaussian-distributed) PEs and background  
442 (uniformly distributed) PEs. In these cases, we estimate the 50<sup>th</sup> and 75<sup>th</sup> percentiles of the signal  
443 component and scale the difference between these percentiles based on the expected width of  
444 these percentiles for a Gaussian distribution. We refer to this measure as “robust spread  
445 including background” and describe its implementation in section 5.

446 **3.1.1 Land-ice height definition**

447 The land-ice height is defined as estimated surface height of the segment center for each  
448 reference point, using median-based statistics. We calculate this the sum of the least-squares  
449 height fit, the first-photon-bias median correction, and the pulse-truncation median correction.  
450 Height increment values on the product allow removal of the corrections and calculation of the  
451 segment mean height, and first-photon-bias and pulse-truncation corrections appropriate to the  
452 segment mean.

453

454 **3.2 Outline of processing**

455 The outline of the process is as follows for each cycle for each along-track point. First, heights  
456 and along-track slopes are calculated for each beam in each pair:

- 457 1. PEs from the current cycle falling into the along-track bin for the along-track point are  
458 collected (3.3)
- 459 2. The heights and surface windows are iteratively refined (3.3.5.2)
- 460 3. Corrections and error estimates are calculated based on the edited PEs. ( 3.4, 3.5, 3.6 )

461 Once these steps are complete, based on the height values for the two beams,

- 462 4. The across-track slope is calculated (3.7)

463 Each of these steps is described in turn below.

464 **3.3 PE selection**

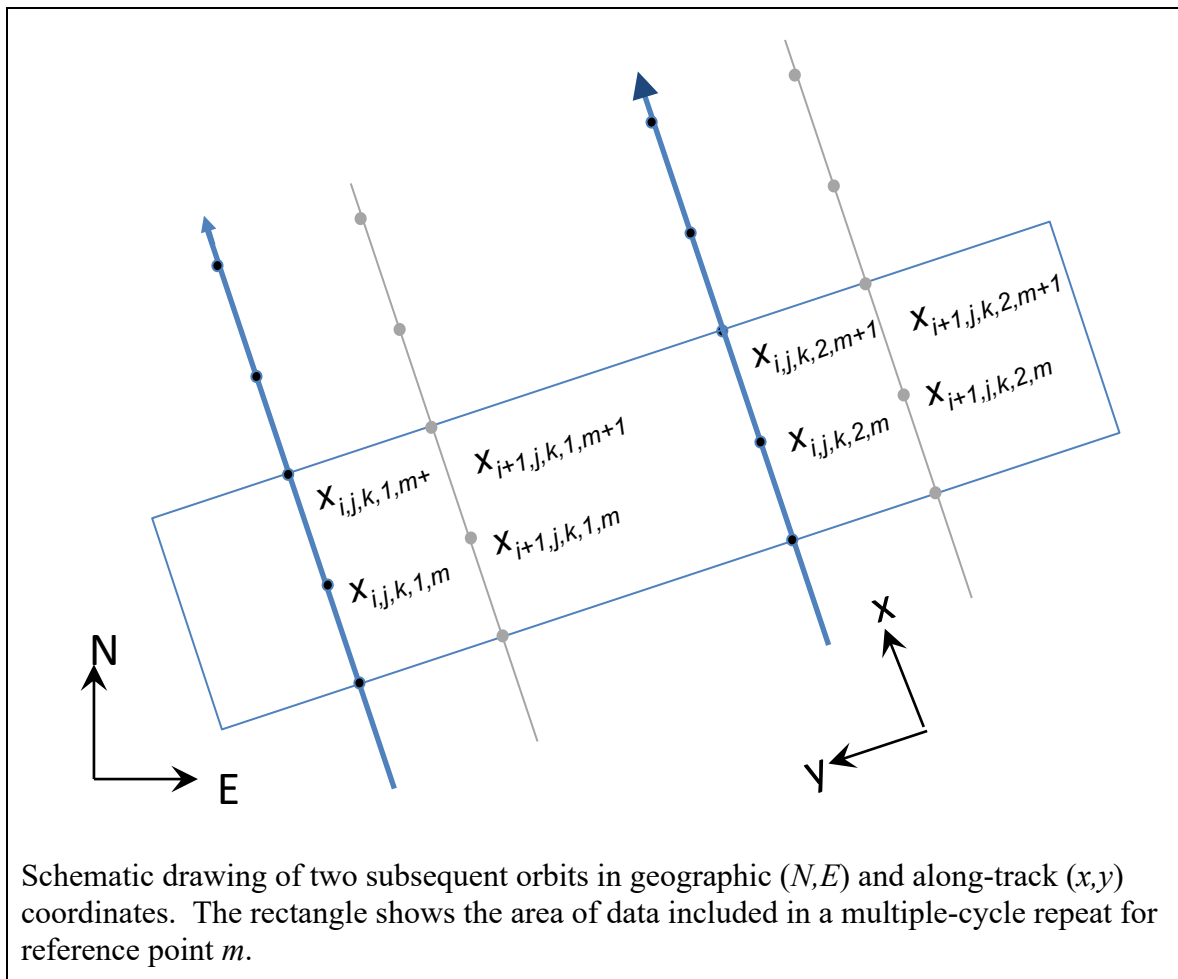
465 ATL03 provides PE locations and timings for each beam. The first step in ATL06 processing is  
466 to select groups of PEs that determine the segment height at each along-track point. Processing  
467 is only carried out if the ATL03 *podppd\_flag* indicates that the PE geolocation was of high  
468 quality for all pulses in the segment, otherwise the segment is skipped.

469 **3.3.1 Along-track segments**

470 Our height- and height-change schemes rely on dividing the data into repeatable along-track  
471 segments. We define these segments relative to the pre-defined RGT (see ATL06 Appendix A  
472 for definitions related to the ICESat-2 ground and reference tracks) and use them to select groups  
473 of PEs for each beam and each pass, and to define local coordinates relative to the RGT. We  
474 define a set of reference points, spaced every 20 m in the along-track coordinate  $x$  along the  
475 RGT, which specify the locations of the height estimates reported in ATL06. One set of  
476 reference points is defined for each RPT (Reference Pair Track). An ATL06 segment of data  
477 includes all PEs whose  $x$  coordinates are within approximately 20 m of that of a given reference  
478 point, for a total length of 40 m, so that each segment overlaps its neighbors by 50%. Each

479 individual segment is fit with a least-squares model that gives the slope and height of the  
 480 segment (Figure 3-3 and Section 3.1.2.4), and height corrections are derived based on the  
 481 residuals to this model.

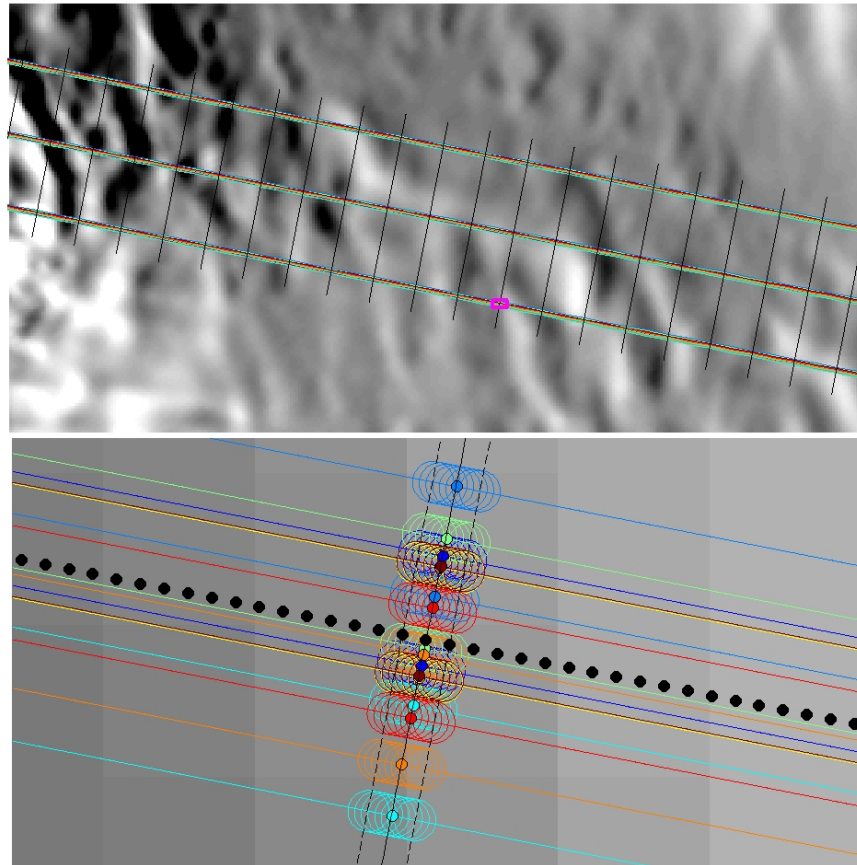
Figure 3-3. Reference point numbering schematic



482  
 483 Along-track segments are designated by five subscripts (Figure 3-3):  
 484        -i, the cycle number, numbered from the start of the mission;  
 485        -j, the track number, numbered consecutively within the cycle;  
 486        -k, the pair number, numbered from left to right across the satellite swath;  
 487        -l, the beam number within the pair, numbered from left to right;  
 488        -m, the reference point number, counted from the equator crossing of the RGT.

489 An along-track repeat measurement for a segment is made up of segments with the same  $j$ ,  $k$ , and  
490  $m$ , meaning that the track, the pair, and the along-track coordinates of the measurements are the  
491 same. Each cycle,  $i$ , contributes measurements from two beams, with different  $l$  values, to the

Figure 3-4. Example PE selection



Selecting PEs for a reference point. Top: GT locations for eight simulated repeat measurement of track 188 (colored lines). Black lines are plotted every 2 km in the along-track coordinate  $x$ . Bottom: selected footprint locations for a reference point on PT 3 (circles, every 10<sup>th</sup> shown). Lines and circles are color coded by repeat. Solid points show reference-point locations, dashed lines show the 40-m along-track extent of the segments, filled circles show segment centers. Background image from (Scambos and others, 2007)

492 repeat; these different measurements allow the across-track slope to be constrained  
493 independently from the height change, and the along-track segment fitting procedure allows us to  
494 correct for the along-track slope. Both ATL03 and ATL06 use this segment numbering scheme;

495 however, ATL06 segments are 40 m long and overlap their neighbors by 50%, while ATL03  
496 segments are 20 m long and are disjoint. ATL06 segments are defined as including PE from pairs  
497 of adjacent ATL03 segments, and are numbered to match the second of the two, so that ATL06  
498 segment  $m$  includes ATL03 segments  $m$  and  $m-1$ .

### 499 **3.3.2 Local Coordinate Systems**

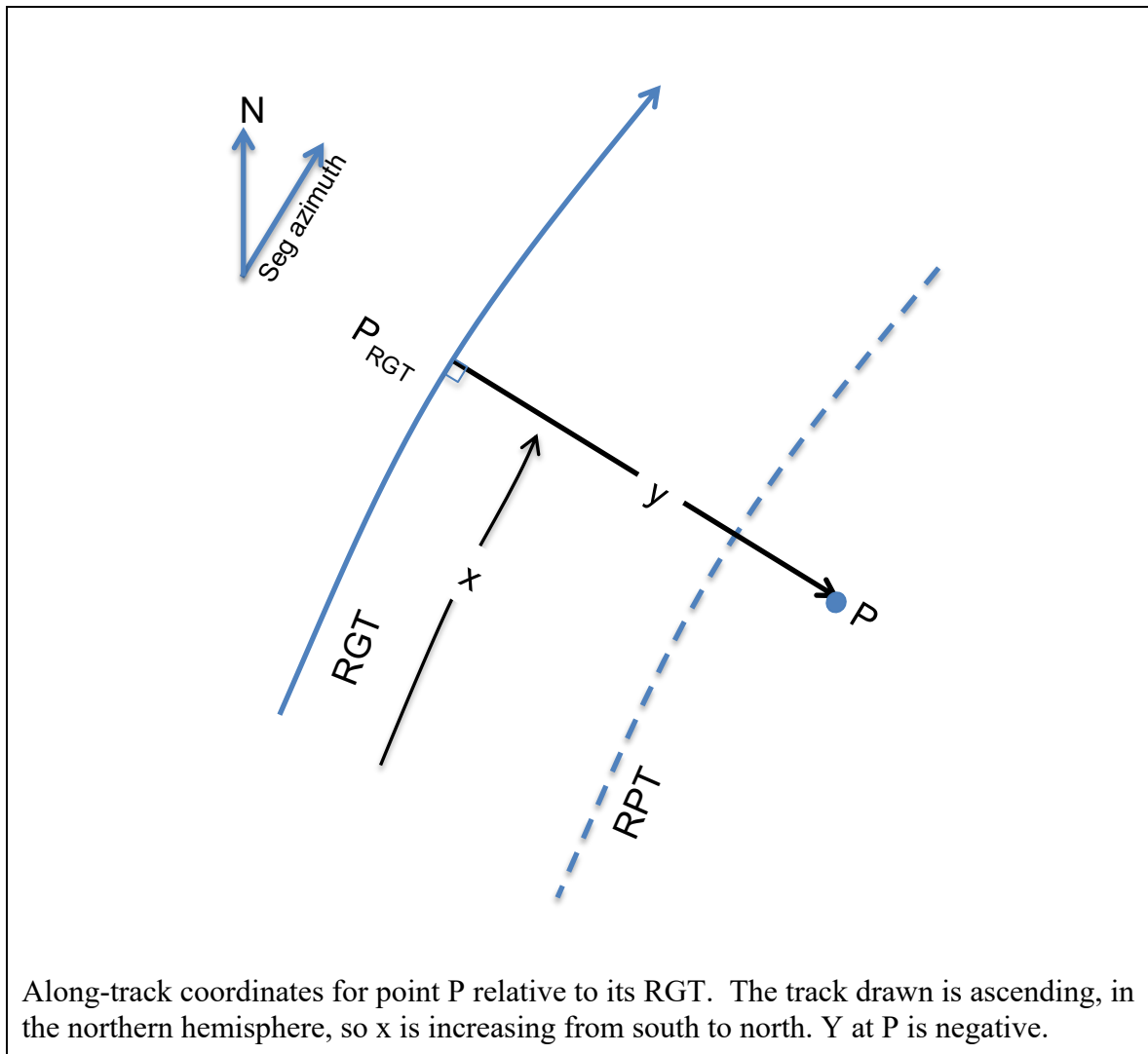
500 To select the PEs associated with each reference point, the height data are grouped in local  
501 coordinates. The local coordinate system is defined in the ATL03G ATBD. Briefly, the  
502 coordinate system is defined separately for each RGT with an  $x$  coordinate that follows the RGT,  
503 starting at its equator crossing going north. The  $y$  coordinate is measured perpendicular to the  $x$   
504 coordinate and is positive to the left. Thus, the  $x$  coordinate runs from zero to around forty  
505 thousand km for each track, the  $y$  coordinate runs from approximately -3.3 km for the right beam  
506 pair to approximately 3.3 km for the left beam pair, although its values may be larger if ATLAS  
507 is pointed off nadir.

508 To calculate along-track coordinates for any point  $P$  adjacent to an RGT, we define the  $x$   
509 coordinate to be equal to the  $x$  coordinate of the nearest point on the RGT,  $P_{RGT}$ . The  $y$   
510 coordinate is equal the distance between  $P$  and  $P_{RGT}$ , measured to the left of the along-track  
511 direction (Figure 3-5). This calculation is carried out for each PE in ATL03: The  $x$  coordinate  
512 for each PE is equal to the sum of the ATL03 parameters */geolocation/segment\_dist\_x* and  
513 */heights/dist\_ph\_along*. The  $y$  coordinate is equal to the ATL03 *dist\_ph\_across* parameter. Our  
514 reference points are defined to be equal to the start of the first ATL03 segment, so that ATL06  
515 segment  $m$  encompasses all PE from ATL03 segments  $m-1$  and  $m$ .

516

Figure 3-5. RGT coordinates

---



517

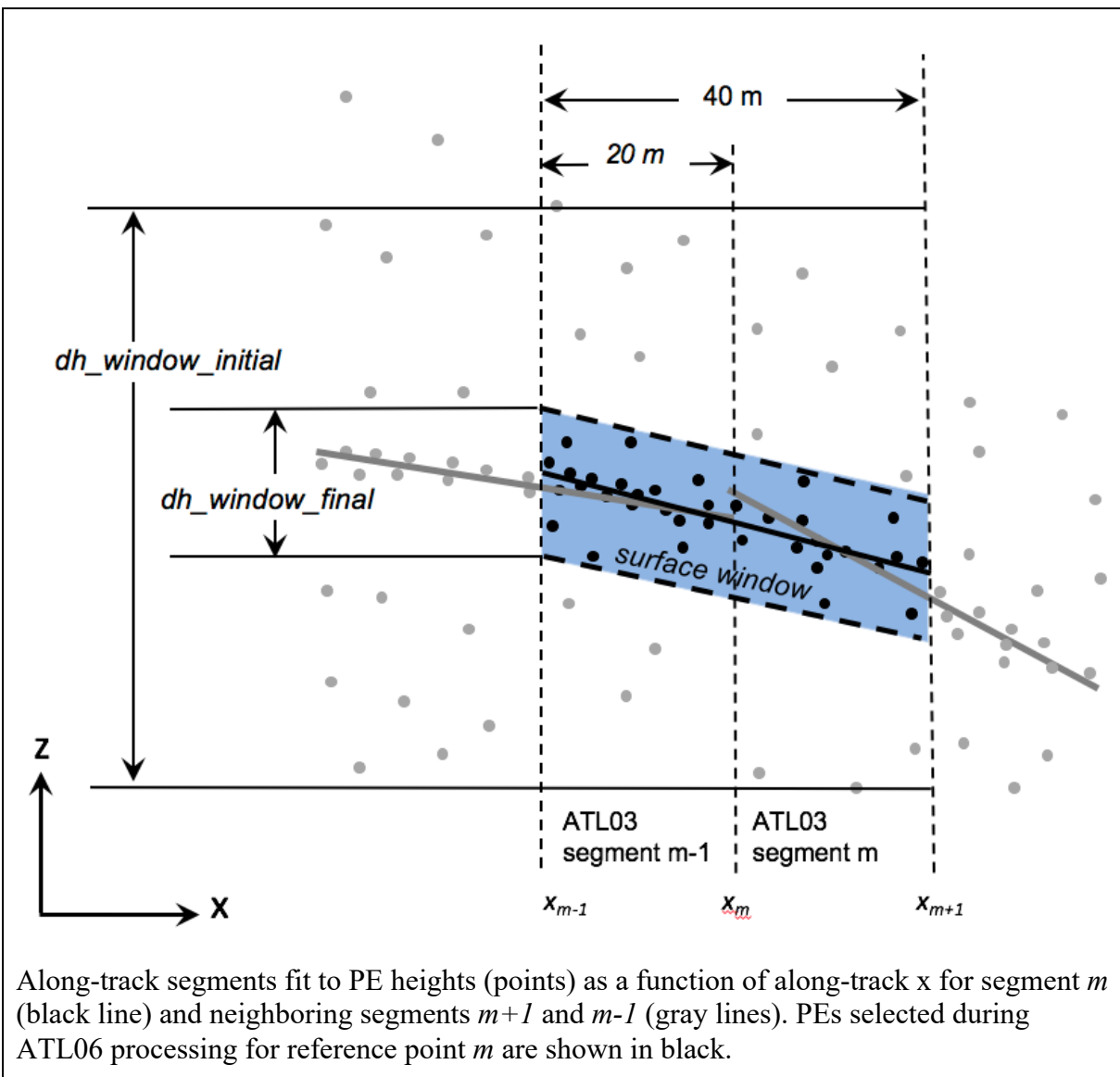
518 The AL06 along-track coordinate for each segment is given by the parameter  $x_{atc}$ . The across-  
519 track coordinate is given by  $y_{atc}$ , and the angle between the along-track vector and local north  
520 is given in the parameter  $seg\_azimuth$ . To allow easy referencing between ATL06 and ATL03,  
521 we provide the number for the second ATL03 segment in each ATL06 segment in the variable  
522  $segment\_id$ .

### 523 3.3.3 Parameters describing selected PEs

524 ATL06 heights and slopes are estimated by piecewise-linear fits to PEs within each overlapping  
525 40-m segment. Since ATL06 segments are 40-meters long and overlap by 50%, we can collect

526 the photons for each segment,  $m$ , by selecting all ATL03 PE that have  $segment\_id$  equal to  $m-1$   
 527 or  $m$ .

Figure 3-6 Segment fitting



528  
 529 The initial PE selection is shown in Figure 3-6. ATL03 data give a ground-finding confidence  
 530 flag that indicates whether each PE was detected high confidence (SNR > 100, flag value of 4),  
 531 medium (100 < SNR < 40, flag value of 3) low confidence (SNR < 40, yet still passes threshold

532 test, flag value of 2), or is included because it falls within 10m of the detected surface (flag value  
533 of 1).

534 An initial surface window is valid if it contains at least 10 PE, and if the along-track distance  
535 between the first and last PE is greater than 20 m. This ensures that there are enough PE to  
536 determine both the height and slope of the segment. We define three possible sources for signal-  
537 selection data:

- 538 1. ATL03 confident PE (*signal\_selection\_source=0*): PE with *confidence\_flag* values  $> 1$   
539 (low or better confidence)
- 540 2. All ATL03 detected PE (*signal\_selection\_source=1*): PE with *confidence\_flag* flag  
541 values  $\geq 1$  (including low or better, and pad PE).
- 542 3. A backup signal-finding algorithm (*signal\_selection\_source=2*)

543 3.3.3.1 Setting the surface window based on ATL03 flagged PE.

544 If sources 1 or 2 define a valid surface window, we calculate the slope of that window using an  
545 initial least-squares fit to  $h$  as a function of  $x$  for the flagged PE. Based on the slope of this  
546 window, we calculate *sigma\_expected* using equation 1, and calculate the robust spread of the  
547 residuals for the flagged PE (correcting for the background PE rate), *r\_flagged*. If ATL03  
548 confident PE define a window (case 1), the minimum surface window size,  $w_{min}$ , is set to 3 m,  
549 and if ATL03 confident PE do not define a window but the combination of ATL03 detected and  
550 pad PE do (case 2),  $w_{min}$  is set to 10 m. The initial surface window, *w\_surface\_window\_initial*  
551 is then set to  $\max(w_{min}, 6 \sigma_{expected}, 6 r_{flagged})$ . The residuals for all of the segment PE  
552 are then calculated, and PE with residuals within  $\pm w_{surface\_window\_initial}/2$  are selected and  
553 passed on to the iterative along-track fitting.

554 3.3.3.2 Setting the surface window using the backup signal-finding algorithm

555 If any ATL03 PE are detected but they do not define a window or if no ATL03 PE are present, a  
556 backup algorithm is used. First, if any ATL03-flagged PE are present, the along-track slope of  
557 the initial window is set to zero, its width is set to 10 m, and it is centered vertically on the mean  
558 height of the flagged PE. If the PE within this window fail the along-track-spread test or the ten-  
559 PE test, then PE within 40 m along track of the reference point are examined to find the 10-  
560 meter-high by 80-meter-long window, centered on the reference point, containing the largest  
561 number of PE. Typically, there will be a range of center heights whose PE counts are not  
562 significantly different from the maximum; if the maximum count is  $C_{max}$ , then any window with  
563 a count greater than  $C_{max} - C_{max}^{1/2}$  will be included. The initial window will extend from 5 m  
564 below the minimum of these centers to 5 m above the top of these centers, and its length is set to  
565 40 m. If this best window does not contain a good distribution of PE (i.e. more than 10 PE, with  
566 a horizontal spread greater than 20 m), the segment is considered invalid. If  $C_{max}$  is less than 16  
567 (the number of PE that would be detected in an 80-meter long window with a signal strength of

568 10 PE/40 m, minus one standard deviation), no PE are selected, and the signal selection is  
569 marked as invalid.

**Table 3-1 *signal\_selection\_source* values**

Value	Meaning
0	Signal selection succeeded using ATL03 confident-or-better flagged PE
1	Signal selection failed using ATL03 confident-or-better flagged PE but succeeded using all flagged ATL03 PE
2	Signal selection failed using all flagged ATL03 PE, but succeeded using the backup algorithm
3	All signal-finding strategies failed.

570  
571 The *signal\_selection\_source* parameter describes the success or failure of each step in this  
572 process, and Table 3-1 describes the meaning of each value. For each signal-selection algorithm  
573 that was attempted, the *signal\_selection\_status\_confident*, *signal\_selection\_status\_all*, and  
574 *signal\_selection\_status\_backup* parameters in the *segment\_quality* group give details of the  
575 success or failure of each part of the algorithm. The *signal\_selection\_source* parameter is  
576 provided for all segments (successful or not) in the *segment\_quality* group, and is provided for  
577 segments for which at least one pair has an elevation in the *fit\_statistics* subgroup.

**Table 3-2 Status parameters for signal-selection algorithms**

<i>Signal_selection_status_confident</i>	
0	Signal selection succeeded using ATL03 low-or-better confidence PEs
1	Signal selection using ATL03 low-or-better confidence PEs failed the 20-meter-spread test
2	Signal selection using ATL03 low-or-better confidence PEs failed the 10-photon-count test

<b>3</b>	Signal selection using ATL03 low-or-better confidence PEs failed both tests
<b><i>Signal_selection_status_all</i></b>	
<b>0</b>	Signal selection succeeded using all ATL03 flagged PEs (or algorithm not attempted)
<b>1</b>	Signal selection using all ATL03 flagged PEs failed the 20-meter-spread test
<b>2</b>	Signal selection using all ATL03 flagged PEs failed the 10-photon-count test
<b>3</b>	Signal selection using all ATL03 flagged PEs failed both tests
<b><i>Signal_selection_status_backup</i></b>	
<b>0</b>	Signal selection succeeded using the backup signal finder after centering the window on flagged PE (or backup signal finder not attempted)
<b>1</b>	Signal selection succeeded using the backup signal finder after searching for the strongest-signal window using four adjacent ATL03 segments
<b>2</b>	Signal selection using the backup signal finder failed the 20-meter-spread test
<b>3</b>	Signal selection using the backup signal finder failed the 10-photon-count test
<b>4</b>	Signal selection using the backup signal finder failed both tests

578  
 579 The final, refined window is described in the *fit\_statistics* subgroups. The height of the window  
 580 is given as *dh\_window\_final*, and the number of pulses that might contribute PE to the ATL06  
 581 segment is given in the *n\_seg\_pulses* parameter. Note that not all of the pulses in the segment

582 necessarily contribute to the received PEs if the signal strength is low. We calculate  
583  $n_{seg\_pulses}$  based on the speed of the nadir point,  $v_{nadir}$ , of the spacecraft along the ground  
584 track, the pulse repetition frequency, and the nominal 40-m length of the ATL06 segment:  
585  $N_{seg\_pulses} = PRF \times 40 \text{ m} / v_{nadir}$ . This parameter has non-integer values, because it is intended  
586 to represent the expected number of pulses in each segment. There is no straightforward way to  
587 determine exactly which pulses might have targeted a particular ground segment.

### 588 3.3.4 Handing of invalid segments

589 Segments must pass a series of tests before their elevations are reported in the ATL06  
590 *gtxx/land\_ice\_segments* groups. The signal selection routines must return at least 10 PE, spread  
591 over at least 20 m. Fitting does not proceed if these criteria are not met. For segments that  
592 continue to the surface window refinement routine, after the surface window refinement is  
593 complete, the final PE count and surface-window height are checked against the *snr\_significance*  
594 parameter, to ensure that the probability of the measured signal-to-noise ratio resulting from a  
595 random signal selection is small. Only segments with *snr\_significance* < 0.05 (indicating that,  
596 given a random-noise input, the algorithm would converge to the calculated SNR less than 5% of  
597 the time) proceed to the next stage.

598 These criteria allow a significant number of low-quality segment heights to be reported in  
599 ATL06. This intended for the benefit of users who need to measure surface heights under  
600 marginal conditions. To help other users remove these segments, the  
601 *land\_ice\_segments/ATL06\_quality\_summary* parameter gives a synopsis of the parameters  
602 relevant to segment quality (Table 4-3), any one of which could indicate unusable data. The  
603 subset of segments with *ATL06\_quality\_summary* = 0 are unlikely to contain blunders due to  
604 signal-finding errors. This choice of parameters may reject useful elevations collected over  
605 rough, strongly sloping, or low-reflectivity surfaces and under clouds so obtain more height  
606 estimates, users may need to examine additional parameters in ATL06, or regenerate a similar  
607 flag for themselves based on a less-stringent set of parameters.

608 A variety of data flags are available to indicate why a particular segment does not have a  
609 reported height parameter. In many cases, the strong-beam segment in a pair will have a  
610 reported height, and the weak beam will not; in these cases, a full record is available for the  
611 weak-beam segment, providing all parameters up to the step where the fitting process failed. In  
612 cases where neither the strong nor the weak beam returned a surface height, the *segment\_quality*  
613 group provides the *signal\_selection\_source* parameter, which will show a value of 3 if all signal-  
614 selection strategies failed. Only in cases where both segments passed the signal-selection tests  
615 but did not pass the *snr\_significance* < 0.05 test will there be an entry in *segment\_quality* and no  
616 entry in the remainder of the ATL06 records.

617

618 Users wishing to apply more- or less-stringent criteria to the data than those described above can  
619 examine the refined surface window width *fit\_statistics/w\_surface\_window\_final*, the signal-to-

620 noise ratio,  $fit\_statistics/snr$ , the range-based-error parameter,  $land\_ice\_segments/h\_li\_sigma$  and  
621 the uncorrected reflectance,  $r\_eff$ , to ensure that they are within expected ranges.

### 622 **3.3.5 Surface-window refinement and least-squares height estimate**

623 The ATL06 ground-finding algorithm refines the ATL03 surface detection estimate by iterative  
624 fitting of the initially-selected ATL03 PEs with the along-track segment model, rejecting PEs  
625 with large residuals to the model at each step (3.3.5.2). After the iterations are terminated, the  
626 final model height, based on this fit,  $h\_mean$ , is used as an input to the next stage of the  
627 algorithm, in which the model residuals are used to derive corrections to the model height.

#### 628 **3.3.5.1 Least-squares fitting**

629 For each segment, we first calculate a least-squares best-fitting segment to the initially selected  
630 ATL03 PEs, then use an iterative procedure based on the least-squares fit to refine this window.  
631 Each time we perform the least-squares fit, we construct a design matrix,  $\mathbf{G}_0$ , from the vector  $\mathbf{x}$ ,  
632 of along-track coordinates for the selected PEs:

$$\mathbf{G}_0 = [1 \ \mathbf{x}] \quad 2$$

633 The segment height and along-track slope are calculated based on  $\mathbf{G}_0$  and the vector of ATL03  
634 heights,  $\mathbf{h}$ , as:

$$\left[ h_{fit}, \frac{dh}{dx} \right] = (\mathbf{G}_0^T \mathbf{G}_0)^{-1} \mathbf{G}_0^T \mathbf{h} \quad 3$$

635 The residuals to this model are then calculated:

$$r_o = h - \mathbf{G}_0 \left[ h_{fit}, \frac{dh}{dx} \right] \quad 4$$

636

#### 637 **3.3.5.2 Iterative ground-window refinement**

638 The initial surface window height may be as large as 20 meters from top to bottom, larger in  
639 rough terrain or when the signal-to-noise ratio is small. This means that it may include many  
640 noise PEs mixed with the signal PEs. If included in the calculation, these will lead to large  
641 random errors in the surface slope and height. We can increase the proportion of signal PEs by  
642 shrinking the surface window, but need to avoid shrinking it so much that we lose signal PEs.  
643 To do this, we seek to find a window centered on the median height of the surface-return PEs,  
644 whose height is three times the spread of the surface PE height residuals. Because the spread and

645 the median of the surface PEs are not initially known, we use an iterative procedure to shrink the  
646 size of the surface window, estimating the median and spread at each step.

647 We have two ways of calculating a value for the spread of the surface return, which we combine  
648 as part of our calculation of the width of the surface window. The first is to predict the RMS  
649 spread of the surface return using an initial estimate of the surface-slope vector and Equation 1 to  
650 give  $h\_expected\_RMS$ , assuming zero roughness. The second is to calculate it based on the  
651 spread of the residuals to the current model,  $\sigma_o$ . In low-signal-to-noise conditions, we include a  
652 correction for the background signal level in this calculation (described in 3.11). Since either of  
653 these might provide a good estimate of the spread of the surface PEs we take the maximum of  
654 these two values as our spread estimate. To avoid excessive trimming, we eliminate PEs only if  
655 their residual magnitude is greater than the maximum of 1.5 m and three times our spread  
656 estimate.

657 We initialize the iterative procedure with the PE selection described in the previous two sections.  
658 In cases where the signal selection was initialized with flagged PE ( $signal\_selection\_source=0$   
659 or 1), the iterative ground-window refinement is forced to use only PE included in the initial  
660 selection. In all other cases, iterations after the first may include PE that were not included in the  
661 initial selection, so the window may expand or migrate as iterations progress. In either case the  
662 PE that might be selected are the *selectable* PE.

663 At each step, we

- 664 a) Perform a least-squares fit to the currently selected PEs using equation 3, giving a current  
665 model estimate,  $[h\_mean, dh/dx]$  and residuals to the model,  $r$ .
- 666 b) Calculate the median and background-corrected RDE (see 3.11) of the distribution of the  
667 residuals for the selected PEs,  $r_{med}$  and  $\sigma_o$ , and update  $h\_expected\_RMS$  based on the  
668 current  $dh/dx$  estimate. The residual spread ( $\sigma_o$ ) is limited to a maximum value of 5 m.
- 669 c) Calculate the residuals of all of the *selectable* PEs to the current model estimate,  $r$ .
- 670 d) Select PEs from among the *selectable* PEs for which  $|r-r_{med}| < H\_window/2$ , where  
671  $H\_window = \max(6 \sigma_o, 6 h\_expected\_RMS, 0.75 H\_window\_last, 3 \text{ m})$ .

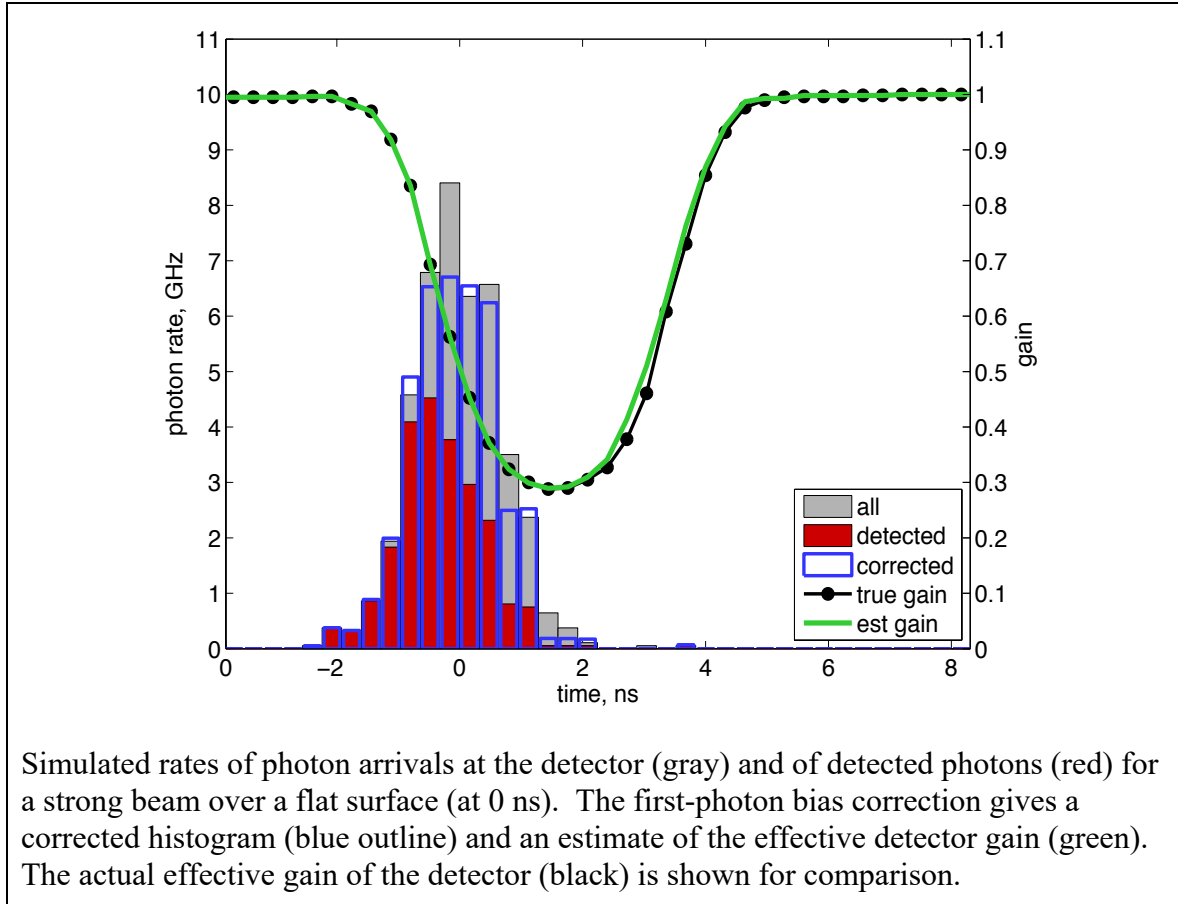
672 The iterations are terminated if no further PEs are eliminated in a given step. If a given iteration  
673 eliminates PE such that the selected PE no longer define a window, then that step is reversed,  
674 and the iterations are terminated. The inclusion of  $0.75 H\_window\_last$  as the minimum size of  
675 the window in each step of the calculation attempts to ensure that the calculation does not  
676 converge too fast to a spurious value of  $h\_mean$ .

677

678 The window width after the final step is reported as  $w\_surface\_window\_final$ , and the number of  
679 PEs in the window is reported as  $n\_fit\_photons$ . The final slope of the along-track segment is  
680 reported as  $dh\_fit\_dx$ . The median residual to the along-track fit is given in the parameter  
681  $med\_r\_fit$ , and is used to convert between a mean-based height estimate for each segment and a  
682 median-based estimate.

683 3.4 First-Photon Bias

Figure 3-7. First-photon bias correction



684

685 The first-photon bias (FPB) results from an inherent problem with the photon-counting detectors  
 686 selected for ATLAS. For a short time,  $t_{dead}$ , after an individual pixel of each detector detects a  
 687 photon, it cannot detect another. This means that photons early in a ground return are more  
 688 likely to be detected than those later on, and, for a symmetric return-photon distribution, the  
 689 mean surface height estimate is biased upwards, an effect that is largest for more intense pulses  
 690 and for pulses from flat surfaces where the return energy is concentrated in a short period of  
 691 time. Note that for ATLAS's asymmetric transmit pulse, the first-photon bias may result in either  
 692 positive or negative height errors, because for small roughness values, the FPB suppresses  
 693 detection the early, intense part of the waveform, while the tail of the waveform is unaffected,  
 694 resulting in a negative height bias. For larger roughness values, FPB affects the tail and the peak  
 695 more equally, and the bias becomes positive. For clarity, we will describe modeling results using

696 a simulated symmetric Gaussian transmit pulse, but the corrections provided on the ATL06  
697 products may have either positive or negative signs.

698 For ATLAS,  $t_{dead}$  is quite short, at approximately 3.2 ns, and there are multiple pixels in each  
699 detector (16 for the strong beams, 4 for the weak), to which photons are assigned at random as  
700 they reach the detector, resulting in fewer photons reaching each pixel while it is inactive.  
701 Despite this, up to several cm of bias may be observed for flat bright surfaces. Figure 3-7 shows  
702 simulated instantaneous photon rates for photons incident on the detector, and of detected  
703 photons for returns from a flat, smooth surface for a strong spot, under moderately saturated  
704 conditions (1.2 photons per pixel per pulse), aggregated over 40 m. Background PE are not  
705 included in the simulation, but their effect is likely to be minor, because their contribution to the  
706 total PE count is, in strong-signal conditions, a small fraction of the total, and the correction is  
707 negligible if the signal is not strong.

708 We have found that we can generate a correction for the first-photon bias based on a model of  
709 the detector for PEs aggregated over a 40-m ground-track segment. In this algorithm, we  
710 generate a histogram representing the distribution of heights around the ground return for the  
711 segment, as represented by the histogram of PE residuals to the best-fitting sloping segment  
712 model. We then estimate the effective gain of the detector, a function that represents the  
713 probability that a photon would have been detected if it reached the detector. We use this  
714 function to correct the received histogram to an estimate of the histogram of all the photons,  
715 detected and undetected. Statistics of this histogram are used to improve estimates of the  
716 surface height.

717 Using the residuals to the best-fitting segment in this calculation assumes that each pulse  
718 experiences the same distribution of photon-arrival times, shifted in time by the along-track  
719 surface slope, so that a typical distribution can be found by correcting for the along-track slope.  
720 If the surface slope or the reflectance has strong variations within a segment this assumption will  
721 fail, but for segments where the correction is large (i.e., in the interior of the ice sheets), it should  
722 not introduce large errors because ice-sheet surfaces are typically very homogeneous.

### 723 3.4.1 Mathematical Description for the First-Photon Bias

724 The photon distribution incident on the detectors is written as a function of  $t_i - t_g$ , where  $t_i$  is the  
725 PE time and  $t_{gi}$  is the time of the ground return. In practice, this is calculated as  $t_i - t_{gi} = -r c/2$ ,  
726 where  $r$  is the height residual to the best-fitting segment. We can express the histogram over  $N$   
727 PE times as:

$$N(t; t_i - t_{gi}) = \sum_{i=1:N} \sum_{t_i - t_{gi} \in (t, t + \Delta t]} 1 \quad 5$$

728 Only some of these photons are detected: After a photon hits a detector, that detector cannot  
729 detect another photon until it becomes active, after receiving no photons for a time  $t_{dead}$ . This can  
730 be expressed by a function giving the status of each pixel for each pulse at time  $t$ :

$$A(t, p, pixel) = \begin{cases} 1 & \text{if pixel is active at time } t \text{ for pulse } p \\ 0 & \text{if pixel is inactive at time } t \text{ for pulse } p \end{cases} \quad 6$$

731 The detected photon distribution is then:

$$N_d(t; t - t_g) = \sum_{i=1:N} \sum_{t_i - t_{gi} \in (t, t + \Delta t]} A(t_i - t_{gi}, pixel_i, P_i) \quad 7$$

732 If the photon distribution in  $t - t_g$  is constant over the pulses and over all pixels, then we can write:

$$N_d(t - t_g; \Delta t) = G(t - t_g) N(t - t_g; \Delta t) \quad 8$$

733 Where:

$$G(t - t_g) = \frac{1}{N_{pulses} N_{pixels}} \sum_{pulses, pixels} A(t - t_g) \quad 9$$

734 This function is effectively a gain for this collection of pulses. It ranges between zero, when all  
735 pixels are inactive, and one, when all pixels are active. The detector gain is shown by the black  
736 line in Figure 3-7. It falls rapidly from unity to about 0.3 during the early part of the surface  
737 return, then recovers gradually over a period slightly longer than  $t_{dead}$ , about 3.2 ns.

### 738 3.4.2 Correction Formulation for the First-Photon Bias

739 We implement the gain correction based on channel dead-time estimates from ATL03 and a  
740 histogram of residual times relative to the best-fitting segment model from 3.3.5.2, truncated by  
741  $\pm h\_window\_final/2$ . We represent the deadtime for the detector with the mean deadtime for all  
742 channels in the detector, and assume that all pixels (and channels) have identical sensitivity.  
743 Although the algorithm's function does not depend strongly on the spacing of the histogram bins,  
744 our test software has used a bin spacing of 0.05 ns. We express the timing for the correction as a  
745 function of time relative to the ground-return time, under the assumption that for an entire  
746 segment, the return shape will be consistent relative to the ground-return time:

$$\tau = t - t_g \quad 10$$

747 Our strategy in this calculation is to correct an initial histogram of PE arrivals for the effects of  
748 detector dead time ( $G < 1$ ) by dividing  $N_d(\tau)$  by  $G(\tau)$ :

$$N_{est}(\tau; \Delta t) = \frac{1}{G(\tau)} N_d(\tau, \Delta t) \quad 11$$

749 To correct waveforms for the effects of dead time, we can use an *a posteriori* estimate of  $G(\tau)$   
750 calculated with a simple model of the detector. In this model, we calculate a detected  
751 distribution,  $N_d$ , as the histogram of PE arrivals relative to the ground bin for a single-segment  
752 (40 m) section of track. For each bin in the histogram, we then determine the average number of  
753 pixels in the detector that were inactive. This is calculated:

$$P_{dead}(\tau) = \frac{\text{number of photons in } [\tau - t_{dead}, \tau)}{N_{pix}N_{pulses}} \quad 12$$

754

755 The estimated gain is then  $1 - P_{dead}$ . This calculation can be carried out efficiently by convolving  
756 the histogram of residuals with a rectangular window of height  $1/N_{pix}N_{pulses}$ , and shifting the  
757 result by the width of the window.

758 For our simulated example (in Figure 3-7) the recovered gain (green) is approximately equal to  
759 the true detector gain; this example is fairly typical of other simulations of this process, where  
760 the estimated gain is usually within a few percent of the true gain. There are visible differences  
761 between the corrected photon-timing histogram (blue) and the incident photon histogram, but the  
762 effects of these variations on the recovered heights are relatively small and have approximately  
763 zero bias.

### 764 3.4.3 Statistics Derived from the First-Photon-Bias Correction

765 The output of the gain estimation is a corrected histogram of height differences relative to a  
766 reference surface. Statistics of this histogram (e.g. its vertical centroid, its median) can be  
767 calculated as they would for the uncorrected PE heights. Since these statistics are calculated on  
768 the histogram of uncorrected photon residuals, their values give the correction relative to the  
769 mean of the PE heights. Thus, to calculate the corrected mean or median surface height, we add  
770 the gain-corrected mean or median of the residuals, respectively, to the uncorrected mean height.  
771 Because we expect the transmitted pulse to be skewed, we expect the median height correction to  
772 be much larger than the mean height correction.

773

#### 774 3.4.3.1 Mean Height Correction

775 The mean height correction based on the corrected histogram is:

$$f_{pb\_mean\_corr} = \sum \frac{N_{corr,i}}{N_{tot}} dz_i \quad 13$$

776 Here  $dz_i$  are the bin centers of the histogram of the PE residuals (i.e. the difference between the  
777 PE heights and the linear segment fit. The error in the mean correction is found using the error

778 propagation formula for a centroid, assuming that the measured PE counts are Poisson  
 779 distributed and ignoring the error in the gain estimate. For each bin in the corrected histogram,  
 780 the corrected count at that bin has an error:

$$\sigma_{N,corr,i} = \frac{N_{0,i}^{1/2}}{G_i} \quad 14$$

781 The error in the mean height based on the corrected counts is then:

$$\sigma_{fpb-corr} = \left[ \sum \left( \sigma_{N,corr,i} \frac{dz_i - fpb\_corr}{N_{corr,tot}} \right)^2 \right]^{1/2} \quad 15$$

### 782 **3.4.3.2 Median Height Correction**

783 The median correction and its error are calculated from the CDF (Cumulative Distribution  
 784 Function) of the corrected histogram as a function of dz:

$$CDF(dz_0) = \sum_{dz_i < dz_0} \frac{N_{corr,i}}{N_{corr,tot}} \quad 16$$

785 The median of the corrected histogram is found by interpolating into  $dz$  as a function of  $CDF(dz)$   
 786 at an abscissa value of 0.5:

$$median\ fpb = CDF^{-1}(0.5) \quad 17$$

787 Because CDF is a function of the residuals to the linear segment-fit model, the median calculated  
 788 in this way gives an offset relative to  $h\_mean$ .

789 The uncertainty of the median interpolated from the CDF is the slope of the inverse function of  
 790  $CDF(dz)$  with respect to CDF times the statistical uncertainty in the CDF at the median point:

$$\sigma_{med} = \left. \frac{dz}{dCDF} \right|_{CDF=0.5} \sigma_{CDF}(h_{med}) \quad 18$$

791 The statistical uncertainty in the CDF achieves half its total variance at the median, so we can  
 792 calculate its uncertainty at the median as:

$$\sigma_{cdf}(dz_{med}) = \left[ \frac{1}{2} \sum \frac{\sigma_{N,corr,i}^2}{N_{tot,corr}^2} \right]^{1/2} \quad 19$$

793 We estimate the slope of the CDF based on the 60<sup>th</sup> and 40<sup>th</sup> percentiles of  $dz$ , calculated from  
 794 the CDF of  $dz$ , and noting that 20% of the residuals should fall within this range. The error in  
 795 the median correction is then:

$$fpb_{md\_corr\_sigma} = \frac{dz_{60} - dz_{40}}{0.2} \sigma_{cdf}(dz_{med}) \quad 20$$

796 For both the mean and the median corrections, the error calculated in this way gives the total  
 797 error in the surface height due to the Poisson sampling in the data. It does not take into account  
 798 the effects of the along-track distribution of the photons, as the propagated least-squares error  
 799 (equation 19) does, so the error in the final, corrected height measurement ( $h_{li\_sigma}$ ) is the  
 800 maximum of  $sigma_{h\_mean}$  and  $fpb_{med\_corr\_sigma}$ . Note that neither the combined error nor  
 801 the median error calculated above are rigorous estimates of the error guaranteed to work under  
 802 all circumstances. However, numerical experiments have shown that these error estimates match  
 803 the RMS spread of recovered values to within ~10% for numbers of PEs greater than ~20. For  
 804 smaller numbers of PE, the error estimates may be up to 20% too small.

### 805 3.4.3.3 Corrected Return Count

806 The corrected number of returned photons is calculated:

$$fpb_{N\_photons} = \sum N_{corr} \quad 21$$

807 This sum is carried out over the ground window calculated during ground-bin refinement  
 808 (3.3.5.2). This is similar to the dead-time correction on ATL03.

### 809 3.4.3.4 Correction Validity

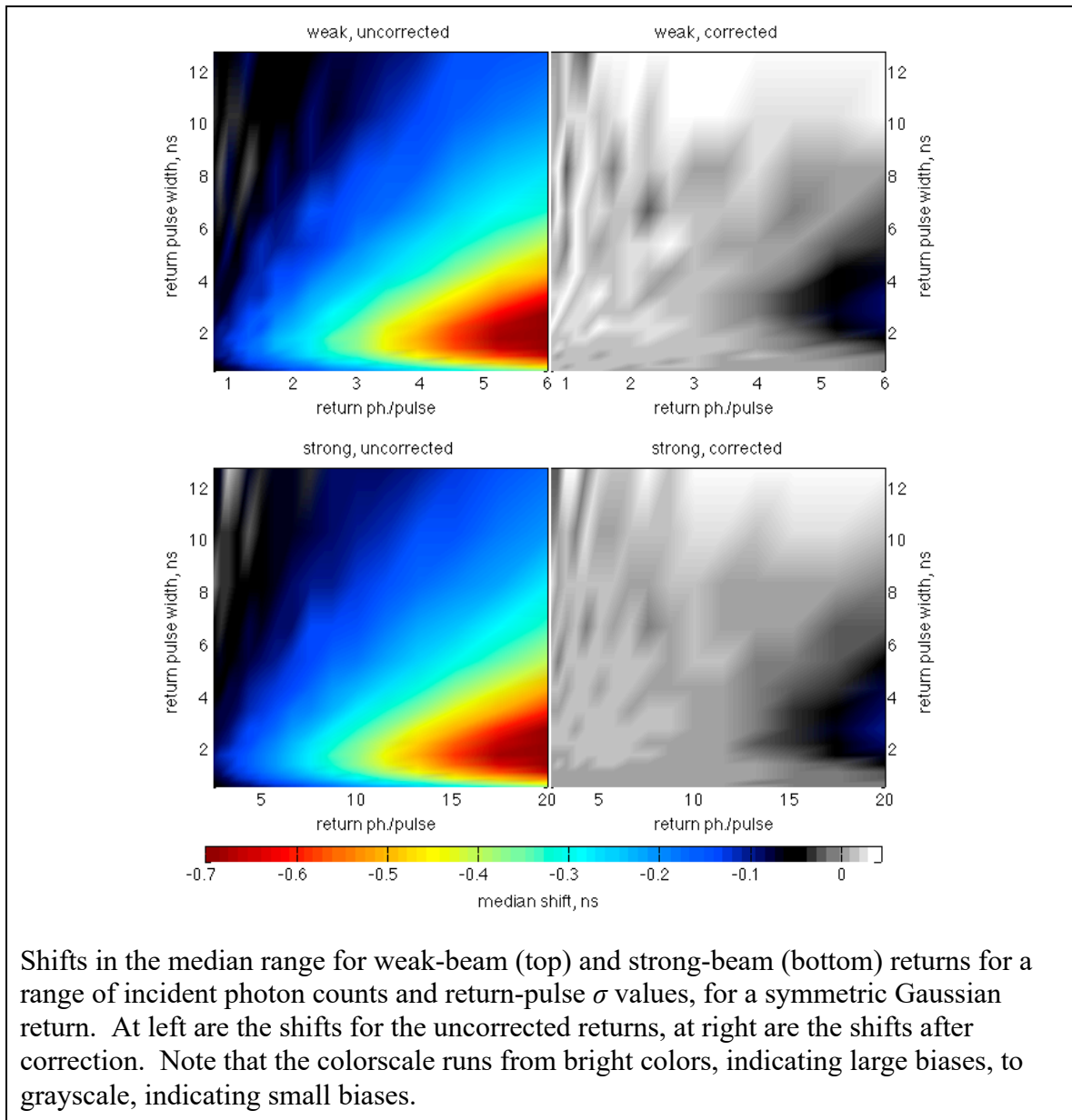
810 The correction should provide accurate height and signal-strength corrections as long as there are  
 811 at least a few active detector pixels during each time increment. If the estimated detector gain for  
 812 a segment falls below  $2/(N_{seg\_pulses} \times n_{pixels})$ , the correction values are set to their invalid  
 813 value ( $NaN$ ), so that any value that uses these corrections (e.g.  $h_{li}$ ,  $fpb_{n\_corr}$ ) will also be  
 814 marked invalid.

815

### 816 3.4.3.5 Accuracy of the first-photon bias correction

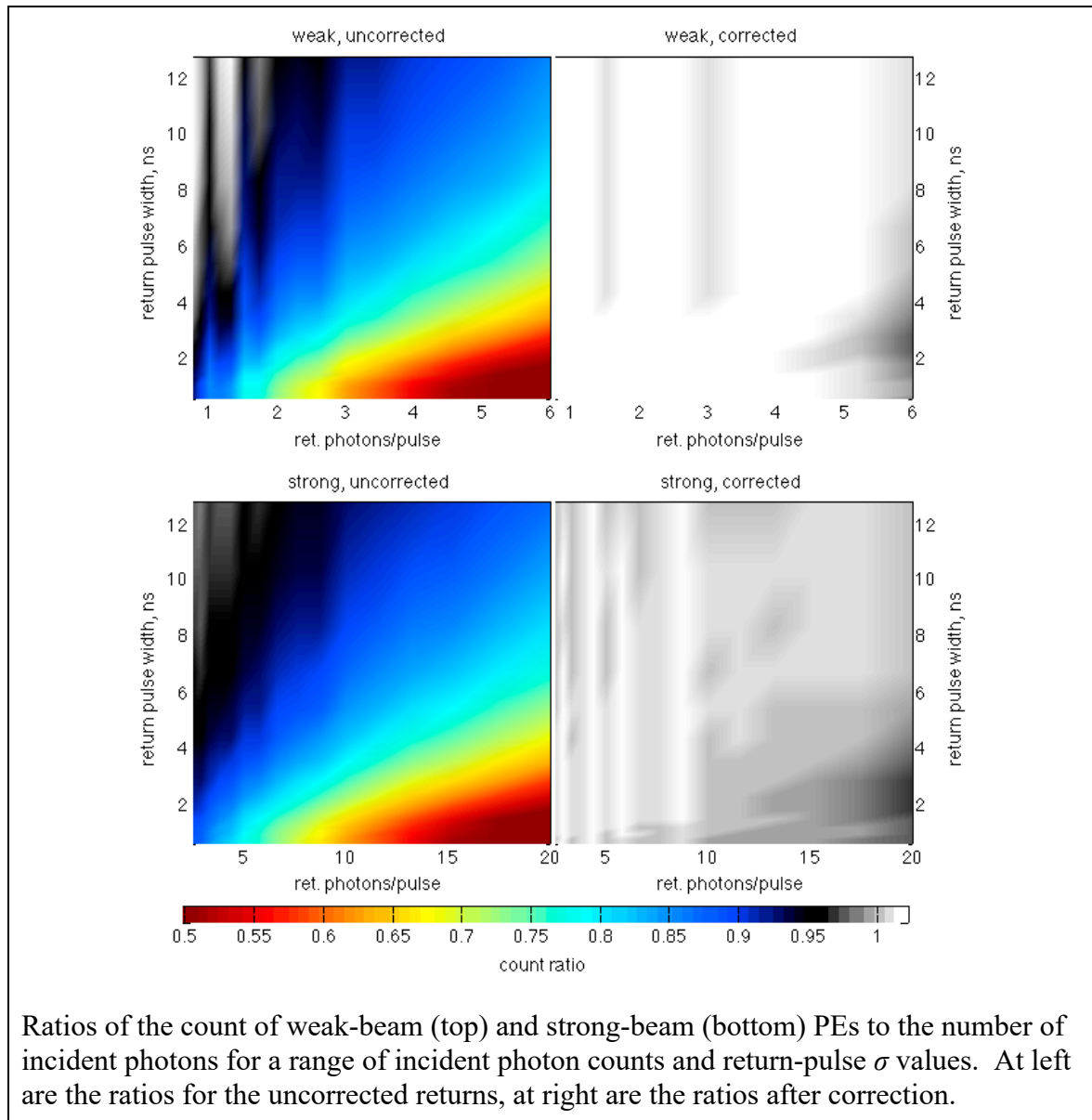
---

Figure 3-8. Accuracy of first-photon bias correction elevation recovery



817 We assess the potential accuracy of this calculation with a simple simulation of elevation  
 818 recovery for a strong and a weak ATLAS beam. For each realization of this simulation, we  
 819 generate random arrival times for a collection of  $N_{inc}$  incident return-pulse photons, with  
 820 standard deviation  $\sigma_{inc}$ . These photons are assigned at random to detector pixels (4 pixels for a  
 821 weak beam, 16 for a strong beam) and are labeled as detected or undetected based on the detector  
 822 model described in 3.4 with a dead time of 3.2 ns. Based on these PE times, we then calculate a  
 823 corrected arrival-time histogram as described in 3.4.2 and calculate statistics for this distribution  
 824 as described in 3.4.3.

Figure 3-9. Accuracy of first-photon-bias-correction signal strength recovery



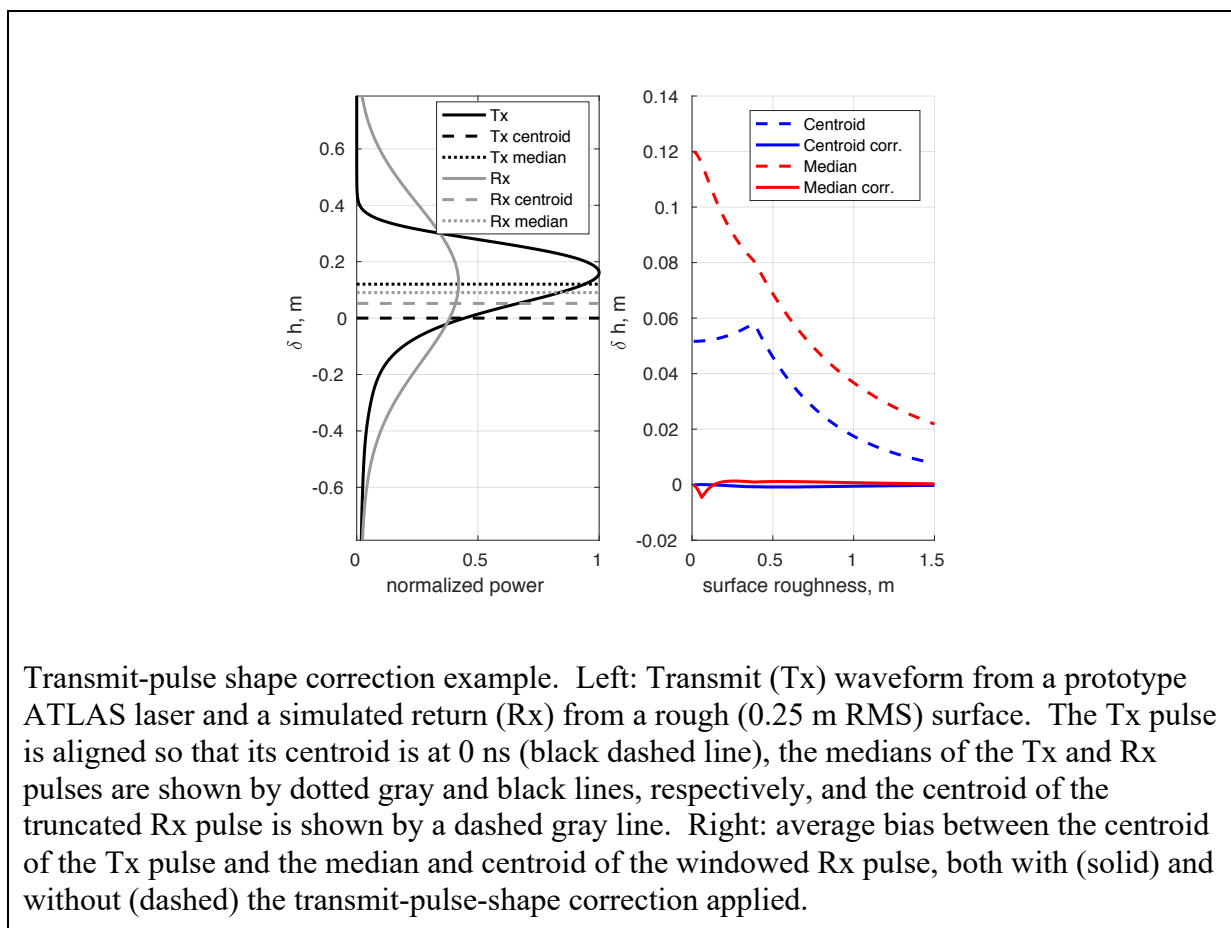
825

826 Results of this simulation are shown in Figure 3-8 and Figure 3-9. For the strongest simulated  
 827 returns, with around two photons per pulse per detector pixel, uncorrected time biases are as  
 828 large as -0.7 ns, corresponding to positive elevation biases of about 0.1 m. For these returns,  
 829 only about 60% incident photons are detected. For expected return strengths, of 0.8 photons per  
 830 pulse per pixel, elevation biases are smaller, around -0.2 ns, and about 85% of incident photons

831 are detected. The largest elevation errors come for return-pulse widths of around 2 ns, and the  
 832 largest loss of signal photons happens for the smallest pulse widths and the strongest returns.  
 833 Applying the correction removes the majority of the bias, both for return times and for signal  
 834 strengths. Corrected returns have much smaller time biases, accurate to 0.1 ns (1.5 cm) for the  
 835 strongest (2 photons/pixel/pulse) returns, and 0.02 ns (0.03 cm) for expected (0.8 ph/pixel/pulse)  
 836 return strengths. Corrected PE counts are within 2% of the incident counts.

837 **3.5 Transmit-pulse shape correction**

Figure 3-10. Transmit-pulse-shape correction



838  
 839 The ATL06 surface-fitting routine and the ATL06 first-photon bias correction both give  
 840 estimates of the median height of the surface for each segment, relative to the centroid of the  
 841 transmit pulse, for a ‘windowed’ collection of photons of limited vertical extent (typically  $\pm 1.5$   
 842 m around the median height). However, the ATL03 PE heights are calculated relative to an

843 estimate of the centroid of the entire transmit pulse. Because the transmitted pulse is not  
844 symmetric in time around its centroid, its median is different from its mean, and the centroid of  
845 any truncated subset of the photons from this pulse will have a nonzero bias relative to those  
846 from the full waveform. This introduces a potential bias in ATL06 height estimates.

847 The magnitude of the bias depends on three factors: the shape of the ‘tail’ of the transmitted  
848 waveform, the width of the surface window, and the effective surface roughness (i.e. the total  
849 broadening introduced by surface slope and roughness). The effects of the tail shape and the  
850 surface-window height were described previously (1.1). The effect of increasing effective  
851 surface roughness is to increase the scatter in the PEs, producing returns that are closer to  
852 symmetrical, as shown for 0.25 m noise in Figure 3-10 (left panel). This larger scatter results in  
853 return-waveform medians that have smaller biases than those from a smooth surface, and in  
854 smaller biases in the truncated-waveform centroids. Figure 3-10 (right panel) shows the  
855 magnitude of biases in return centroids and medians for prototype-laser waveforms, broadened to  
856 simulate the effects surface roughness values between 0 and 1.5 meters. For each waveform, we  
857 calculated the centroid and median surface height relative to the centroid and median of the  
858 transmitted pulse, using a surface window height of a maximum of 3 m and three times the RDE  
859 of the returned PEs. The worst of the biases, for the zero-roughness median, is around 15 cm,  
860 and biases decrease with increasing roughness. The bias in the centroid is smaller than that of the  
861 median, but both are large relative to other expected instrumental biases.

862 We have found that we can correct for this effect by modeling expected return-pulse shapes and  
863 calculating the biases for these shapes, then subtracting the bias from the measured height  
864 estimates. The model is based on transmitted-waveform shapes measured periodically during the  
865 ICESat-2 orbit using the transmitter-echo-pulse (TEP). Using this TEP waveform and the width  
866 of the return, we estimate the extent to which reflection from the sloped, rough surface has  
867 broadened the return, and smooth the TEP waveform to broaden it to the same width. We then  
868 truncate the broadened synthetic waveform around its mean using the surface window  
869 determined in 3.3, then calculate the median and centroid of the broadened, truncated waveform.  
870 This gives corrections to the median and mean surface heights.

871 Note that at the time of writing of this document the relationship between the absolute values of  
872 the photon times measured in the TEP and the transmit times of the lasers has not been  
873 established. On-orbit calibration exercises and further analysis of pre-launch calibration data  
874 should be helpful in this regard, but for now, we take the TEP as a measurement of the shape of  
875 the waveform, not the timing of the transmission. Accordingly, we shift the time values on the  
876 TEP measurements obtained from ATL03 so that the centroid of the signal photons arrival times  
877 is equal to zero, and assume that this shifted TEP represents the transmit pulse.

878 To estimate the broadened transmit-pulse shape, we begin with an estimate of the transmitted  
879 pulse shape derived from ATL03,  $P_{tx}(t)$ , and  $RDE(t_i)$ , our estimate of the degree to which the  
880 distribution of surface returns,  $t_i$ , has been spread by its reflection from a rough or sloping  
881 surface:

$$\sigma_s^2 = \max \left( (0.01 \text{ ns})^2, RDE(t_i)^2 - RDE(P_{tx}(t))^2 \right) \quad 22$$

882 The  $\max((0.01 \text{ ns})^2, \dots)$  function here is included to ensure that the broadening estimate is  
883 positive. From this we generate an estimate of the surface broadening function S(t):

$$S(t) = \exp \left( -\frac{t^2}{2\sigma_s^2} \right) \quad 23$$

884 The estimated broadened pulse shape,  $P_B(t)$  is the temporal convolution of  $P_{tx}(t)$  and S(t):

$$P_B(t) = P_{tx}(t) * S(t) \quad 24$$

885 We apply a windowing function,  $W_s(t)$ , to account for the truncation of the surface return during  
886 the ground-bin-selection process:

$$W_s(t) = \begin{cases} 0 & |t - \text{mean}(P_B(t))| > h\_window\_final/2 \\ 1 & |t - \text{mean}(P_B(t))| \leq h\_window\_final/2 \end{cases} \quad 25$$

887

888 The height correction for the median based on this waveform estimate is then:

$$dh_{tx} = \frac{c}{2} \text{median}_t(P_B(t)W_s(t)) \quad 26$$

889 Here  $\text{median}_t()$  represents the temporal median of a function:

$$\text{median}_t(f(t)) \equiv t \text{ such that } \int_{-\infty}^t f(t') dt' = \frac{1}{2} \int_{-\infty}^{\infty} f(t') dt' \quad 27$$

890 The correction for the mean is identical, but uses the mean instead of the median in equation 26.  
891 Figure 3-10 shows that after applying this correction, the remaining bias in the median and mean  
892 heights is less than 3 mm. The value calculated in equation 26 is included in the standard  
893 surface-height estimate,  $h_{li}$ , and is provided in the  $tx\_median\_corr$  and  $tx\_mean\_corr$  fields in  
894 the  $bias\_correction$  parameter subgroup.

895

896 **3.6 Signal, Noise, and Error Estimates**

897 Before we can calculate the error in the retrieved surface height, we must form estimates of  
 898 relative contributions of signal and noise PEs to the observed PE count. Under ideal conditions,  
 899 when the signal level is high and the background count rate is low, few noise PEs will be present  
 900 among those selected by editing process described above. However, under cloudy conditions  
 901 when the sun is above the horizon this will often not be true, and it is important that the error  
 902 estimates reflect the potential presence of background PEs.

903 **3.6.1 Background PE rate**

904 The background PE rate (*bckgrd* in the *geophysical* subgroup) is derived from the ATL03  
 905 parameter */bckgrd\_atlas/bckgrd\_rate*, and is derived from a 50-shot, 200Hz count of PE within  
 906 the ATLAS signal-finding window, corrected for the number of PE detected by the ATL03  
 907 ground-finding algorithm. In general, we expect this parameter to be sufficiently accurate to  
 908 allow us to predict the number of PE within 10 m of the ground to a precision of better than 10  
 909 PE/segment.

910 The expected background rate,  $E_{bckgrd}$ , is also predicted based the solar elevation, assuming a  
 911 flat, Lambertian surface at the ground. The calculation of this parameter is described in the  
 912 ATL07 ATBD, section 4.2.3.1. This parameter, when compared against the measured *bckgrd*, is  
 913 a potential indicator of the surface reflectance and cloud properties.

914 **3.6.2 Signal PE count**

915 The total number of PEs selected in the window, as a function of the number of signal PEs, the  
 916 background rate, the number of pulses in the window, and the background window height is:

$$N_{tot} = N_{sig} + N_{BG} \quad 28$$

917 The number of background PEs in the window has a mean value:

$$N_{BG} = 2 N_{pulses} h_{window} BGR/c \quad 29$$

918 Subtracting the two gives an estimate of the number of signal PE,  $N_{signal}$ . Because the number of  
 919 background PE is a Poisson random variable, the calculated  $N_{signal}$  may be less than zero in  
 920 weak-signal conditions. The ratio between the number of signal and noise photons is reported as  
 921 *fit\_statistics/snr*.

922 To help distinguish high-quality surface returns from returns that are likely a result of  
 923 signal-finding blunders, we provide the *fit\_statistics/snr\_significance*, which gives the  
 924 probability that in the absence of any real ground signal, a segment with at least the observed  
 925 SNR would be found by the ATL06 signal-selection routine, for the initial range of heights,  
 926 *h\_range\_initial* and background rate *bckgrd*. If ATL03 detected photons were used in the signal

927 selection (*signal\_selection\_source* of 0 or 1, or *signal\_selection\_status\_backup* of 0),  
 928 *h\_range\_input* is equal to the range of photon heights. Otherwise it is set to the full range of PE  
 929 heights provided from ATL03 for the segment. The values of *snr\_significance* are calculated  
 930 from a look-up table based on 1,000,000 realizations of random noise for background-noise  
 931 values, *bckgrd\_table*, between 1 and 10 MHz, and for initial window sizes, *w\_table*, between 3  
 932 and 80 meters. For each set of random-noise PE, the backup signal-selection algorithm is run to  
 933 select the input PE for the iterative ground-window refinement routine (3.3.5.2), which is then  
 934 run to convergence, and the final SNR is recorded. Then, for each value of *bckgrd\_table* and  
 935 *w\_table*, the probability of reporting a segment with an SNR value greater than a set of values  
 936 between -10 and 10, in steps of 0.1, is calculated, and the value is stored in *F\_table*. To find  
 937 *snr\_significance* for each segment, we interpolate into *F\_table* as a three-dimensional linear  
 938 function of *h\_range\_input*, *bckgrd*, and *snr* for that segment.

### 939 3.6.3 Per-Photon Errors

940 Noise PEs are vertically distributed throughout the window with a standard deviation of  
 941 approximately

$$\sigma_{BG} = 0.287 h_{window} \quad 30$$

942 where the factor 0.287 equals the standard deviation of a uniform random variable on a unit  
 943 interval.

944 The signal PEs have an approximate skewed Gaussian distribution, whose width depends on the  
 945 transmit-pulse duration, the surface roughness, the surface slope, and the footprint width, as  
 946 described in equation 1, with additional broadening possible due to atmospheric or subsurface  
 947 scattering. For ice-sheet surfaces and near-vertical beams we assume that the angle between the  
 948 beam and the surface slope is equal to the magnitude of the surface slope. The total standard  
 949 deviation of the surface return heights,  $\sigma_{\text{photon,est}}$  is then:

$$\sigma_{\text{photon,est}} = \left( \frac{N_{BG} \sigma_{BG}^2 + N_{\text{signal}} \sigma_{\text{signal}}^2}{N_{BG} + N_{\text{signal}}} \right)^{1/2} \quad 31$$

950 With the exception of the surface roughness, all of the quantities needed for this equation are  
 951 estimated from the data: the slope spreading is estimated from the along-track component of the  
 952 surface slope and the transmitted pulse width using equation 1, and the background and signal  
 953 PE counts are estimated from the total number of PEs and the background rate. If we assume the  
 954 roughness to be zero, and neglect atmospheric and subsurface scattering errors, equation 31 gives  
 955 a minimum error estimate. An alternate estimate of the per-PE error is the vertical spread of PEs  
 956 relative to the along-track fit, *h\_rms\_misfit*. We combine these two estimates by setting our error  
 957 estimate,  $\sigma_{\text{photon}}$ , to the maximum of *h\_rms\_misfit* and  $\sigma_{\text{photon,est}}$ .

958 **3.6.4 Propagated Height Errors:**

959 Given the established per-PE error,  $\sigma_{photon}$ , the error propagation for the linear fitting equation  
 960 gives an estimate of the covariance matrix for the fit (Menke, 1989):

$$\mathbf{C}_{fit} = ((\mathbf{G}^T \mathbf{G})^{-1} \mathbf{G}^T)((\mathbf{G}^T \mathbf{G})^{-1} \mathbf{G}^T)^T \sigma_{photon}^2 \quad 32$$

961 The height error estimate,  $\sigma_{h\_mean}$  is the square root of the upper-left element of  $\mathbf{C}_{fit}$ .  
 962 This error is combined with the sampling error estimated during the first-photon-bias calculation  
 963 to give the total surface ranging error,  $\sigma_{h\_li\_sigma}$ . The error in the along-track slope  
 964  $\sigma_{dh\_fit\_dx}$ , is equal to the square root of the lower-right element of  $\mathbf{C}_{fit}$ .

965 **3.6.5 Uncorrected reflectance**

966 The uncorrected reflectance gives the ratio of the measured return energy to the energy expected  
 967 from a white surface, through a nominal clear atmosphere (Yang and others, 2013). Following  
 968 the strategy outlined in the ATL09 ATBD, we calculate:

$$r_{eff} = \frac{\pi E_{RX} r^2 F}{N_{seg\_pulses} E_{TX} A T_{opt}} \quad 33$$

969 Here  $E_{RX}$  is the received energy,  $r$  is the range to the surface,  $A$  is the telescope area, and  $T_{opt}$  is a  
 970 factor that combines the optical efficiency of the instrument optics and the detector sensitivity.  $F$   
 971 is a calibration factor that will be determined and maintained as part of the atmospheric science  
 972 operations.  $E_{TX}$  is the transmitted energy per pulse from the ATL03 parameter  $tx\_pulse\_e$ . We  
 973 calculate  $E_{RX}$  based on the number of returned PE as:

$$E_{RX} = (f_{pbN} - N_{BG}) \frac{hc}{\lambda} \quad 34$$

974 Here  $f_{pbN}$  is the dead-time-corrected segment signal photon count,  $N_{BG}$  is the background-photon  
 975 count (from equation 29), and  $hc/\lambda$  is the energy received per photon. Note that this is the same  
 976 calculation as equation 4.7 in the ATL09 ATBD, except that we use the ATL06 first-photon-  
 977 bias-corrected photon count, instead of the correction factor used in ATL09. For an atmospheric  
 978 transmittance 0.95, we expect to see  $r_{eff}$  of about 0.88 over unit-reflectance surfaces.

979 **3.7 Across-track slope calculation**

980 After the iterative editing process is complete, the across-track slope is computed for the pair  
 981 based on the first-photon-bias-corrected median heights for the two segments:

$$\frac{dh}{dy} = \frac{h_{LI,R} - h_{LI,L}}{y_{ATC,R} - y_{ATC,L}} \quad 35$$

982 If only one beam has returned a height, then *across\_track\_slope* is set to *invalid* for both beams.

### 983 **3.8 Subsurface-Scattering Bias**

984 The subsurface-scattering, or volume-scattering, bias comes from photons that experience  
985 multiple scattering within the snow or ice before returning to the satellite. Ice absorbs green  
986 light only weakly, with attenuation lengths of tens of meters or more, but ice grains in firn and  
987 air bubbles in ice both scatter green light strongly (Warren and others, 2006). While most  
988 photons from an ATLAS pulse are expected to exit the surface of a firn pack within a fraction of  
989 a nanosecond, others will likely be delayed significantly, producing a long tail on the histogram  
990 of return times. Averaging return times of PEs from this tail with PEs from the surface return  
991 leads to a delay in the mean PE return time, and a downward bias in the apparent surface height.  
992 The median surface height is modestly less sensitive than the mean, because it is less sensitive to  
993 outlying data values far from the central peak of the return distribution. This error and its  
994 temporal variability is expected to be small for fine-grained snow surfaces such as those found  
995 on the Antarctic Plateau and in central Greenland, but it may be more significant in coastal areas  
996 where seasonal snow melt leads to large temporal variations in the surface grain size.

997 The magnitude of the subsurface-scattering bias delay depends in part on the scattering density  
998 of the snow and its bulk absorbance, both of which are determined by the density and grain or  
999 bubble size close to the surface, and on the impurity content of the snow or ice. Since none of  
1000 these properties may be known at the time of ATLAS processing, each must be determined  
1001 independently using external information about the snow, such as meteorological model output  
1002 or infrared reflectance data.

1003 We do not expect to be able to offer an accurate correction for this effect with our current  
1004 understanding of the process. This remains an area of active research.

### 1005 **3.9 Atmospheric-Scattering Bias**

1006 A second important source of bias in ATLAS height measurements may come from atmospheric  
1007 scattering of the down-going laser pulse. Scattering by ice particles in the atmosphere redirects  
1008 much of the light through small angles, often less than about one degree. These photons may fall  
1009 outside the field of view of the ATLAS detectors, in which case they will be lost and will have  
1010 no impact on altimetry beyond attenuation of the received pulse, or they may reflect from the  
1011 surface within the field of view, in which case they may then be detected by ATLAS. However,  
1012 because their down-going path was longer than the assumed straight down-and-back path  
1013 assumed in the PRD model, they will give erroneously long ranges, and therefore low surface  
1014 heights. This effect is increasingly severe for thicker clouds, which scatter more photons, and for  
1015 clouds closer to the surface, where photons scattered through large angles may still remain in the  
1016 field of view.

1017 Under cloudy conditions, the received pulse contains a mixture of scattered and unscattered  
1018 photons, yielding a tail of delayed photons on the downward side of the return pulse; mean and

1019 median delays for a segment’s aggregate PEs will depend on the relative fraction of the two  
 1020 groups of photons, and the mean path delay per photon. This process has been modeled and  
 1021 found to produce 1-cm level biases on ATLAS height retrievals under most circumstances (Yang  
 1022 and others, 2011) but since the bias may be correlated over large spatial scales it may have a  
 1023 non-negligible impact on continental-scale surface-change retrievals.

1024 As is the case with the subsurface-scattering bias, parameters relating to a possible correction  
 1025 must be determined from datasets external to ATLAS, likely from atmospheric models that give  
 1026 an estimate of the cloud optical depth and the particle size. Potential corrections and data editing  
 1027 strategies for this effect remain an active topic of research.

1028

### 1029 **3.10 Segment geolocation**

1030 After ground-window refinement we calculate the final location of the segment. The segment  
 1031 location is defined as the reference-point location plus the across-track unit vector times the  
 1032 mean across-track coordinate of the selected PEs.

1033 To calculate the latitude and longitude of each segment, including the offset between the  
 1034 segment and the reference point, we use the latitude, longitude, and along-track distance  
 1035 provided by ATL03 for the selected PE. We assume that latitude and longitude for the selected  
 1036 PE in the segment are linear functions of along-track distance, and fit a linear function,  $f_{lat}$ , to the  
 1037 PE latitudes, and a second linear function,  $f_{lon}$ , to the PE longitudes, each as a function of  $x-x_0$ .  
 1038 The intercepts of these functions give the segment latitude and longitude.

1039 Geolocation errors in the along- and across-track direction are calculated based on the ATL03  
 1040 parameters  $\sigma_{geo\_AT}$ , and  $\sigma_{geo\_XT}$  and the radial orbit error,  $\sigma_{geo\_r}$ .

1041 With the surface-slope vector and the geolocation estimate we can calculate the geolocation  
 1042 contribution to the uncertainty in the surface height:

$$\sigma_{geo,h} = \left( \sigma_{geo,r}^2 + \left( \sigma_{geo,AT} \frac{dh}{dx} \right)^2 + \left( \sigma_{geo,XT} \frac{dh}{dy} \right)^2 \right)^{1/2} \quad 36$$

1043 This value is reported in the *land\_ice\_segments* group as  $\sigma_{geo\_h}$ , and the contributing  
 1044  $\sigma_{geo\_r}$ ,  $\sigma_{geo\_xt}$ , and  $\sigma_{geo\_at}$  are reported in the *ground\_track* group.

### 1045 **3.11 Noise-corrected robust estimators of spread**

1046 Many of the parameters in this document are based on ordinal statistics. These statistics use the  
 1047 percentiles of a distribution, which are defined based on the cumulative distribution function  
 1048 (CDF) of the distribution. We define the CDF of a discrete sample of values S as:

$$C(x; S) = \frac{\text{the number of values in } S \text{ that are less than } x}{\text{the number of values in } S} \quad 37$$

1049 For a binned distribution (e.g. a histogram or a probability distribution function),  $C(x; D(x_0))$ , we  
1050 define the CDF as

$$C(x; D(x_0)) = \frac{\int_{x_1}^x D(x') dx'}{\int_{x_1}^{x_2} D(x') dx'} \quad 38$$

1051 Here  $x_1$  and  $x_2$  are the bounds over which the distribution is defined. The percentiles of a  
1052 distribution are found by calculating the inverse function of the CDF of the distribution:

$$p(r; D) = C^{-1}\left(\frac{r}{100}; D\right) \quad 39$$

1053 Thus the median of a distribution  $D$  is:

$$\text{Median}(D) = x \text{ such that } C(x; D) = 0.5 \quad 40$$

1054 We also define the robust dispersion estimate (RDE) of a distribution as

$$RDE(D) = \frac{p(0.84; D) - p(0.16; D)}{2} \quad 41$$

1055 This is analogous to the standard deviation of a normal distribution, which is equal to half the  
1056 difference between its 84<sup>th</sup> and 16<sup>th</sup> percentiles, but is less influenced by outlying background  
1057 values.

1058

1059 In most cases, distributions of ATLAS PEs include a mix of signal and noise PEs. In these  
1060 cases, the noise PEs and the signal PEs both contribute to the distribution  $D$ . We expect the  
1061 noise PEs are generally uniformly distributed, so we can assume that

$$C(x; D) = \frac{BGR(x - x_1) + \int_{x_1}^x D_{\text{signal}}(x') dx'}{\int_{x_1}^{x_2} D(x') dx'} \quad 42$$

1062 Here  $D_{\text{signal}}$  is the distribution of the signal PEs, and  $\text{bckgrd}$  is the background PE rate, in units of  
1063  $x^{-1}$ . We can solve this for  $C_{\text{signal}}$ :

$$C(x; D_{\text{signal}}, BGR) = \frac{\int_{x_1}^x D_{\text{signal}}(x') dx'}{N_{\text{signal}}} = \frac{\int_{x_1}^x D(x') dx' - \frac{BGR(x - x_1)}{N_{\text{total}}}}{N_{\text{signal}}} \quad 43$$

1064 Here  $N_{\text{total}} = \int_{x_1}^{x_2} D(x') dx'$  and  $N_{\text{signal}} = N_{\text{total}} - (x_2 - x_1)BGR$ .

1065 Estimating the percentiles of  $D_{\text{signal}}$  is complicated because  $C(x; D_{\text{signal}}, \text{bckgrd})$  generally does  
 1066 not have an inverse function in  $x$ . However, if we evaluate  $C(x; D_{\text{signal}}, \text{bckgrd})$  for a set of  
 1067 values,  $x_i$ , we can find  $x_{\text{LT}}$ , the largest value of  $x_i$  for which  $C(x; D_{\text{signal}}, \text{bckgrd}) < r/100$  and  $x_{\text{GT}}$ ,  
 1068 the first value of  $x_i$  for which  $C(x; D_{\text{signal}}, \text{bckgrd}) > r/100$ , and interpolate linearly into  $[x_{\text{LT}}, x_{\text{GT}}]$   
 1069 as a function of  $[C(x_{\text{LT}}; D_{\text{signal}}, \text{bckgrd}), C(x_{\text{GT}}; D_{\text{signal}}, \text{bckgrd})]$  at the point  $r/100$ .

1070 The above procedure defines the background-corrected percentiles of a distribution. Based on  
 1071 this we define the noise-corrected median of a distribution, which we designate:  $\text{median}(D; \text{bckgrd})$ . We define the noise-corrected RDE of a distribution somewhat differently from its  
 1072 uncorrected counterpart. For low-noise distributions, the standard deviation of the population  
 1073 can accurately be estimated as half the difference between its 16<sup>th</sup> and 84<sup>th</sup> percentiles. In the  
 1074 presence of significant noise, the standard deviation can be estimated more accurately based on  
 1075 the difference between the 25<sup>th</sup> and 50<sup>th</sup> percentiles of the distribution, divided by a correction  
 1076 factor of 1.349, equal to the width of the central 50% of a normalized Gaussian distribution.  
 1077

1078

1079 The surface-window-refinement procedure in section 3.3.5 uses least-squares fitting and the  
 1080 RDE to progressively narrow the surface window. This procedure will not converge under all  
 1081 circumstances. Consider an initial surface window spanning from  $-H_i/2$  to  $H_i/2$ , with noise rate  
 1082  $R$  (in PE/m), containing  $s$  signal PEs at the center of the window. The normal (non-background-  
 1083 corrected) RDE will find a spread of:

$$\hat{\sigma} = 0.34 H - \frac{S}{R} \quad 44$$

1084 If  $s$  is small,  $\hat{\sigma} \approx 0.34 H$  so the three-sigma interval will have a width of  $2.04 H$ , and the  
 1085 refinement will not converge. Convergence requires  $6\hat{\sigma} < H$ , or:

$$s > 1.73HR \quad 45$$

1086 For a background rate of 10MHz (0.067 PE/m) and a weak beam (three surface PE per pulse),  
 1087 the procedure will converge if  $H < 26$  m. For a strong beam (10 PE per pulse), it will converge if  
 1088  $H < 86$ m. The convergence intervals become smaller in proportion to the signal PE count as the  
 1089 surface return is weakened by cloud attenuation or by reduced surface reflectance.

1090 The noise-corrected RDE and median improve on the performance of their uncorrected  
 1091 counterparts, but their performance is limited by the accuracy of the signal-level estimate. The

1092 estimate of  $N_{\text{signal}}$  has an approximate error of  $(N_{\text{pulses}} (HR+s))^{1/2}$  due to the Poisson statistics of  
1093 the PE. In contrast to the non-robust RDE and median, the process works increasingly well as  
1094 more shots are aggregated, because  $N_{\text{signal}}$  increases in proportion to  $N_{\text{pulses}}$ , while its error  
1095 increases in proportion to  $N_{\text{pulses}}^{1/2}$ . If we require that  $N_{\text{pulses}} s > a\sigma_n$ , we find convergence  
1096 intervals:

$$H < \frac{N_{\text{pulses}} s^2 - a^2 s}{a^2 R} \quad 46$$

1097 For 10 MHz noise, 3 PE/pulse, and for 57 pulses, this gives  $s > 3\sigma_n$  for  $H < 806$  m, implying  
1098 that the accuracy of the signal-level estimate will not be the limiting factor for any reasonable  
1099 initial window size.

1100

1101

## 1102 4 ATL06 DATA PRODUCT DESCRIPTION

1103 Here we describe how the parameters appear in the ATL06 product. The ATL06 parameters are  
1104 arranged by beam, and within each beam in a number of groups and subgroups. Where  
1105 parameter descriptions in the ATL06 data dictionary are considered adequate, they are not  
1106 repeated in this document.

### 1107 4.1 Data Granules

1108 ATL06 data are provided as HDF5 files. The HDF format allows several datasets of different  
1109 spatial and temporal resolutions to be included in a file. ATL06 files contain data primarily at the  
1110 single-segment resolution, divided into different groups to improve the conceptual organization  
1111 of the files. Each file contains data from a single cycle and a single RGT.

1112 Within each file there are six top-level groups, each corresponding to data from GT: *gt1l*, *gt1r*,  
1113 *gt2l*, etc. The subgroups within these *gtxx* groups are *segment\_quality*, *land\_ice\_segments*, and  
1114 *residual\_histogram*.

1115 In the *segment\_quality* group, the data are nearly dense, providing signal-selection and location  
1116 information for every segment attempted (i.e. those that contain at least one ATL03 PE) in the  
1117 granule, at the 20-meter along-track segment spacing. Datasets in this group can be used to check  
1118 the geographic distribution of data gaps in the ATL06 record.

1119 In the *land\_ice\_segments* group, data are sparse, meaning that values are reported only for those  
1120 pairs for which adequate signal levels (i.e. more than 10 PE, *snr\_significance* > 0.05) were found  
1121 for at least one segment: This means that within each pair, every dataset has the same number of  
1122 values, and that datasets are pre-aligned between pairs, with invalid values (NaNs) posted where  
1123 the algorithm provided a value for only one beam in a pair. Conversely, if neither beam in a pair  
1124 successfully obtained a value for *h\_li*, that segment is skipped for both beams in the pair. The  
1125 *segment\_id*, timing, and geolocation fields for the valid segments should allow the along-track  
1126 structure of the data to be reconstructed within these sparse groups. For segments without valid  
1127 heights that still appear on the product (because the other beam in the pair did contain a valid  
1128 height) the latitude and longitude are reported for the mean location of all PE for the segment (if  
1129 any PE are present) or as the location for the valid segment in the pair, displaced by the 90-meter  
1130 within-pair separation (if no PE are present).

1131 The *residual\_histogram* group is at lower resolution than the other groups, giving the distribution  
1132 of PE relative to the segment heights at a horizontal resolution of 200 m, or around 280 pulses.  
1133 The *segment\_id\_list*, *x\_atc\_mean*, *lat\_mean*, and *lon\_mean* fields in this group all can be used to  
1134 connect the *residual\_histogram* group to the per-segment groups.

1135 In the native format archived at the National Snow and Ice Data Center (NSIDC), each granule  
1136 (file) of data contains segments from a single pass over a one-degree increment of latitude for a  
1137 particular RGT, with corresponding data from all six beams. Over most of the globe, ICESat-2  
1138 travels in a roughly north-south direction, so each granule will contain approximately 111 km of

1139 data for each beam, or approximately 5660 segments. The granules containing the southernmost  
1140 extent of Antarctica, south of 87S, will contain a considerably longer stretch of data, but because  
1141 this area will likely be of most interest to researchers investigating continental-scale Antarctic  
1142 mass balance, the additional coverage will likely be desirable. We expect that because most  
1143 users will obtain their data through subsetting services provided by the NSIDC, the native  
1144 granule structure will be of minor importance.

1145 **4.2 Segment\_quality group**

1146 The segment\_quality group contains a nearly dense record of the success or failure of the  
1147 surface-finding strategies, and gives the locations of the reference points on the RPTs. It  
1148 contains a record of the success or failure of the surface-finding strategies, and gives the  
1149 locations of the reference points on the RPTs.

1150 Locations provided within this group are for the reference points on the pair tracks, not for the  
1151 segments themselves. This means that both beams in a pair will have the same location (because  
1152 they are not displaced relative to the reference point), and that the actual segment locations will  
1153 usually be displaced from the values in *reference\_pt\_lat* and *reference\_pt\_lon* in this group by  
1154 more than 45 m in the across-track direction. The laser beam and spot numbers corresponding to  
1155 the ground tracks are available in the attributes of the *ground\_track* group.

1156

**Table 4-1 Segment\_quality group**

Parameter	Units	Description
<i>delta_time</i>	seconds	Elapsed GPS seconds since the reference epoch. Use the metadata attribute <i>granule_start_seconds</i> to compute the full GPS time.
<i>segment_id</i>	unitless	segment number corresponding to the second of two ATL03 segments in the ATL06 segment, counted from the RGT equator crossing
<i>reference_pt_lat</i>	degrees	Latitude of the reference segment location on the RPT
<i>reference_pt_lon</i>	degrees	Longitude of the reference segment location on the RPT

<i>record_number</i>	unitless	For those segments that have adequate signal strength, this parameter gives the record for the pair within the other groups in the granule.
<i>signal_selection_source</i>	unitless	Indicates the last algorithm attempted to select the signal for ATL06 fitting, see table Table 3-1. A value of 3 indicates that all algorithms failed.

1157

1158 **4.2.1 Signal\_selection\_status subgroup**

1159 This subgroup includes the *Signal\_selection\_status\_confident*, *Signal\_selection\_status\_all*, and  
1160 *Signal\_selection\_status\_backup* parameters. Their values are described in Table 3-2. Its density  
1161 structure matches that of the *segment\_quality* group.

1162

1163 **4.3 Land\_ice\_segments group**

1164 The primary set of derived ATL06 parameters are given in the *land\_ice\_segments* group (Table  
1165 4-2). This group contains geolocation, height, and standard error and quality measures for each  
1166 segment. This group is sparse, meaning that parameters are provided only for pairs of segments  
1167 for which at least one beam has a valid surface-height measurement. This group contains the  
1168 *bias correction*, *fit statistics*, *ground\_track*, and *geophysical* subgroups, which all have the same  
1169 sparsity structure as the *land\_ice\_segments* group.

1170

1171

**Table 4-2 land\_ice\_segments group**

Parameter	Units	Description	Defined
<i>ATL06_quality_summary</i>	Unitless	Flag indicating: 0: No likely problems identified for the segment 1: One or more likely problems identified for the segment	4.3

*ICESat-2 Algorithm Theoretical Basis Document (ATBD) for Land Ice Along-Track Height (ATL06)*

*Release 003*

<i>delta_time</i>	Seconds	Elapsed GPS seconds since the reference epoch. Use the metadata attribute <i>granule_start_seconds</i> to compute the full gpstime.	Interpolated to the segment center from ATL03
<i>h_li</i>	Meters	Standard land-ice segment height determined by land ice algorithm, corrected for first-photon bias, representing the median-based height of the selected PEs	Equation 47
<i>h_li_sigma</i>	Meters	Propagated error due to sampling error and FPB correction from the land ice algorithm	Equation 48
<i>sigma_geo_h</i>	meters	Total vertical geolocation error due to PPD and POD, including the effects of horizontal geolocation error on the segment vertical error	3.10
<i>latitude</i>	degrees north	Latitude of segment center, WGS84, North=+	3.10
<i>longitude</i>	degrees east	Longitude of segment center, WGS84, East=+	3.10
<i>segment_id</i>	counts	Segment number, counting from the equator. Equal to the <i>segment_id</i> for the second of the two 20-m ATL03 segments included in the 40-m ATL06 segment	ATL03

1172  
 1173 The standard surface height will be given on the ATL06 product as *h\_li*. This height is the  
 1174 segment-center height obtained from the along-track slope fit, with the mean-median correction  
 1175 applied so that it represents the median surface height for the segment. By default, *h\_li* will be  
 1176 corrected for all height increments in the *geophysical* parameter group except for the ocean tide,

1177 the equilibrium tide, and the dynamic atmosphere correction (*dac*); this includes earth, load, and  
1178 pole tides, and troposphere corrections. Since these parameters are included in the standard  
1179 ATL03 PE height, the only correction made here is to remove the ocean tide by adding the  
1180 ocean-tide model value for each segment, a correction that is made when the data are read from  
1181 the ATL03 product. Using the names for product variables:

$$h_{li} = h_{mean} + fpb_{med\_corr} + tx_{med\_corr} \quad 47$$

1182 Other tide and troposphere corrections may be removed from *h* by adding the values provided in  
1183 the ATL06 *geophysical* group. The correction values for the waveform-based corrections are  
1184 provided in the *bias\_correction* group, so that users may convert, for example, from a median-  
1185 based height estimate to a mean-based estimate.

1186 The errors in the standard land-ice height product are calculated as the maximum of the median  
1187 error (calculated during the first-photon-bias correction) and the linear-fit error (calculated in  
1188 3.6), ignoring errors in the tidal and atmospheric corrections.

$$h_{li\_sigma} = \max(\sigma_{h\_fit}, fpb_{med\_corr\_sigma}) \quad 48$$

1189 This value does not include the effects of geolocation errors on the height estimate, because  
1190 while the components of *h<sub>li</sub>\_sigma* should be uncorrelated at the segment-to-segment scale, the  
1191 geolocation errors are likely to be correlated on much longer scales. The vertical component of  
1192 the geolocation error, as calculated from the surface-slope vector and the mean horizontal  
1193 geolocation accuracies of the selected PEs are given in parameter *sigma\_geo\_h* (see 3.10). The  
1194 error on a single segment height measurement taken independently of all adjacent measurements  
1195 should be  $(h_{li\_sigma}^2 + \sigma_{geo\_h}^2)^{1/2}$ . Averaged over several tens of segments with a  
1196 consistent surface slope, the error should approach *sigma\_geo\_h*, but the relative scatter between  
1197 individual adjacent segments should be *h<sub>li</sub>\_sigma*.

1198 The geolocation of the segment is given in geographic coordinates by parameters *latitude* and  
1199 *longitude*. These each represent the horizontal centers of the segments. The corresponding  
1200 along-track coordinates are given in the *ground\_track* group as *x\_atc* and *y\_atc*.

1201 The *land\_ice\_segments* group includes the *ATL06\_quality\_summary* parameter, which indicates  
1202 the best-quality subset of all ATL06 data. A zero in this parameter implies that no data-quality  
1203 tests have found a problem with the segment, a one implies that some potential problem has been  
1204 found. Users who select only segments with zero values for this flag can be relatively certain of  
1205 obtaining high-quality data, but will likely miss a significant fraction of usable data, particularly  
1206 in cloudy, rough, or low-surface-reflectance conditions. Table 4-3 gives the parameter values  
1207 needed for *ATL06\_quality\_summary* to be reported as zero. The last of these characteristics, the  
1208 vertical density of photons, helps remove the effects of a common problem where the ATL03  
1209 photon selection identifies a cloud top as a likely surface return. In these cases, ATL06 can  
1210 converge to a large (10+ m) vertical window containing tens of signal photons. Requiring a

1211 minimum ratio between the number of photons and the height of the window eliminates most  
1212 clouds, and eliminates only a few returns from rough or steep surfaces.

**Table 4-3 Segment characteristics for ATL06\_quality\_summary to be zero**

Characteristic	Threshold	Description
<b>h_robust_spread</b>	< 1 m	Robust spread of photons less than one meter suggests moderate spreading due to slope or roughness
<b>h_li_sigma</b>	< 1 m	Errors in surface height are moderate or better
<b>snr_significance</b>	< 0.02	Surface detection blunders are unlikely
<b>Signal_selection_source</b>	<=1	Signal selection must be based on ATL03 photons
<b>N_fit_photons/ W_surface_window_final</b>	>1 PE /m for weak beams, > 4 PE/m for strong beams	The vertical density of photons in the final surface window.

1213

1214

1215

### 1216 4.3.1 geophysical subgroup

1217 The *geophysical* group (Table 4-4) contains tidal and atmospheric corrections that may be added  
1218 to or removed from *h\_li*, and inferred atmospheric properties that may be used to determine  
1219 whether the elevation of a given segment might be affected by atmospheric forward scattering.  
1220 Note that the *neutat\_delay* parameter and all *tide\_* parameters in this group are applied by default  
1221 except for *tide\_ocean* and *dac* (dynamic atmosphere correction).. The sign of the parameters is  
1222 such that adding the parameter value to *h\_IS* removes the correction (for applied corrections) and  
1223 subtracting the parameter includes the correction (for *tide\_ocean*). These parameters are  
1224 interpolated from the corresponding ATL03 parameters for the ‘nominal photons’, interpolated  
1225 as a piecewise linear function of along-track distance to the segment centers. This group is  
1226 sparse, meaning that parameters are provided only for pairs of segments for which at least one  
1227 beam has a valid surface-height measurement.

1228 The ocean-tide value (*tide\_ocean*) and dynamic atmosphere correction(*dac*) are provided to  
 1229 allow interested users to correct for tides and the inverse-barometer effect over ice shelves.  
 1230 These parameter are not applied because the locations of ice-sheet grounding lines (defining the  
 1231 inland extent of floating ice shelves) are not always precisely known, and may change over time.  
 1232 Different users will want to apply the ocean-tide model to different areas within the grounding  
 1233 zone.

1234 This group also include parameters related to solar background and parameters indicative of the  
 1235 presence or absence of clouds. Some of these parameters are derived from the ATLAS  
 1236 atmospheric channel, and should help identify segments strongly affected by clouds or blowing  
 1237 snow: parameters *cloud\_flg\_asr* and *cloud\_flg\_atm* give estimates of the probability of clouds  
 1238 between ATLAS and the ground, based on the apparent surface reflectance and on atmospheric  
 1239 backscatter, respectively. Their values are described in the ATL09 ATBD, and should be  
 1240 evaluated against the standard that cloud optical thickness greater than 0.5 in the lower 3 km of  
 1241 the atmosphere is required to produce a substantial altimetry error. (Yang and others, 2011) .  
 1242 Note that over surfaces other than bright snow (e.g. over blue ice or dirty snow) the  
 1243 *cloud\_flg\_asr* may indicate clouds when none are present.

1244 Blowing snow has a larger potential to produce altimetry errors, and has been assigned its own  
 1245 flag; the estimated height of a detected blowing-snow layer is given in *bsnow\_h*, which is set to  
 1246 zero if no such layer can be detected; the confidence with which a blowing-snow layer can be  
 1247 detected or ruled out is given in *bsnow\_conf*. For both flags, cautious users may require a value  
 1248 of 0 or 1 (clear with high/medium confidence) but under sunlit conditions, neither flag may  
 1249 clearly indicate cloud-free conditions. The estimated optical thickness of blowing snow layers,  
 1250 if found, is given in *bsnow\_od*.

1251

1252

**Table 4-4 geophysical subgroup**

Parameter	Units	Description	Defined
<i>bckgrd</i>	Hz	Background count rate, derived from the ATL03 50-shot average, interpolated to the segment center.	Interpolated from ATL03
<i>bsnow_conf</i>	unitless	Blowing snow confidence. -3=surface not detected; -2=no surface wind; -1=no scattering layer found; 0=no top layer found; 1=none-little; 2=weak; 3=moderate; 4=moderate-high; 5=high; 6=very high	ATL09

**ICESat-2 Algorithm Theoretical Basis Document (ATBD) for Land Ice Along-Track Height (ATL06)**

**Release 003**

<i>bsnow_od</i>	unitless	Blowing snow layer optical depth	ATL09
<i>bsnow_h</i>	meters	Blowing snow layer top height	ATL09
<i>cloud_flg_asr</i>	counts	Cloud flag (probability) from apparent surface reflectance. 0=clear with high confidence; 1=clear with medium confidence; 2=clear with low confidence; 3=cloudy with low confidence; 4=cloudy with medium confidence; 5=cloudy with high confidence	ATL09
<i>cloud_flg_atm</i>	counts	Number of layers found from the backscatter profile using the DDA layer finder.	ATL09
<i>layer_flag</i>	counts	This flag is a combination of multiple flags (cloud flag atm, cloud flag asr, and bsnow_con) and takes daytime/nighttime into consideration. A value of 1 means clouds or blowing snow are likely present. A value of 0 indicates the likely absence of clouds or blowing snow.	ATL09
<i>e_bckgrd</i>	Hz	Expected background count rate based on sun angle, surface slope, for unit surface reflectance	Calculated following ATL07
<i>msw_flag</i>	unitless	Multiple Scattering warning flag. The multiple scattering warning flag (ATL09 parameter msw_flag) has values from -1 to 5 where zero means no multiple scattering and 5 the greatest. If no layers were detected, then msw_flag = 0. If blowing snow is detected and its estimated optical depth is greater than or equal to 0.5, then msw_flag = 5. If the blowing snow optical depth is less than 0.5, then msw_flag = 4. If no blowing	ALT09

		<p>snow is detected but there are cloud or aerosol layers detected, the <i>msw_flag</i> assumes values of 1 to 3 based on the height of the bottom of the lowest layer: &lt; 1 km, <i>msw_flag</i> = 3; 1-3 km, <i>msw_flag</i> = 2; &gt; 3km, <i>msw_flag</i> = 1. A value of -1 indicates that the signal to noise of the data was too low to reliably ascertain the presence of cloud or blowing snow. We expect values of -1 to occur only during daylight.</p>	
<i>r_eff</i>	unitless	Effective reflectance, uncorrected for atmospheric effects.	Equation 33
<i>solar_azimuth</i>	degrees_east	The direction, eastwards from north, of the sun vector as seen by an observer at the laser ground spot.	ATL03 <i>solar_azimuth</i> parameter, interpolated to the segment center from the reference photons
<i>solar_elevation</i>	degrees	Solar Angle above or below the plane tangent to the ellipsoid surface at the laser spot. Positive values mean the sun is above the horizon, while negative values mean it is below the horizon. The effect of atmospheric refraction is not included. This is a low-precision value, with approximately TBD degree accuracy.	ATL03 <i>solar_elevation</i> parameter, interpolated to the segment center from the reference photon
<i>tide_earth</i>	meters	Earth tide	Inherited from ATL03
<i>dac</i>	meters	dynamic atmosphere correction	Inherited from ATL03
<i>tide_load</i>	meters	Load Tide	Inherited from ATL03
<i>tide_ocean</i>	meters	Ocean Tide	Inherited from ATL03

<i>tide_pole</i>	meters	Pole Tide	Inherited from ATL03
<i>tide_equilibrium</i>	meters	Equilibrium tide	Inherited from ATL03
<i>neutat_delay_total</i>	meters	Total neutral atmospheric delay correction (wet+dry)	Inherited from ATL03

1253

1254 In some circumstances, the estimated background rate may also give an indication of cloud  
 1255 conditions. The estimated background rate is provided in parameter *bckgrd*, which may be  
 1256 compared with the background rate expected for a unit-reflectance Lambertian surface, with a  
 1257 slope equal to the measured surface slope, *E\_bckgrd*. In sunlit conditions, these parameters  
 1258 together allow an estimate of the total sub-satellite reflectance. The effective, uncorrected surface  
 1259 reflectance, *r\_eff*, based on first-photon-bias-corrected PE count and the range to the ground,  
 1260 may be compared to these numbers; if *bckgrd* is approximately equal to *e\_bckgrd*, the  
 1261 atmosphere and the surface must together have a reflectance close to unity; if *r\_eff* is  
 1262 approximately equal to unity, this indicates that the surface below the satellite is likely snow, and  
 1263 likely cloud free; if *bckgrd* is approximately equal to *e\_bckgrd* and *r\_eff* is small, clouds must be  
 1264 present, and if *bckgrd* is less than *e\_bckgrd*, the surface must be dark, and, most likely not snow  
 1265 covered.

1266 Also included in this group are the solar azimuth (*solar\_azimuth*) and elevation  
 1267 (*solar\_elevation*), used in estimating the expected background rates.

### 1268 4.3.2 ground\_track subgroup

1269 The *ground\_track* subgroup (Table 4-5) contains parameters describing the GT and RGT for  
 1270 each segment, as well as angular information about the beams. All the components needed to  
 1271 identify a given segment's orbit number, reference track, pair track, and beam number are given,  
 1272 along with the azimuth and elevation of the beam relative to the ellipsoid surface normal. The  
 1273 orientation of the RPT with respect to local north is given in *seg\_azimuth*.

1274 Note that in land-ice products, the ground tracks and pair tracks are numbered separately from  
 1275 the laser beams: the ground tracks are numbered from left to right relative to RGT, and the  
 1276 ground track number is associated with group names within the product: From left to right, they  
 1277 are *gt1l*, *gt1r*, *gt2l*, *gt2r*, *gt3l*, and *gt3r*. The laser beams are numbered from left to right relative  
 1278 to the spacecraft flight direction. When the spacecraft is flying with its x axis pointing forwards,  
 1279 the beam numbers are in the same order (beam numbers 1...6 correspond to tracks *gt1l...gt3r*),  
 1280 but when it is in the opposite orientation, the laser-beam numbers are reversed relative to the  
 1281 ground-track numbers (beam numbers 1...6 correspond to tracks *gt3r...gt1l*).

1282 This group is sparse, meaning that parameters are provided only for pairs of segments for which  
 1283 at least one beam has a valid surface-height measurement. Data-set attributes give:

- 1284            -the reference ground track number
- 1285            -the correspondence between laser beam numbers and ground tracks
- 1286            -the cycle number
- 1287    The RMS accuracy of the horizontal geolocation for the segment is described by the geolocation
- 1288    error ellipse, which is calculated based on the PE-medians of the ATL03 parameters
- 1289    *sigma\_geo\_xt*, *sigma\_geo\_at* and *sigma\_geo\_r*. The along-track and across-track coordinates of
- 1290    the segments are provided by parameters *x\_atc* and *y\_atc*.

**Table 4-5 *ground\_track* subgroup**

Parameter	Units	Description	Derived
<i>ref_azimuth</i>	degrees	The direction, eastwards from north, of the laser beam vector as seen by an observer at the laser ground spot viewing toward the spacecraft (i.e., the vector from the ground to the spacecraft).	ATL03
<i>ref_coelv</i>	degrees	Coelevation (CE) is direction from vertical of the laser beam as seen by an observer located at the laser ground spot.	ATL03
<i>seg_azimuth</i>	degrees	The azimuth of the pair track, east of local north	3.1.2.2
<i>sigma_geo_at</i>	meters	Geolocation error in the along-track direction	3.10
<i>sigma_geo_xt</i>	meters	Geolocation error in the across-track direction	3.10
<i>sigma_geo_r</i>	Meters	Radial orbit error	3.10
<i>x_atc</i>	meters	The along-track x-coordinate of the segment, measured parallel to the RGT, measured from the ascending node of the equatorial crossing of a given RGT	3.1.2.2
<i>y_atc</i>	meters	Along-track y coordinate of the segment, relative to the RGT, measured along the	3.1.2.2

		perpendicular to the RGT, positive to the right of the RGT.	
--	--	---	--

1291

1292 **4.3.3 bias\_correction subgroup**

1293 The *bias\_correction* subgroup (Table 4-6) contains information about the estimated first-photon  
 1294 bias, and the transmit-pulse-shape bias. The standard correction applied in *h\_li* is  
 1295  $fpb\_med\_corr + tx\_med\_corr$ , and its error is  $fpb\_med\_corr\_sigma$ . The alternate, mean-based  
 1296 correction, is  $fpb\_mean\_corr$ , with error  $fpb\_mean\_corr\_sigma$ . The median-based elevation,  
 1297 without the first-photon-bias correction, may be recovered by subtracting  $fpb\_med\_corr$  and  
 1298 adding  $med\_r\_fit$ . For example, users who prefer to use the mean statistics instead of the median  
 1299 statistics would use  $h\_li - fpb\_med\_corr - tx\_med\_corr + fpb\_mean\_corr + tx\_mean\_corr$  as their  
 1300 height estimate.

1301 The corrected photon count is given as  $fpb\_n\_corr$ ; this gives an estimate of the number of  
 1302 photons in the surface window as estimated during the FPB correction. The transmit-pulse-shape  
 1303 corrections ( $tx\_med\_corr$  and  $tx\_mean\_corr$ ) are also given.

1304

**Table 4-6 *bias\_correction* subgroup**

Parameter	Units	Description	Derived
<i>fpb_mean_corr</i>	meters	First-photon bias correction to the mean segment height	3.4.3.1
<i>fpb_mean_corr_sigma</i>	meters	Estimated error in <i>fpb_mean_corr</i>	3.4.3.1
<i>fpb_med_corr</i>	meters	First-photon-bias correction giving the difference between the mean segment height and the corrected median height	3.4.3.2
<i>fpb_med_corr_sigma</i>	meters	Estimated error in <i>fpb_med_corr</i>	3.4.3.2
<i>fpb_n_corr</i>	counts	Estimated window photon count after first-photon-bias correction	3.4.3.3
<i>med_r_fit</i>	meters	Difference between uncorrected mean and median of linear-fit residuals	3.3.5.2

<i>tx_med_corr</i>	meters	Estimate of the difference between the full-waveform transmit-pulse mean and the median of a broadened, truncated waveform consistent with the received pulse	3.5
<i>tx_mean_corr</i>	meters	Estimate of the difference between the full-waveform transmit-pulse mean and the mean of a broadened, truncated waveform consistent with the received pulse	3.5

1305

1306 **4.3.4 fit\_statistics subgroup**

1307 The *fit\_statistics* subgroup gives a variety of parameters describing the segment fit and its  
 1308 residuals. These parameters may be used to determine whether a particular segment is  
 1309 potentially usable if it is not identified as problem-free in the  
 1310 *land\_ice\_segments/ATL06\_quality\_summary* flag.

**Table 4-7 fit\_statistics subgroup**

Parameter	units	Description
<i>dh_fit_dx</i>	unitless	Along-track slope from along-track segment fit
<i>dh_fit_dx_sigma</i>	Unitless	Propagated error in the along-track segment slope
<i>dh_fit_dy</i>	Unitless	Across-track slope from segment fits to weak and strong beams; the same slope is reported for both laser beams in each pair
<i>signal_selection_source</i>	Unitless	Flag describing the source of the information used to select the signal PE. See Table 3-1

<i>signal_selection_source_status</i>	Unitless	Indicates the status of the last signal selection algorithm attempted (see <i>signal_selection_source</i> ). Values for this flag are given in the sections of Table 3-2.
<i>h_mean</i>	meters	Mean surface height, not corrected for first-photon bias or pulse truncation.
<i>sigma_h_mean</i>	meters	Propagated height error due to PE-height sampling error for height from the along-track fit, not including geolocation-induced error
<i>h_expected_rms</i>	meters	Expected RMS misfit between PE heights and along-track segment fit
<i>h_rms_misfit</i>	meters	RMS misfit between PE heights and along-track segment fit
<i>h_robust_sprd</i>	meters	RDE of misfit between PE heights and the along-track segment fit.
<i>n_seg_pulses</i>	counts (pulse ID)	The number of pulses potentially included in the segment (floating-point number)
<i>n_fit_photons</i>	counts	Number of PEs used in determining <i>h_li</i> after editing
<i>w_surface_window_final</i>	meters	Width of the surface window, top to bottom
<i>snr</i>	unitless	Signal-to-noise ratio in the final refined window

<i>snr_significance</i>	unitless	Probability that signal-finding routine would converge to at least the observed SNR for a random-noise input. Small values indicate a small likelihood of a surface-detection blunder.
-------------------------	----------	--

1311

1312 **4.3.5 DEM subgroup**

1313 This subgroup (Table 4-8) contains DEM elevations interpolated at the segment centers. It  
 1314 contains only three parameters: the DEM elevation (*dem\_h*), the geoid height (*geoid\_h*), and the  
 1315 DEM source (*dem\_flag*). The best DEMs available in time for the ICESat-2 launch may be  
 1316 significantly better than those available at present (February 2015), but the best current choices  
 1317 are:

- 1318 • For Antarctica, the REMA DEM : <https://www.pgc.umn.edu/data/rema/>, filtered to 40-m  
 1319 resolution before interpolation to the ICESat-2 segment centers, with gaps filled with  
 1320 ATL06 data from cycles 1 and 2.
- 1321 • For the Arctic, the Arctic DEM, based on stereophotogrammetry  
 1322 <https://www.pgc.umn.edu/data/arcticdem>. The DEM should be filtered to 40-m  
 1323 resolution before interpolation to the ICESat-2 reference points.
- 1324 • For areas outside the poles, a multi-sensor global DEM, posted at 7.5 arcsec  
 1325 ([http://topotools.cr.usgs.gov/gmted\\_viewer](http://topotools.cr.usgs.gov/gmted_viewer)).

1326 This group is sparse, meaning that parameters are provided only for pairs of segments for which  
 1327 at least one beam has a valid surface-height measurement.

Table 4-8 DEM subgroup

Parameter	Description
<i>dem_h</i>	Height of the DEM, interpolated by cubic-spline interpolation in the DEM coordinate system to the PE location
<i>dem_flag</i>	source for the DEM. 1=Antarctic DEM, 2=Arctic DEM, 3=global DEM.
<i>geoid_h</i>	Geoid height, meters

1328

1329 **4.4 residual\_histogram group**

1330 This group contains histograms of the residuals between PE heights and the least-squares fit  
1331 segment heights, at 200-meter along-track resolution. It is intended to allow visualization of the  
1332 surface-return shapes, and investigation of changes in the return pulse shape or of near-surface  
1333 scattering, such as that due to dense blowing snow. Each column of the histogram gives the  
1334 number of PE in a set of bins distributed between -50 and +50 m around the surface. The  
1335 distribution of these bins is as follows:

1336 From 50 to 20 m below the surface, bins are spaced at 1 m

1337 From 20 m to 10 m below the surface, bins are spaced at 0.5 m

1338 From 10 m to 4 m below the surface, bins are spaced at 0.25 m

1339 From 4 m to 2 m below the surface, bins are spaced at 2 cm

1340 From 2 m below the surface to 2 m above the surface, bins are spaced at 1 cm

1341 From 2 m to 4 m above the surface, bins are spaced at 2 cm

1342 From 4 to 10 m above the surface, bins are spaced at 0.25 m

1343 From 10 to 20 m above the surface, bins are spaced at 0.5 m

1344 From 20 m above the surface to 50 m above the surface, bins are spaced at 1 m.

1345 This distribution of bin edges gives 749 ( $N_{bins}$ ) vertical bins, with 750 edges. The heights of  
1346 the bin tops are given in the *bin\_top\_h* parameter, listed in order from bottom to top. For any bin  
1347 in the histogram, the bottom elevation is equal to the top of the previous bin, and the elevation of  
1348 the bottom of the bottom bin is 1 m below its top. The residuals from collections of 10 along-  
1349 track ATL06 segments are combined into each histogram; because adjacent ATL06 segments  
1350 overlap by 50%, only those PE within 10 m of each segment center in the along-track direction  
1351 are included in the histograms. Only those segments with high-quality signals  
1352 (*ATL06\_quality\_summary* = 0) are included in the histogram, and a list of the *segment\_id* values  
1353 of included segments is provided in the group (recall that the *segment\_id* for a segment  
1354 corresponds to the second of the two ATL03 segments included in each ATL06 segment). To  
1355 allow reconstruction of the per-pulse signal levels, the sum of the number of pulses in the valid  
1356 segments is given for each histogram, and the *background\_per\_m* parameter is given to indicate  
1357 the number of background photons expected in each vertical meter of each histogram. The  
1358 expected number of photons in each histogram bin can be found by multiplying the height  
1359 difference between the edges of the bin by *background\_per\_m*. The counts for any histogram  
1360 bins that are not entirely encompassed by at least one of the two possible telemetry band window  
1361 ranges are marked as invalid.

1362

Table 4-9 Parameters in the *residual\_histogram* group

Parameter	Dimensions	Description
<i>count</i>	N_bins x N_hist	Residual count in 1-cm bins, for PE within 10 (horizontal) m of segment centers for each histogram. Bin-top heights may be found in <i>residual_histogram/bin_top_h</i> .
<i>delta_time</i>	1xN_hist	Elapsed GPS seconds since the reference epoch. Use the metadata attribute <i>granule_start_seconds</i> to compute the full gpstime. Calculated from the mean of the <i>delta_time</i> for the segments in each histogram bin.
<i>bin_top_h</i>	N_bins	Height of the top of each histogram bin, listed in increasing order. The bottom of each bin is equal to the top of the next-lowest bin, and the bottom of the lowest bin is 1 m below its top
<i>bckgrd_per_m</i>	1xN_hist	Number of background PE expected for each vertical meter of the histogram based on the observed background rate ( <i>bckgrd</i> )
<i>segment_id_list</i>	10xN_hist	Segments ids included in each column of the histogram
<i>lat_mean</i>	1x N_hist	Mean latitude of the segments included in the histogram
<i>lon_mean</i>	1x N_hist	Mean longitude of the segments included in the histogram
<i>pulse_count</i>	1xN_hist	Number of pulses potentially included in the histogram (pulses are counted if they are in the central 20 m of each segment, even if no PE from the pulse are selected)

<i>x_atc_mean</i>	1x N_hist	Mean along-track coordinate of the segments included in the histogram.
-------------------	-----------	--

1363

1364

1365 **5 ALGORITHM IMPLEMENTATION: LAND ICE HEIGHT (ATL 06/L3A)**

1366 This section gives detailed procedures for estimating heights from ATL03 PEs. The procedures  
1367 are presented as an outline of the steps that need to be programmed to calculate the main  
1368 parameters from each group; we assume that after interaction with the programming team these  
1369 outlines will be updated to ensure their accuracy and consistency with the rest of this document.

1370 **5.1 Outline of Procedure**

1371 The following steps are performed for each along-track reference point:

- 1372 1. PEs from the current cycle falling into the along-track bin for the along-track point are  
1373 collected
- 1374 2. The initial height and along-track slope are estimated for each beam in the pair
- 1375 3. The heights and surface windows are iteratively refined for each beam in the pair
- 1376 4. Corrections for subsurface scattering, first-photon bias, median offsets, and error  
1377 estimates are calculated for each beam based on the edited PEs
- 1378 5. The across-track slope is calculated

1379 Steps 1-5 are described in the “Processing Procedure” subsection.

1380 **5.2 Input Parameters**

1381 Steps 1-6 in 5.1.1 can be calculated based on ATL03 inputs. Steps 5 and 6 require information  
1382 about the background rate, which is provided with the atmospheric data

1383 **Table 5-1** lists parameters needed from ATL03 and ATL09 for generation of ATL06.

1384 Individual PE heights, times, IDs, and geolocations are provided by ATL03. A variety of tidal  
1385 and atmospheric-delay parameters are derived from subsamples of ATL03 fields or by  
1386 interpolation into data tables used during ATL03 processing. Some ATL03 parameters are  
1387 provided for every PE (e.g. height and horizontal position). These are averaged over the selected  
1388 PEs for each segment. Others are provided for ‘reference’ photons spaced approximately every  
1389 40 m along track. For these fields, ATL06 values are interpolated as a function of along-track x  
1390 from the values for the ‘nominal’ photons to the segment centers.

1391 In addition, parameters from the atmospheric channel are used to define the blowing-snow height  
1392 parameter, the blowing-snow confidence parameter, and the cloud-flag confidence parameter.

1393 The 200-Hz background-rate parameter is used to estimate background rates for each segment, as  
1394 is the 50-Hz background-rate parameter based on the full atmospheric window. An estimate of  
1395 the optical depth for the 3 km above the ground and a blowing-snow height estimate and  
1396 confidence flag are also calculated based on ATL09 parameters.

1397 The transmit-pulse shape is used to correct the truncated means and medians used in estimating  
1398 the surface shape to reduce potential biases in the recovered surface height.

Table 5-1. Inputs for ATL06

Parameter	Source	Description
podppd flag	<i>/gtxx/geolocation/podppd_flag</i>	Flag indicating low/high quality geolocation
Segment_ID	ATL03: <i>/gtxx/geolocation</i>	ATL03 segment ID
Ph_index_beg	ATL03: <i>/gtxx/geolocation</i>	First photon in the segment
Segment_ph_cnt	ATL03: <i>/gtxx/geolocation</i>	Number of PE in each segment
Segment_dist_x	ATL03: <i>/gtxx/geolocation</i>	Along-track distance for each ATL03 segment
Segment_length	ATL03: <i>/gtxx/geolocation</i>	Along-track length of each ATL03 segment.
Velocity_sc	ATL03: <i>/gtxx/geolocation</i>	Spacecraft ground speed
Sigma_across	ATL03: <i>/gtxx/geolocation</i>	across-track component of geolocation error
Sigma_along	ATL03: <i>/gtxx/geolocation</i>	Along-track component of geolocation error
Sigma_h	ATL03: <i>/gtxx/geolocation</i>	Vertical component of geolocation error
Delta_time	ATL03: <i>/gtxx/geolocation</i>	Time for each PE

**ICESat-2 Algorithm Theoretical Basis Document (ATBD) for Land Ice Along-Track Height  
(ATL06)**

**Release 003**

H_ph	ATL03: /gtxx/heights	WGS-84 PE height
Lat_ph	ATL03: /gtxx/heights	PE latitude
Lon_ph	ATL03: /gtxx/heights	PE longitude
Signal_conf_ph	ATL03: /gtxx/heights	Signal-classification confidence
Ph_id_channel	ATL03: /gtxx/heights	Channel number for each PE
Ph_id_pulse	ATL03: /gtxx/heights	Pulse number for the current PE
Pce_mframe_cnt	ATL03: /gtxx/heights	Major frame number for the current PE
Dist_ph_along	ATL03: /gtxx/heights	Along-track distance relative to the current segment start
Dist_ph_across	ATL03: /gtxx/heights	Along-track distance relative to the RGT
bckgrd_rate	ATL03: /gtxx/bckgrd_atlas	Background rate calculated from the 50-pulse altimetric histogram
delta_time (corresponding to bckgrd_rate)	ATL03: /gtxx/bckgrd_atlas	Time for the first shot in the 50-pulse altimetric histogram
DEM elevation	Standard DEMs	Best-available DEMs (see 4.3.5) interpolated to each segment location

*ICESat-2 Algorithm Theoretical Basis Document (ATBD) for Land Ice Along-Track Height (ATL06)*

*Release 003*

Tide model values	ATL03: /gtxx/geophys_corr	Various tide-model parameters
Tep_hist	ATL03: Atlas_impulse_response/ beam_x/histogram	Transmitter-echo-pulse histogram for the strong/weak spot (should match current spot)
Tep_hist_x	ATL03: Atlas_impulse_response/ beam_x/histogram	Times for transmitter-echo-pulse histogram bins
Tep_bckgrd	ATL03: Atlas_impulse_response/ beam_x/histogram	Transmitter-echo-pulse per-bin background count
Tep_tod	ATL03: Atlas_impulse_response/ beam_x/histogram	Day/time for the TEP measurement used
Channel dead-time estimates	ATL03	dead-time estimates for each channel, from ATL03 parameters /atlas_impulse_response/dead_time
Blowing-snow flag	ATL09	Blowing-snow flag
Blowing-snow confidence	ATL09	Blowing-snow confidence
Cloud flag	ATL09	Cloud flag and confidence

1399

1400 Note that some parameters that are provided for each segment in ATL03 are needed for each PE  
 1401 in ATL06. For example, the along-track distance for a PE is the sum of *segment\_dist\_x*  
 1402 (provided per segment) and *dist\_ph\_along* (provided for each PE). To allow us to access these  
 1403 fields, we generate an internal *ph\_seg\_num* variable, based on the ATL03  
 1404 *geolocation/ph\_index\_beg* variables, assigning all photons between the *i*-th value of  
 1405 *geolocation/ph\_index\_beg* and 1 less than the *i+1*-th value a *ph\_seg\_num* value of *i*. The

1406 background rate is provided in ATL03 on a 50-shot sampling interval; we convert this to the per-  
1407 PE rate by interpolating as a function of *delta\_time*.

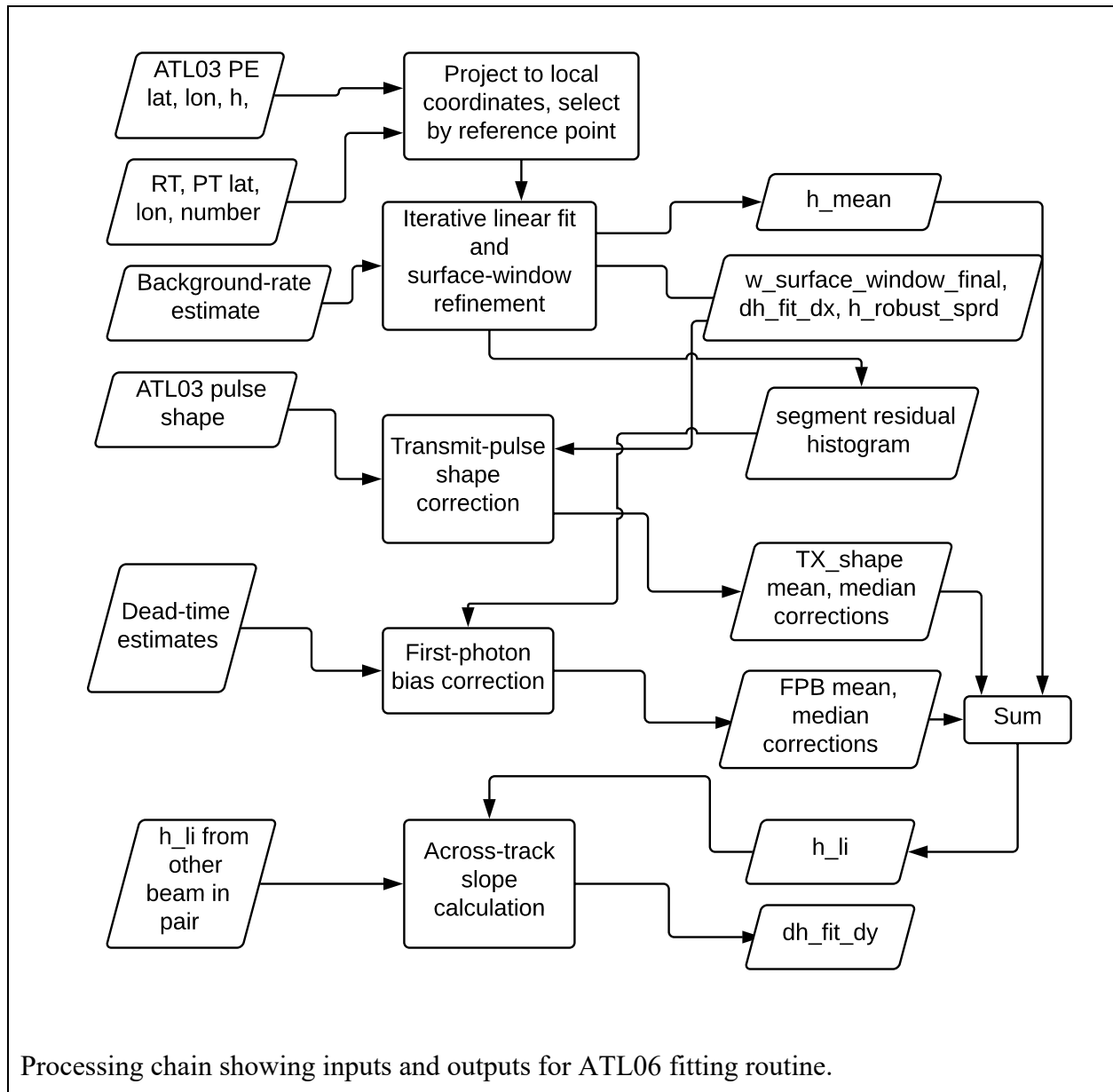
1408

### 1409 **5.3 Processing Procedure for Parameters**

1410 In this section, we give pseudocode for the calculation of ATL06 parameters. The flow chart for  
1411 this process is summarized in Figure 5-1. The code is made up of several functions that call one  
1412 another, following the process described in Section 5.1.

Figure 5-1. Flow chart for top-level ATL06 processing

---



1413

1414 **5.4 Top-Level Fitting Routine**

1415 This routine calls the other routines in the processing chain to derive the final heights and  
 1416 corrections. It corresponds to all the steps described in 3.2.

1417

1418 **Inputs**, for each beam, for ATL03 segments  $m-1$  and  $m$ :

1419  $x_{PE}$ : along-track coordinates of the land-ice PEs, meters

1420  $y_{PE}$ : across-track coordinates of the land-ice PEs, meters

1421  $h_{PE}$ : heights of the PE, meters

1422  $t_{PE}$ : times for PE.

1423  $Ice\_confidence\_flag$ : Confidence with which the PE has been identified as coming from  
1424 the surface, unitless

1425  $bckgrd$ : estimated background PE rate for the current segment, counts/second

1426  $ch\_deadtime$ : Deadtime estimate for each channel

1427  $x0\_seg$ : along-track coordinate of the current reference point

1428  $bckgrd\_rate$ : 50-shot-resolution background rate, derived from ATL03, interpolated to  
1429 the center of the segment.

1430  $Spacecraft\_ground\_speed$ : The speed of the nadir point below the spacecraft as it moves  
1431 along the geoid.

1432  $Podppd\_flag$ : ATL03 flag indicating high or low quality geolocation

1433 **Outputs** (repeated for left and right beams)

1434  $delta\_time$ : time offset with respect to the beginning of the granule

1435  $h_{li}$ : land-ice height, meters

1436  $h_{li\_sigma}$ : error in the ice-sheet height, meters

1437  $h_{robust\_sprd}$ : ice-sheet residual robust spread, meters

1438  $h_{rms\_misfit}$ : RMS residual for the residual spread, meters

1439  $n_{fit\_photons}$ : The number of photons used to define the segment.

1440  $w_{surface\_window}$ : width of the refined window used to select PEs, meters

1441  $h_{expected\_rms}$ : expected standard deviation of PEs based on surface geometry and  
1442 signal levels, meters

1443  $dh_{fit\_dx}$ : along-track slope for the segment, unitless

1444  $signal\_selection$  parameters: parameters indicating how the initial PE were selected

1445  $f_{pb\_corr\_mean}$ : first-photon bias correction for the mean surface height, meters

1446  $f_{pb\_corr\_median}$ : first-photon bias correction for the median surface height, meters

1447  $tx_{median\_corr}$ : return-truncation correction to the median-based segment height

1448  $tx_{mean\_corr}$ : return-truncation correction to the mean-based segment height

1449        *fpb\_n\_corr* : corrected PE count from the first-photon bias, meters  
1450        *y\_seg\_RGT*: segment across-track coordinate  
1451        *lat\_seg\_center*: segment-center latitude  
1452        *lon\_seg\_center*: segment-center longitude  
1453        *tide* and *dac* parameters: geophysical parameters that are averaged and passed on from  
1454        ATL03  
1455        *SNR*: Estimated signal-to-noise ratio for the segment  
1456        *atl06\_quality\_summary*: Summary parameter indicating whether a problem in the  
1457        segment fitting was identified  
1458        **Output** for both beams together:  
1459        *dh\_fit\_dy* : across-track slope, unitless  
1460        **Internal variable**, that is tracked through the fitting procedure:  
1461        *h\_range\_input*: The range of heights provided as an input to the fitting algorithm.  
1462        **Parameters:**  
1463        *granule\_start\_time*: the starting time of the granule  
1464        *dx\_seg* = 40 meters  
1465        *sigma\_beam*: sigma value for pulse surface footprint (expected to be equal to 4.25 m)  
1466        *SNR\_F\_table*: 3-d table giving the probability of finding a segment with the given SNR  
1467        for noise-only inputs  
1468        *PRF*: Pulse repetition frequency for ATLAS (equal to 10,000 s<sup>-1</sup>)  
1469        **Procedure:**  
1470        1. Select PE for the initial fit.  
1471            1a. If the *podppd\_flag* indicates degraded geolocation for any pulses, skip to the next  
1472            segment.  
1473            1b. For each beam, select PE with ATL03 *segment\_id* of *m* or *m-1*. Set *h\_range\_input*  
1474            equal to the difference between the maximum and minimum of the PE heights. Eliminate any  
1475            photons that are identified by ATL03 as part of the TEP.  
1476            1c. Set initial values for the geolocation and time parameters: set *lat\_seg\_center*,  
1477            *lon\_seg\_center* and *delta\_time* to the means of the corresponding reference photon values.  
1478            1d. Calculate *n\_seg\_pulses* based on the spacecraft ground speed, and the lengths of  
1479            segments *m-1* and *m*:  $n\_seg\_pulses = (\text{sum of segment lengths} * PRF) / \text{spacecraft\_ground\_speed}$ .

1480           1e Based on the *ice\_confidence\_flag* values (see **PE selection based on ATL03 flags**),  
1481 and assign values to *signal\_selection\_source*, *signal\_selection\_status\_confident*, and  
1482 *signal\_selection\_status\_all*. If *signal\_selection\_source* is equal to 0 or 1, set *h\_range\_input* equal  
1483 to *H\_win*.

1484           1f. If both *signal\_selection\_status\_confident* and *signal\_selection\_status\_all* are nonzero,  
1485 select PE using the **backup PE selection** routine. If *signal\_selection\_status\_backup* is greater  
1486 than 1, skip fitting for the current beam and reference point, report invalid for *h\_mean*, and for  
1487 *n\_fit\_photons*. If *signal\_selection\_status\_backup* is equal to 0 set *h\_range\_input* equal to  
1488 *H\_win*.

1489           Note: If *h\_range\_input* is not set in 1d or 1e, it remains equal to the value set in 1a: the  
1490 difference between the maximum and minimum heights of all photons found in segments *m* and  
1491 *m-1*.

1492

1493   Output values assigned: *signal\_selection\_source*, *signal\_selection\_status\_confident*,  
1494 *signal\_selection\_status\_all*, *signal\_selection\_status\_backup*.

1495   Internal values assigned: *PE\_selection\_flag*.

1496   2. For each beam, estimate the surface height and slope using the **iterative least-squares fitting**  
1497 routine. Set *n\_fit\_photons* to the number of PE in the final selection. If the final selection  
1498 includes fewer than 10 PE, or if the along-track spread is less than 20 m, or if the final window  
1499 width is larger than 20 m, report an invalid fit and set *h\_mean* to its invalid value (*NaN*) and  
1500 return.

1501   Output values assigned, for each beam: *n\_fit\_photons*, *dh\_fit\_dx*, *h\_mean*, *h\_rms\_misfit*,  
1502 *h\_robust\_sprd*, *med\_r\_fit*, *w\_surface\_window\_final*, *SNR*.

1503   Internal values assigned, for each beam: *h\_mean*, *r\_fit*, *selected\_PE*, *h\_range\_input*

1504

1505   3. For each beam, calculate the first-photon bias correction

1506           For each beam, estimate the first-photon bias correction to the mean height, the first-  
1507 photon-bias corrected median height, and the corrected return-time histogram based on the  
1508 residuals to the segment heights calculated in step 3.

1509           3a. Run the first-photon-bias-correction routine on PE flagged with *selected\_PE* (see  
1510 below)

1511   Internal values assigned: fpb-corrected residual histogram, estimated gain.

1512   Output values assigned for each beam: *fpb\_mean\_corr*, *fpb\_mean\_corr\_sigma*,  
1513 *fpb\_median\_corr*, *fpb\_median\_corr\_sigma*, *FPB\_N\_PE*

1514

1515 4. Calculate the pulse-truncation correction

1516 Based on the  $h\_robust\_sprd$  and  $w\_surface\_window\_final$  values calculated in the last  
1517 step of the iterative least-squares fit and the  $SNR$  calculated in step 2, calculate the pulse-  
1518 truncation correction (See pulse-truncation-correction section).

1519 Output values assigned for each beam:  $tx\_med\_corr$ ,  $tx\_mean\_corr$

1520

1521 5. Calculate remaining output parameters

1522 5a. Calculate  $h\_li$ :

1523 
$$h\_li = h\_mean + fpb\_med\_corr + tx\_med\_corr$$

1524 Output values assigned:  $h\_li$

1525

1526 5b. Calculate  $y\_seg\_RGT$ , equal to the median of all  $y\_PE\_RGT$  values.

1527 Output values assigned:  $y\_seg\_RGT$

1528 5c. Calculate  $seg\_time$ ,  $lat\_seg\_center$  and  $lon\_seg\_center$  by regressing (respectively)  
1529  $time\_PE$ ,  $lat\_PE$  and  $lon\_PE$  as a function of  $x\_PE$  to  $x0\_seg$  for selected PE. For those  
1530 segments for which fitting has failed, but for which the other beam in the pair has a valid  
1531 segment, report the latitude and longitude of the valid segment, displaced by 90 m to the left or  
1532 right in the across-track direction (depending on which segment is valid).

1533 Output values assigned:  $seg\_time$ ,  $lat\_seg\_center$ ,  $lon\_seg\_center$ ,  $delta\_time$

1534 5d. Estimate the final cross-track slope, equal to the difference between the  $h\_li$  values  
1535 divided by the difference between the  $y\_seg\_RGT$  values for the two beams.

1536 Output values assigned:  $dh\_fit\_dy$

1537 5e. Calculate error estimates for each beam.

1538 *i.* For each segment, calculate  $h\_expected\_RMS$  based on the footprint size, the along-  
1539 track track slope, and the transmit pulse duration (equation 1):

1540 
$$h\_expected\_RMS = \sqrt{(dh\_fit\_dx \sigma_{beam})^2 + (c/2 \sigma_{xmit})^2}$$

1541 *ii.* Add the effects of background noise to  $\sigma_{expected}$  to calculate  $\sigma_{PE\_est}$ .

1542 
$$\sigma_{PE\_est} = ((N_{signal} h\_expected\_RMS^2 + N_{noise}(0.287 H_{win})^2) / N_{tot})^{1/2}$$

1543 *iii.* Calculate linear-fit-model errors. Multiply  $h\_mean\_sigma\_unit$  and  
1544  $dh\_fit\_dx\_sigma\_unit$  by  $\max(\sigma_{PE\_est}, h\_rms\_misfit)$  to obtain  $h\_mean\_sigma$  and  
1545  $dh\_fit\_dx\_sigma$ .

1546 Output values assigned:  $\sigma_{h\_mean}$ ,  $\sigma_{dh\_fit\_dx}$ ,  $\sigma_{PE\_est}$ ,  $h\_rms\_misfit$ .

1547           5f. Set  $h\_li\_sigma$  equal to the maximum of  $sigma\_h\_mean$  and  $fpb\_med\_corr\_sigma$ .

1548   Output values assigned for each beam:  $h\_li\_sigma$ .

1549           5g. Calculate the uncorrected reflectance, based on the first-photon-bias-corrected total  
1550 PE count. Equation given in 3.4.3.3.

1551   Output values assigned, for each beam:  $r\_eff$

1552           5h. Calculate  $SNR\_significance$ , by interpolating into the  $SNR\_F\_table$  as a linear  
1553 function of the table parameters  $BGR$ ,  $SNR$ , and  $w\_surface\_window\_initial$ .

1554   Output value assigned:  $SNR\_significance$

1555           5i: calculate  $atl06\_quality\_summary$ :  $atl06\_quality\_summary$  is zero unless  
1556  $h\_robust\_sprd > 1\text{ m}$  or  $h\_li\_sigma > 1\text{ m}$  or  $SNR\_significance > 0.02$  or  
1557  $N\_fit\_photons/w\_surface\_window\_final < 4$  (for strong beams) or  $< 1$  (for weak beams) or  
1558  $signal\_selection\_source > 1$ .

1559           5j: Calculate pass-through parameters: For tide parameters, error parameters, and the  $dac$ ,  
1560 calculate ATL06 values from the average values for the ATL03 segments.

1561           5k: Calculate systematic error estimates: Based on geolocation error estimates and surface  
1562 slope, calculate  $h\_li\_sigma\_systematic$  based on equation 36.

## 1563   **5.5 Signal selection based on ATL03 flags**

1564   **Inputs**, from one beam only, for each PE

1565            $x\_PE$ : along-track coordinates of the land-ice PE for the current segment

1566            $h\_PE$ : height of PE for the current segment

1567            $Ice\_confidence\_flag$ : ATL03 classification of the land-ice PE. 0=undetected, 1=PE in the  
1568 pad region, but not identified as signal PE, 2=low confidence, 3=medium confidence, 4=high  
1569 confidence.

1570   **Input**, one per segment:

1571            $x0$ : the along-track location of the segment center.

1572            $BGR$ : the interpolated background PE rate for the segment.

1573   **Parameters**:

1574            $Sigma\_beam$ : The one-sigma expected horizontal spread of the photons on the ground.  
1575 Equal to 4.25 m (pre-launch estimate)

1576            $Sigma\_xmit$ : The one-sigma temporal duration of the transmit pulse.

1577   **Outputs**:

1578 *PE\_selection*: binary flag, one per input PE, showing whether to use that PE in the initial  
1579 fit.

1580 *Signal\_selection\_source*: parameter indicating the how the signal was selected. See  
1581 Table 3-1 for values.

1582 *signal\_selection\_status\_confident*: parameter indicating the success/failure of signal  
1583 selection using low-or-better confidence PEs.

1584 *signal\_selection\_status\_all*: parameter indicating the success/failure of signal selection  
1585 using all flagged PEs.

1586 *H\_win*: Height of the window around the best-fitting line used to select PE.

1587

1588 **Procedure:**

1589 1. If the inputs are empty (no PE are in the along-track window), set *signal\_selection\_source* to  
1590 3, set *signal\_selection\_status\_confident* to 3, set *signal\_selection\_status\_all* to 3 set  
1591 *signal\_selection\_status\_backup* to 4, and return.

1592 2. Check if the confidently detected PE are adequate to define an initial segment.

1593 2a. Set *PE\_selection* to true for all PE with *Ice\_confidence\_flag*  $\geq 2$ , to zero for all  
1594 others

1595 2b: If the difference in *x\_PE* between the first and last PE in *PE\_selection* is less than 20  
1596 m set *signal\_selection\_status\_confident* to 1.

1597 2c: If there are fewer than 10 true elements in *PE\_selection*, but the spread between the  
1598 first and last PE in *PE\_selection* is greater than 20 m, set *signal\_selection\_status\_confident* to 2.

1599 2d. If there are fewer than 10 true elements in *PE\_selection*, and the spread between the  
1600 first and last PE is less than 20 m, set *signal\_selection\_status\_confident* to 3.

1601

1602 3. Check if the combination of confidently detected PE and the padded PE are adequate to define  
1603 an initial segment. If *signal\_selection\_status\_confident* is zero, skip this step.

1604 3a. Set *PE\_selection* to true for all PE with non-zero *ice\_confidence\_flag*.

1605 3b: If the difference in *x\_PE* between the first and last PE in *PE\_selection* is less than 20  
1606 m set *signal\_selection\_status\_all* to 1.

1607 3c: If there are fewer than 10 true elements in *PE\_selection*, but the spread between the  
1608 first and last PE in *PE\_selection* is greater than 20 m, set *signal\_selection\_status\_all* to 2.

1609 3d. If there are fewer than 10 true elements in *PE\_selection*, and the spread between the  
1610 first and last PE is less than 20 m, set *signal\_selection\_status\_all* to 3.

1611           3e: If *signal\_selection\_status\_all* is equal to zero, set *signal\_selection\_source* to 1 and  
1612 proceed to step 4, otherwise set *signal\_selection\_source* to 2, and return.

1613 4. Calculate the vertical spread of the selected PE, make the selection consistent with a vertical  
1614 window around a sloping segment.

1615           4a. Calculate the least-squares fit line between (*x*<sub>PE</sub>-*x*<sub>0</sub>) and *h*<sub>PE</sub> for the selected PE.  
1616 Internal variables set: *along\_track\_slope*, *seg\_center\_height*.

1617           4b. Calculate *r*<sub>PE</sub>, the residual between the best-fitting line and *h*<sub>PE</sub>.

1618           4c. Calculate *sigma\_r*, the robust spread (accounting for noise) of *r*<sub>PE</sub>, based on the  
1619 background density, *BG\_density*, with *z\_min* and *z\_max* set to the minimum and maximum  
1620 values of *r*<sub>PE</sub>. See the **robust dispersion** section for description.

1621           4d. Calculate the expected PE spread, *sigma\_expected*, based on the current slope  
1622 estimate:

1623           
$$sigma\_expected = [(c/2 \sigma_{xmit})^2 + \sigma_{beam}^2 \text{along\_track\_slope}^2]^{1/2}$$

1624           4e. Calculate *H\_win*:

1625           
$$H\_win = \max(H\_win\_min, 6 \sigma\_expected, 6 \sigma\_r)$$

1626           4f. Select all PE that have  $abs(r_{PE}) < H\_win/2$ . Report the number of selected PE as  
1627 *N\_initial*.

## 1628 **5.6 Backup PE-selection routine.**

### 1629 **Inputs:**

1630           *x*<sub>PE</sub> : along-track coordinates of all PE for the current beam

1631           *h*<sub>PE</sub>: heights of all PE for the current beam

1632           *x0*: along-track bin center for the current bin.

1633           *Ice\_confidence\_flag*: ATL03 classification of the land-ice PE. 0=undetected, 1=PE in the  
1634 pad region, but not identified as signal PE, 2=low confidence, 3=medium confidence, 4=high  
1635 confidence

1636           *signal\_selection\_source*: Flag indicating the how the signal was selected. See Table 3-1  
1637 for values.

### 1638 **Outputs:**

1639           *PE\_selection*: selected PE for the current bin.

1640           *signal\_selection\_source*: Flag indicating the how the signal was selected. See Table 3-1  
1641 for values, updated based on the results of this algorithm

1642 *signal\_selection\_status\_backup* flag indicating the success/failure of signal selection  
1643 using backup selection algorithm

1644 *H\_win*: Vertical extent of the selected window

1645 **Internal variables:**

1646 *Test\_window\_center*: Vector of test window centers

1647 *Window\_center\_height*: Estimated window center height

1648 **Procedure:**

1649 1. Attempt to center the window on any ATL03 flagged PE that are present.

1650 1a. If any padded or detected PE are found, set  $w_0$  to the maximum of 10 m and the  
1651 difference between the maximum and minimum selected PE heights, and set *PE\_selection* to true  
1652 for all PE that have heights within 5 m of the median of the selected PE heights. Set *H\_win*  
1653 equal to 10 m.

1654 1b. If the horizontal spread in the PE marked in *PE\_selection* is greater than 20 m, and if  
1655 10 or more PE are selected, then set *signal\_selection\_status\_backup* to zero, set  
1656 *signal\_selection\_source* to 2, and return.

1657 2. Find the 80-m along-track by 10-m vertical bin that contains the largest number of PEs

1658 2a. Select all PE from ATL03 segments  $m-2$  to  $m+1$ , inclusive.

1659 2b. Loop over *test\_window\_center* values between  $\text{floor}(\min(h_{PE})) + 0.25$  and  
1660  $\text{ceil}(\max(h_{PE}))$  in 0.5 m steps. For each *test\_window\_center* value, count the PE in a 10-m  
1661 (vertical) bin centered on the *test\_window\_center* value.

1662 2c. Find the maximum of the window counts,  $C_{max}$ , and calculate its uncertainty,  
1663  $C_{sigma} = \text{sqrt}(C_{max})$ . If  $C_{max}$  is less than 16, then set *PE\_selection* to null (no selected PE) and  
1664 skip to step 3.

1665 2d. Set *window\_center\_height* equal to the center of the range of *test\_window\_center*  
1666 values that have a count greater than  $C_{max} - C_{sigma}$ . Set *H\_win* to the difference between the  
1667 minimum and maximum of *test\_window\_center* values that have a count greater than  $C_{max} -$   
1668  $C_{sigma}$ , plus 10 m.

1669 2e. Set *PE\_selection* to 1 for all PE in ATL03 segments  $m-1$  and  $m$ , with a height within  
1670  $H_{win}/2$  of *window\_center\_height*.

1671 3. Evaluate the selection.

1672 3a. Set *signal\_selection\_status\_backup* to 1.

1673 3b: If the difference in  $x_{PE}$  between the first and last PE in *PE\_selection* is less than 20  
1674 m set *signal\_selection\_status\_backup* to 2.

1675           3c: If there are fewer than 10 true elements in *PE\_selection*, but the spread between the  
1676 first and last PE in *PE\_selection* is greater than 20 m, set *signal\_selection\_status\_backup* to 3.

1677           3d. If there are fewer than 10 true elements in *PE\_selection*, and the spread between the  
1678 first and last PE is less than 20 m, set *signal\_selection\_status\_backup* to 4.

1679           3e. If *signal\_selection\_status\_backup* is 1, set *signal\_selection\_source* to 2, if greater  
1680 than 1, set *signal\_selection\_source* to 3.

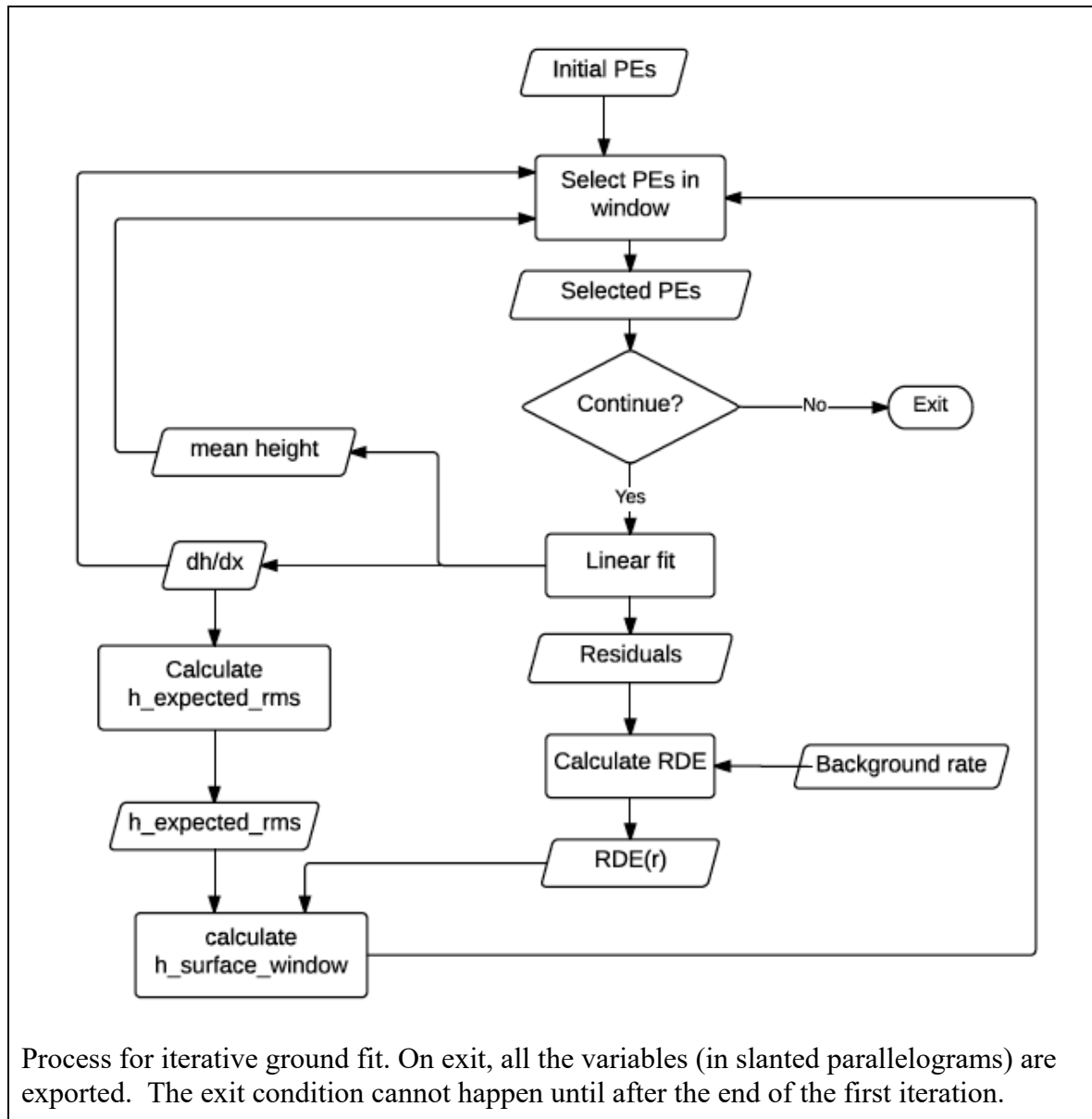
1681

## 1682 **5.7 Iterative Least-Squares Fitting Routine**

1683 This routine performs the iterative least-squares fit to refine the surface window and determine  
1684 the along-track slope. The process for this step is shown in Figure 5-2.

Figure 5-2. Flow chart for iterative ground fit

---



1685

1686 **Inputs:**

1687  $x_{PE}$  : along-track coordinates of PE for the current beam

1688  $y_{PE}$  : across-track coordinates of PE for the current beam

1689  $input_{PE\_selection}$ : Flag defining the PE selected by the initial selection routine

1690  $h_{PE}$ : heights of selected PE for the current beam

1691  $x0$ : along-track bin center for the current bin.  
1692  $bckgrd$ : Interpolated background-PE rate estimate for the segment  
1693  $H\_win$ : Initial surface-window height.  
1694  $signal\_selection\_source$ : Flag indicating the source of the initial signal selection  
1695  $N\_it$ : maximum number of iterations

1696 **Parameters:**

1697  $Sigma\_xmit$ : transmitted pulse duration (seconds)  
1698  $Sigma\_beam$ : sigma value for pulse surface footprint (expected to be equal to 4.25 m)  
1699  $L0$ : Along-track length of the window  
1700  $N\_seg\_pulses$ : Number of pulses in a 40-meter segment (equal to 58 assuming 7 km/s  
1701 ground-track speed)  
1702  $H\_win\_min$ : Minimum allowed surface window height, equal to 3m.

1703 **Outputs:**

1704  $H\_win$ : the height of the window around the best-fitting segment within which PE are  
1705 selected.  
1706  $dh\_fit\_dx$ : The along-track slope of the best-fitting segment  
1707  $h\_mean$ : The mean-based height of the best-fitting segment  
1708  $PE\_fit\_flag$ : A flag indicating whether a particular PE has been selected based on the  
1709 segment height and slope and  $H\_win$ .  
1710  $r0$ : Residuals to the best-fitting segment  
1711  $h\_mean\_sigma\_unit$ : Estimated error in  $h\_mean$  per unit of PE-height error  
1712  $dh\_fit\_dx\_sigma\_unit$ : Estimated error in  $dh\_fit\_dx$  per unit of PE-height error.  
1713  $N\_signal$  : Estimated number of signal PE  
1714  $N\_BG$  : Estimated number of background PE  
1715  $h\_robust\_sprd$  : robust spread of residuals  
1716  $h\_rms\_misfit$ : RMS misfit of residuals  
1717  $SNR$ : signal-to-noise ratio for window.

1718 **Procedure:**

1719 1. Initialize the fit.  
1720 1a. If  $signal\_selection\_source$  is zero or 1, eliminate all PE not marked as 1 in  
1721  $input\_PE\_selection$ , set  $PE\_fit\_flag$  to 1 for all remaining PE.

1722           1b. If *signal\_selection\_source* is nonzero, Set *PE\_fit\_flag* to 1 for all PE marked in  
1723 *input\_PE\_selection*, zero for all others.

1724           1c. Calculate the vertical noise-photon density:  
1725                    $BG\_density = N\_seg\_pulses\ median(bckgrd) / (c/2)$

1726           2. Iterate the fit.

1727           2a. Check whether enough PE are selected to define a window. If fewer than 10 PE are  
1728 selected in *PE\_fit\_flag*, set *H\_win*, *dh\_fit\_dx*, *H\_mean*, and *r0* to invalid, and return.

1729           2b. Calculate the least-squares linear fit between *h\_PE* and *x\_PE-x0* for the PE selected  
1730 in *PE\_fit\_flag*. The intercept of the fit is *h\_mean*, the slope is *dh\_fit\_dx*. Calculate the residual to  
1731 this fit for the selected PE, *r0* and for all PE, *r*. If the along-track spread between the first and  
1732 last selected PE is less than 10 m, fit for the height only, and set the along-track slope estimate to  
1733 zero.

1734           2c. Calculate *sigma\_r*, the robust spread (accounting for noise) of *r0*, based on the  
1735 background density, *BG\_density*, and current window height, *H\_win*. The variables input to the  
1736 **robust dispersion including a background estimate** routine are  $z=r0$ ,  $zmin=-H\_win/2$ ,  
1737  $zmax=H\_win/2$ ,  $N\_BG=H\_win\ BG\_density$ . If the resulting *sigma\_r* is greater than 5 m, set it to  
1738 5 m.

1739           2d. Calculate the expected PE spread, *sigma\_expected*, based on the current slope  
1740 estimate:  
1741                    $sigma\_expected = [(c/2\ sigma\_xmit)^2 + sigma\_beam^2\ along\_track\_slope^2]^{1/2}$

1742           2e. Save the value of *H\_win* in *H\_win\_previous*, then calculate the window height from  
1743 *sigma\_expected* and *sigma\_r*.  
1744                    $H\_win = max(H\_win\_min, 6\ sigma\_expected, 6\ sigma\_r, 0.75\ H\_win\_previous)$

1745           2f. Save the values of *PE\_fit\_flag* in *PE\_fit\_flag\_last*.

1746           2g. Select PE within *H\_win/2* of the segment fit.  
1747                    $PE\_fit\_flag = 1$  for PE with  $r < H\_win/2$ , 0 for PE with  $r > H\_win/2$

1748           2h. Evaluate the newly selected PE. If there are fewer than 10 selected PE, or if the  
1749 along-track spread between the first and last PE is less than 20 m, set *PE\_fit\_flag* to  
1750 *PE\_fit\_flag\_last*, *H\_win* to *H\_win\_previous*, and continue to step 3.

1751           2i. If fewer than *N\_iterations* have been completed, and if the values for *PE\_fit\_flag* have  
1752 changed since the previous iteration, return to step 2a. Otherwise continue to step 3.

1753           3. Propagate the error in the fit parameters assuming unit data errors (see 3.6, with  $\sigma_{photon}=1$ ).  
1754 This gives the unit errors *h\_mean\_sigma\_unit*, *dh\_fit\_dx\_sigma\_unit*.

1755           4. Calculate the number of signal and background PE, and the SNR.

1756  $N_{BG} = bckgrd\ H\_win\ 2/c\ N\_seg\_pulses$   
1757  $N\_signal = \max(0, \text{number of selected PE} - N_{BG})$   
1758  $SNR = N\_signal / N_{BG}$

1759 5. Calculate output error statistics:

1760  $h\_rms\_misfit = \text{RMS misfit of selected PE}$   
1761  $h\_robust\_sprd = \sigma_r$  from the last iteration

1762 **5.8 Robust dispersion calculation from a collection of points, not including a background**  
1763 **estimate**

1764 **Input:**

1765  $z$ : sampled values

1766 **Output:**

1767  $RDE$  : the robust dispersion estimate for  $z$ .

1768

1769 **Procedure:**

1770 1. Sort  $z$ .  $zs$  is equal to  $z$ , sorted in ascending order. Let  $Nz$  equal to the number of elements in  $z$ .

1771 2. Calculate an abscissa for  $zs$ ,

1772     2a. Generate  $ind$ , equal to the sequence of integers between 1 and  $Nz$ .

1773     2b. Calculate  $ind\_N$ , equal to  $(ind - 0.5) / Nz$ .

1774 3. Interpolate the percentiles of  $z$ . Interpolate the values of  $zs$  as a function of  $ind\_N$  at values  
1775 0.16 and 0.84. Half the difference between these values is  $RDE$ .

1776

1777 **5.9 Robust dispersion calculation from a collection of points, including a background**  
1778 **estimate**

1779 **Inputs:**

1780  $z$ : sampled values

1781  $zmin, zmax$ : window from which the values in  $z$  are sampled

1782  $N_{BG}$ : Estimate of the number of background events between  $z\_min$  and  $z\_max$ .

1783 **Output:**

1784  $RDE$  : the robust dispersion estimate for  $z$ .

1785 **Parameter:**

1786 *Scale\_factor*: equal to  $\sqrt{2}(\text{erfinv}(0.5)-\text{erfinv}(-0.5))$ , where *erfinv()* is the inverse error  
1787 function, or 1.3490.

1788 **Procedure:**

1789 1. Estimate the background rate and signal count.

1790 1a. *bckgrd* is equal to  $N_{BG}$  divided by the difference between *zmax* and *zmin*.

1791 1b.  $N_{sig}$  is equal to the number of elements in *z*, minus  $N_{BG}$ .

1792 1c. If  $N_{sig} \leq 1$ , the RDE is equal to  $(z_{max}-z_{min})/(\text{the number of elements in } z)$ , and the  
1793 rest of the calculation is skipped.

1794 2. Sort *z*. *zs* is equal to *z*, sorted in ascending order. Let  $N_z$  equal to the number of elements in *z*.

1795 3. Calculate an abscissa for *zs*. Generate *ind*, equal to the sequence of integers between 1 and  $N_z$ ,  
1796 minus 0.5.

1797 4. Find the indices for the smallest potential percentiles of *z*.

1798 4a. *i0* is equal to the index of the greatest value of *ind* for which  $ind < (0.25N_{sig} + (z_{s-}$   
1799  $z_{min})bckgrd)$ .

1800 4b. *i1* is equal to the index of the smallest value of *ind* for which  $ind > (0.75N_{sig} + (z_{s-}$   
1801  $z_{min})bckgrd)$ .

1802 5. If  $i1 < i0$ , reselect *i0* and *i1* to measure spread of the central  $N_{sig}/2$  values of the distribution:

1803 5a: *i0* is equal to the index of the greatest value of *ind* for which  $ind < N_z/2 - N_{sig}/4$ .

1804 5b: *i1* is equal to the index of the smallest value of *ind* for which  $ind > N_z/2 + N_{sig}/4$ .

1805 6. Calculate *RDE*. *RDE* is equal to the difference between the *zs* values at *i0* and *i1*, divided by  
1806 *scale\_factor*.

1807 **5.10 First- Photon Bias Correction**

1808 These routines calculate the first-photon bias for a collection of residual photon heights. Most of  
1809 the calculation is done as a function of time, and the results are converted back to height at the  
1810 end of the routine.

1811

1812 **Inputs:**

1813 *r\_p*: PE heights, corrected for the along-track segment fit, converted to time (multiplied by  $-2/c$ )

1814 *N\_seg\_pulses*: the number of pulses in the segment

1815 *N\_px*: the number of pixels in the detector.

1816

1817 **Outputs:**

1818 *G\_est*: the estimated detector gain

1819 *N\_hist*: The uncorrected PE count histogram (in units of PE)

1820 *N\_PECorr*: the estimated PE count histogram (in units of PE)

1821 *t\_full*: the time vector for the PE count histogram.

1822 *FPB\_med\_corr*: the FPB correction to the median height

1823 *Sigma\_FPB\_med\_corr*: the error estimate for *FPB\_med\_corr*

1824 *FPB\_mean\_corr*: The FPB correction to the mean height

1825 *FPB\_mean\_corr\_sigma*: the error estimate for *FPB\_mean\_corr*.

1826 *Fpb\_N\_photons*: the FPB-corrected estimate of the number of PE in the return.

1827

1828 **Parameters:**

1829 *t\_dead* : the mean detector dead time for the beam.

1830 *N\_seg\_pulses*: the number of pulses in the segment

1831 *N\_px*: the number of pixels in the detector.

1832 *dt*: duration of a histogram bin.

1833

1834 **Procedure:**

1835

1836 *1. Generate a residual histogram*

1837 Convert PE height residuals to time residuals (multiply by  $-2/c$ ). Generate a histogram of time  
1838 residuals, *N\_hist*, in bins of size *dt*.

1839 *2. Calculate the gain from the histogram*

1840 *P\_dead* for bin *i* is the sum over bins *i-N\_dead* to *i-1* of *N\_hist*, divided by *N\_seg\_pulses N\_px*.

1841 *G\_est* is equal to  $1 - P_{dead}$ , where *N\_dead* is the deadtime expressed in histogram bins.

1842 *3. Check if the correction is valid. If the minimum value for G\_est is less than  $2/(N_{seg\_pulses}$   
1843  $N_{px})$ , set all return values equal to invalid (NaN) and return.*

1844 *4. Calculated the corrected histogram:*

1845 *N\_PECorr* is equal to *N\_hist* divided by *G\_est*.

1846 *5. Calculate height statistics*

1847 Calculate the gain-corrected mean and median and their errors for the segment, based on the full  
1848 gain estimate and the full histogram:

1849 *FPB\_med\_corr*:  $-1/2c$  times the gain-corrected median time based on  $N_{PE}$  and  $G_{est}$ . See  
1850 5.11.

1851 *Sigma\_FPB\_med\_corr*: the error estimate for *FPB\_med\_corr*

1852 *FPB\_mean\_corr*:  $-1/2c$  times the gain-corrected mean time based on  $N_{PE}$  and  $G_{est}$ . See 5.12.

1853 *FPB\_mean\_corr\_sigma*: the error estimate for *FPB\_mean\_corr*.

1854 *Fpb\_N\_photons*: the sum of  $N_{PEcorr}$ .

1855

1856

### 1857 **5.11 Gain-corrected median**

1858 Inputs:

1859  $N$ : The uncorrected histogram

1860  $G$ : The gain estimate,

1861  $x$ : the abscissa for the bin centers, corresponding to  $N$  and  $G$ .

1862

1863 Outputs:

1864  $x_{med}$ : the median of  $N$  based on  $G$

1865  $\sigma_{x_{med}}$ : the error in  $x_{med}$

1866

1867 **Procedure:**

1868 *1. Calculate the corrected histogram:*

1869  $N_{corr}$  is equal to  $N$  divided by  $G$ .

1870

1871 *2. Calculate the CDF of  $N_{corr}$*

1872 The CDF,  $C$ , is calculated at the bin centers, and at each bin center,  $j$ , is equal to the sum of all  
1873 values of  $N_{corr}$  for bin centers  $i < j$ .  $C$  is normalized so that its last value is equal to 1.

1874

1875 *3. Calculate the 40<sup>th</sup>, 50<sup>th</sup>, and 60<sup>th</sup> percentiles of  $N_{corr}$*

1876  $C$  is treated as a function that increases linearly across each bin, such that the upper edge of the  
1877  $i$ th bin is greater than the lower edge of the  $i$ th bin by  $N_i$ . The abscissa for  $C$  runs from zero at  
1878  $x_l-dx/2$ , to  $x_m+dx/2$ , where  $x_l$  is the first bin center,  $x_m$  is the last bin center, and  $dx$  is the spacing  
1879 between bin centers. The 40<sup>th</sup>, 50<sup>th</sup>, and 60<sup>th</sup> percentiles of  $N_{corr}$  are calculated by interpolating  
1880 into the vector of bin edges as a function of  $C$ . If more than one bin has a CDF within numerical  
1881 precision of the calculated percentile, report the mean  $x$  value of all such bins.

1882

#### 1883 4. Calculate the error in the CDF at the 50<sup>th</sup> percentile

1884 The error in any value of  $N_{corr}$  ( $\sigma_{N_{corr}}$ ) is the inverse gain value for that bin times the  
1885 square root of  $N$  for that bin.  $\sigma_{CDF}$  for any  $x$  is found by calculating the RSS of all  
1886  $\sigma_{N_{corr}}$  values for bins less than  $x$ , and dividing by the sum of  $N_{corr}$ .

1887 The value for  $\sigma_{CDF}$  at the 50<sup>th</sup> percentile is found by interpolating  $\sigma_{CDF}$  as a  
1888 function of  $C$  at a  $C$  value of 0.5.

1889

#### 1890 5. calculate $\sigma_{x_{med}}$

1891  $\sigma_{x_{med}}$  is found:

$$\sigma_{x_{med}} = \frac{dz_{60} - dz_{40}}{0.2} \sigma_{cdf}(dz_{med})$$

1892

1893 Here  $dz_{60}$  and  $dz_{40}$  are the 40<sup>th</sup> and 60<sup>th</sup> percentiles of  $N_{corr}$  from step 3.

1894

### 1895 5.12 Gain-corrected mean

1896 Inputs

1897  $N$ : The uncorrected histogram

1898  $G$ : The gain estimate

1899  $x$ : the abscissa for the bin centers, corresponding to  $N$  and  $G$ .

1900

1901 **Outputs:**

1902  $x_{mean}$ : the mean of  $N$  based on  $G$

1903  $\sigma_{x_{mean}}$ : the error in  $x_{mean}$

1904

1905 1. Calculate the corrected histogram:

1906  $N_{corr}$  is equal to  $N$  divided by  $G$ .

1907

1908 2. Calculate the corrected mean:

1909 Calculate the mean:

$$x_{mean} = \sum \frac{N_{corr,i}}{N_{tot}} x_i$$

1910

1911 3. Calculate the error in the corrected histogram:

$$\sigma_{N,corr,i} = \frac{N_{0,i}^{1/2}}{G_i}$$

1912

1913 4. Calculate the error in the corrected mean:

$$sigma\_x\_mean = \left[ \sum \left( \sigma_{N,corr,i} \frac{x_i - x_{mean}}{N_{corr,tot}} \right)^2 \right]^{1/2} \quad 49$$

1914

### 1915 **5.13 Transmit-pulse-shape correction**

1916 This routine uses the most recent estimate of the transmit-pulse shape calculated from the  
1917 transmitter-echo pulse to calculate median and mean offsets for a windowed, truncated received  
1918 pulse. This correction depends the shape of the transmit pulse, and on three parameters that are  
1919 unique to each segment: the estimated width of the return pulse, the refined surface-window  
1920 height, and the signal-to-noise ratio.

1921

#### 1922 **Inputs:**

1923 -Transmit-pulse-shape estimate ( $t_{tx}$ ,  $P_{tx}$ ). The time vector,  $t_{tx}$  is shifted so that  $P_{tx}$  has a  
1924 zero centroid (see 5.15).

1925 -Received-pulse width estimate ( $W_{rx}$ )

1926 -Surface-window time duration ( $dt_W$ )

1927 -Signal-to-noise ratio estimate within the truncated window (*SNR*)

1928 **Outputs:**

1929 Height offsets for the mean and median transmit-pulse-shape correction.

1930

1931 **Procedure:**

1932 This correction works by generating a synthetic return pulse that matches the width of the actual  
1933 return pulse, and truncating it in the same way that the return pulse has been truncated. The  
1934 median and the mean of the synthetic pulse are then calculated.

1935

1936 *1. Calculate the time by which the received pulse was broadened*

1937 The spreading needed to broaden the transmitted pulse to match the received pulse is equal to  
1938  $W\_spread = \sqrt{\max(0.01e-9^2, W\_RX^2 - W\_TX^2)}$ .

1939

1940 *2. Generate a synthetic received pulse*

1941 *2a: Calculate the shape of the expected spread pulse:*

1942 The synthetic received pulse is generated by convolving the transmitted pulse with a Gaussian  
1943 function of with a sigma parameter equal to  $W\_spread$ . The Gaussian should have enough  
1944 samples to include at least  $4 * W\_spread$  worth of samples on either side of its center. The  
1945 synthetic pulse and its time vector are  $N\_hist\_synthetic$  and  $t\_synthetic$ .

1946

1947 *2b: Calculate the median of the broadened synthetic pulse:*

1948 Calculate the median of the synthetic received pulse,  $t\_synthetic\_med$ , and set  
1949  $t\_ctr = t\_synthetic\_med$ .

1950

1951 *2c: Normalize the waveform and add an estimated noise signal:*

1952  $N\_hist\_synthetic$  is normalized so that its sum is equal to 1, and a background count of  $1/SNR$   
1953  $(dt/dt\_W)$  is added to  $N\_hist\_synthetic$ .

1954

1955 *3. Calculate the centroid of the synthetic received pulse*

1956 To find the centroid of the truncated synthetic waveform, an iterative procedure is used:

1957 *3a: Calculate the centroid of the synthetic waveform*

1958  $t\_ctr$  is set to the centroid of the truncated synthetic received waveform, windowed by  $t\_ctr -$   
1959  $dt\_W/2$  and  $t\_ctr + dt\_W/2$   
1960 *3b: Check for convergence and iterate*  
1961 Unless the current and previous values of  $t\_ctr$  are consistent to within 0.1 mm (0.00067 ns) or if  
1962 50 iterations are complete, return to *4a*.

1963

1964 *4. Calculate the median of the synthetic received pulse*

1965 The median of the synthetic received waveform is calculated the synthetic received waveform  
1966 from 4b, windowed by  $t\_ctr - dt\_W/2$  and  $t\_ctr + dt\_W/2$

1967

1968 5. The corrections for the median and mean heights are equal to  $c/2$  times the median and mean  
1969 time offsets.

## 1970 **5.14 Residual\_histogram calculation**

### 1971 **Inputs:**

1972 *Segment\_lat* : latitude for each segment center

1973 *Segment\_lon* : longitude for each segment center

1974 *Segment\_x\_ATC*: along-track (x) coordinate for each segment center

1975 *Segment\_h\_mean*: mean-based land-ice height for each segment center

1976 *Segment\_slope*: along-track slope for each segment center

1977 *Segment\_SNR*: SNR values for segment fits

1978 *Segment\_BGR*: Background rate estimate for each segment

1979 *N\_seg\_pulses* Number of pulses in each segment (including those contributing no PE to the fit).

1980 *x\_pe*: along-track(x) coordinates for all ATL03 PE in the segment

1981 *h\_pe*: ATL03 surface height for all PE in the segment.

### 1982 **Parameters:**

1983 *N\_hist*: Number of groups of segments in the histogram (number of horizontal divisions)

1984 *N\_bins*: Number of vertical bins in the residual histogram

1985 *bin\_top\_h*: Tops of the histogram bins, listed from bottom to top

### 1986 **Outputs:**

1987 *Count*:  $N\_bins \times N\_hist$ -element array giving the number of residual photons in each bin  
1988 ( $N\_bins$  is the vertical dimension,  $N\_hist$  is the horizontal dimension)

1989 *bckgrd\_per\_m*:  $1 \times N\_hist$ -vector giving the expected background count per vertical  
1990 meter in each column of the histogram based on the observed background rate (*bckgrd*) and the  
1991 number of segments included in the histogram

1992 *Segment\_id\_list*:  $10 \times N\_hist$ -element array list of segment IDs included in the histogram

1993 *Lat\_mean*:  $N\_hist$ -element list giving the mean latitude of all segments included in each  
1994 horizontal histogram bin

1995 *Lon\_mean*:  $N\_hist$ -element list giving the mean longitude of all segments included in  
1996 each horizontal histogram bin

1997 *x\_ATC\_mean*:  $N\_hist$ -element list giving the mean along-track (x) coordinate of all  
1998 segments included in each horizontal histogram bin

1999 **Procedure**

2000 1. Calculate the bin-edge heights. There are  $N\_bins+1$  edges. The second through last edges are  
2001 equal to the input *bin\_top\_h* values. The first (lowest) edge is 1 m lower than the second (i.e.  
2002 equal to the first value of *bin\_top\_h - 1*).

2003 2. Group segment centers into 10-segment groups: For each RGT, segments 1-10 would be in the  
2004 first group, 11-20 in the second, etc.

2005 3. For each group, gather all valid segments that have high-quality surface-height estimates  
2006 (*ATL06\_quality\_summary=0*). If any high-quality segments are present, calculate the histogram  
2007 count. Otherwise, report the histogram count as all zeros, and report *lat\_mean*,  
2008 *lon\_mean*, *x\_atc\_mean*, and *segment\_id\_list* as invalid.

2009 3a. For each valid segment, calculate the histogram and background count.

2010 3a.1: Gather the PE that have  $x\_segment - 10 \text{ m} < x\_pe \leq 10 \text{ m}$ .

2011 3a.2: Calculate the residual between the segment and the gathered PE:  $r = h$ -  
2012  $h\_mean\_segment - (x\_pe - segment\_x\_ATC) \times segment\_slope$ .

2013 3a.3: For each vertical bin in the histogram, count the PE with residuals that fall  
2014 into the bin

2015 3a.4: For each valid segment, add the expected background count per vertical  
2016 meter, as estimated from the segment background count to the total background-per-meter  
2017 (*bckgrd\_per\_m*) for the segment. The contribution for each segment is:  $segment\_BGR \times$   
2018  $N\_seg\_pulses / 2 / (c/2)$ . [N.B. The factors of 2 in the previous statement cancel, leaving :  
2019  $segment\_BGR \times N\_seg\_pulses / c$ .]

2020 3b. Add the segment histograms together to calculate the 10-segment histogram

2021           3c. Calculate the mean values for latitude, longitude, and  $x_{ATC}$  for the segment. List  
2022 the selected segments in  $segment\_id\_list$

2023

## 2024 **5.15 Transmit-echo-pulse initialization**

2025 This calculation centers the transmit-echo-pulse reported by ATL03 on its centroid, after using  
2026 an iterative edit to distinguish between signal and noise. It should be performed each time a new  
2027 night-time TEP estimate of the waveform becomes available. The TEP consists of the power  
2028 ( $tep\_hist$ ) and time ( $tep\_hist\_x$ ) that are input from ATL03. Two TEP histograms are available,  
2029 obtained for laser spot 1 and 3. The ATL03  $tep\_valid\_spot$  parameter specifies with which TEP  
2030 histogram is used for each of the ground tracks, and the ATL03  $tep\_range\_prim$  parameter  
2031 specifies the valid range of times for each TEP histogram.

### 2032 **Inputs:**

2033  $-tep\_hist\_x$ : Time for the Transmit-pulse-shape estimate

2034  $-tep\_hist$ : power (or signal count) for the transmit-pulse-shape estimate

2035 The time-sampling interval these is  $dt\_input$ . The transmit pulse is sampled so that at least the  
2036 first 5 ns and the last 10 ns are representative of the background noise for the transmit pulse.

### 2037 **Outputs:**

2038  $-t\_tx$ : time vector for the transmit pulse estimate, shifted such that  $P\_tx$  has a zero centroid

2039  $-P\_tx$ : Power for the transmit-pulse estimate,

### 2040 **Algorithm:**

2041 1. *Identify noise-only and signal samples:* mark index  $noise\_samples$  as true for the first 5 ns  
2042 and last 10 ns of samples in  $tep\_hist$ . Set  $sig\_samples$  to the inverse of  $noise\_samples$

2043 2. *Calculate the noise value for the transmit pulse:*  $N\_tx$  = the mean of  $tep\_hist$  for the samples  
2044 in  $noise\_samples$ . Subtract  $N\_tx$  from  $tep\_hist$  to give  $P\_tx$ .

2045 3. *Calculate the centroid of the transmit pulse:*  $T0\_tx = sum(P\_tx * t\_tx) / sum(P\_tx)$ . The sum  
2046 is carried out over the samples in  $sig\_samples$ .

2047 4. *Calculate the RDE of the transmit pulse:* The width of the transmitted pulse ( $W\_TX$ ) is equal  
2048 to half the difference between the 84<sup>th</sup> percentile and the 16<sup>th</sup> percentile of the portion of  $P\_tx$  in  
2049  $sig\_samples$ .

2050 5. *Re-establish the noise-only samples:* mark  $noise\_samples$  as true for all samples with times  
2051 more than 6  $W\_TX$  away from  $T0\_tx$ , set  $sig\_samples$  to the inverse if  $noise\_samples$ . If  
2052  $sig\_samples$  has changed from its previous values, and if fewer than 10 iterations have taken  
2053 place, return to 1b.

2054 6. *Center the transmit pulse on its centroid:* Subtract  $T0\_tx$  from  $t\_tx\_input$  to give  $t\_tx$ .

***ICESat-2 Algorithm Theoretical Basis Document (ATBD) for Land Ice Along-Track Height  
(ATL06)***

***Release 003***

2055

2056

2057 **6 TEST DATA AND SOFTWARE REQUIREMENTS**

2058 This section describes a very simple test data set that has been derived to verify the performance  
2059 of the ATL06 surface code.

2060 **6.1 ATL06 Test Data Setup**

2061 The ATL06 test data are a set of synthetic data generated based on a planar, sloping surface with  
2062 a slope of 0.02. Separate data sets are generated for surface reflectance values between 1/16 and  
2063 1, and for surface roughness values between zero and 2 m. A detector model with a dead time of  
2064 3.2 ns is used to simulate the effects of the first-photon bias. For each segment, a full set of  
2065 ATL06 parameters are generated using the Matlab prototype code, and with the ASAS  
2066 production code, and the two are compared. Small numerical differences between the codes can  
2067 produce different results in the early stages of the signal-finding code, so the most valid  
2068 comparisons between the results of the two codes are for segments with moderate signal strength  
2069 (reflectance greater than 0.25). We consider the two codes to produce equally valid results when  
2070 the difference between the results for any parameter is not significantly different from zero, and  
2071 when the spreads of the two sets of parameters are not significantly different from one another  
2072 for segments based on the same number of photons with the same surface window size.

2073 **7 BROWSE PRODUCTS AND Q/A STATISTICS**

2074 **7.1 Browse Products**

2075 Browse products include two kinds of plots: Data-quality maps, and profile plots.

2076 Data-quality maps are based on the *signal\_selection\_source* parameter. Each map shows a  
2077 background image based on the MODIS mosaics of Greenland or Antarctica (Scambos and  
2078 others, 2007), with color-coded points showing the mean segment location for each kilometer of  
2079 the beam track, with the color showing the largest bit in *signal\_selection\_source* that is set for  
2080 more than 50% of all segments in that kilometer of data, assuming that for segments with no  
2081 data, all bits are set. The plots are made separately for the strong and weak beams, because the  
2082 two beams are, at the granule scale, very close to one another and would otherwise overlap.

2083 Profile plots are generated separately for each beam pair in the granule. Each plot shows the  
2084 surface height as a function of along-track distance, and the height for each beam in the pair. A  
2085 second set of axes, aligned with the first, shows the number of PE per segment (*N\_fit\_photons*)  
2086 and the height error estimate, *h\_li\_sigma*.

2087 **7.2 Q/A Statistics**

2088 Quality assessment statistics are provided for each beam, for each 10-km increment along track.  
2089 For each increment we provide:

2090 A synopsis of the *signal\_selection\_source* parameter:

2091 -The fraction of possible segments with *signal\_selection\_source* equal to zero.

2092 -The fraction of segments with *signal\_selection\_source* equal to 1.

2093 -The fraction of segments with *signal\_selection\_source* equal to 2.

2094 -The fraction of segments with *signal\_selection\_source* equal to 3.

2095 [Add parameters for the entire file]

2096

2097

2098 **8 APPENDIX A: GLOSSARY**

2099 This appendix defines terms that are used in ATLAS ATBDs, as derived from a document  
2100 circulated to the SDT, written by Tom Neumann. Some naming conventions are borrowed from  
2101 **Spots, Channels and Redundancy Assignments** (ICESat-2-ATSYS-TN-0910) by P. Luers.  
2102 Some conventions are different than those used by the ATLAS team for the purposes of making  
2103 the data processing and interpretation simpler.

2104

2105 **Spots.** The ATLAS instrument creates six spots on the ground, three that are weak and three that  
2106 are strong, where strong is defined as approximately four times brighter than weak. These  
2107 designations apply to both the laser-illuminated spots and the instrument fields of view. The  
2108 spots are numbered as shown in Figure 1. At times, the weak spots are leading (when the  
2109 direction of travel is in the ATLAS +x direction) and at times the strong spots are leading.  
2110 However, the spot number does not change based on the orientation of ATLAS. The spots are  
2111 always numbered with 1L on the far left and 3R on the far right of the pattern. Not: beams,  
2112 footprints.

2113

2114 **Laser pulse (pulse for short).** Individual pulses of light emitted from the ATLAS laser are  
2115 called laser pulses. As the pulse passes through the ATLAS transmit optics, this single pulse is  
2116 split into 6 individual transmit pulses by the diffractive optical element. The 6 pulses travel to  
2117 the earth's surface (assuming ATLAS is pointed to the earth's surface). Some attributes of a laser  
2118 pulse are the wavelength, pulse shape and duration. Not: transmit pulse, laser shot, laser fire.

2119

2120 **Laser Beam.** The sequential laser pulses emitted from the ATLAS instrument that illuminate  
2121 spots on the earth's surface are called laser beams. ATLAS generates 6 laser beams. The laser  
2122 beam numbering convention follows the ATLAS instrument convention with strong beams  
2123 numbered 1, 3, and 5 and weak beams numbered 2, 4, and 6 as shown in the figures. Not:  
2124 beamlet.

2125

2126 **Transmit Pulse.** Individual pulses of light emitted from the ICESat-2 observatory are called  
2127 transmit pulses. The ATLAS instrument generates 6 transmit pulses of light from a single laser  
2128 pulse. The transmit pulses generate 6 spots where the laser light illuminates the surface of the  
2129 earth. Some attributes of a given transmit pulse are the wavelength, the shape, and the energy.  
2130 Some attributes of the 6 transmit pulses may be different. Not: laser fire, shot, laser shot, laser  
2131 pulse.

2132

2133 **Reflected Pulse.** Individual transmit pulses reflected off the surface of the earth and viewed by  
2134 the ATLAS telescope are called reflected pulses. For a given transmit pulse, there may or may  
2135 not be a reflected pulse. Not: received pulse, returned pulse.

2136

2137 **Photon Event.** Some of the energy in a reflected pulse passes through the ATLAS receiver  
2138 optics and electronics. ATLAS detects and time tags some fraction of the photons that make up  
2139 the reflected pulse, as well as background photons due to sunlight or instrument noise. Any  
2140 photon that is time tagged by the ATLAS instrument is called a photon event, regardless of  
2141 source. Not: received photon, detected photon.

2142

2143 **Reference Ground Track (RGT).** The reference ground track (RGT) is the track on the earth at  
2144 which a specified unit vector within the observatory is pointed. Under nominal operating  
2145 conditions, there will be no data collected along the RGT, as the RGT is spanned by GT2L and  
2146 GT2R (which are not shown in the figures, but are similar to the GTs that are shown). During  
2147 spacecraft slews or off-pointing, it is possible that ground tracks may intersect the RGT. The  
2148 precise unit vector has not yet been defined. The ICESat-2 mission has 1387 RGTs, numbered  
2149 from 0001xx to 1387xx. The last two digits refer to the cycle number. Not: ground tracks, paths,  
2150 sub-satellite track.

2151

2152 **Cycle Number.** Over 91 days, each of the 1387 RGTs will be targeted in the polar regions once.  
2153 In subsequent 91-day periods, these RGTs will be targeted again. The cycle number tracks the  
2154 number of 91-day periods that have elapsed since the ICESat-2 observatory entered the science  
2155 orbit. The first 91-day cycle is numbered 01, the second 91-day cycle is 02, and so on. At the  
2156 end of the first 3 years of operations, we expect the cycle number to be 12. The cycle number  
2157 will be carried in the mid-latitudes, though the same RGTs will (in general) not be targeted more  
2158 than once.

2159

2160 **Sub-satellite Track (SST).** The sub-satellite track (SST) is the time-ordered series of latitude  
2161 and longitude points at the geodetic nadir of the ICESat-2 observatory. In order to protect the  
2162 ATLAS detectors from damage due to specular returns, and the natural variation of the position  
2163 of the observatory with respect to the RGT throughout the orbit, the SST is generally not the  
2164 same as the RGT. Not: reference ground track, ground track.

2165

2166 **Ground Tracks (GT).** As ICESat-2 orbits the earth, sequential transmit pulses illuminate six  
2167 ground tracks on the surface of the earth. The track width is approximately 10m wide. Each  
2168 ground track is numbered, according to the laser spot number that generates a given ground  
2169 track. Ground tracks are therefore always numbered with 1L on the far left of the spot pattern  
2170 and 3R on the far right of the spot pattern. Not: tracks, paths, reference ground tracks, footpaths.

2171  
2172 **Reference Pair Track (RPT).** The reference pair track is the imaginary line half-way between  
2173 the planned locations of the strong and weak ground tracks that make up a pair. There are three  
2174 RPTs: RPT1 is spanned by GT1L and GT1R, RPT2 is spanned by GT2L and GT2R (and may be  
2175 coincident with the RGT at times), RPT3 is spanned by GT3L and GT3R. Note that this is the  
2176 planned location of the midway point between GTs. We will not know this location very  
2177 precisely prior to launch. Not: tracks, paths, reference ground tracks, footpaths, pair tracks.

2178  
2179 **Pair Track (PT).** The pair track is the imaginary line half way between the actual locations of  
2180 the strong and weak ground tracks that make up a pair. There are three PTs: PT1 is spanned by  
2181 GT1L and GT1R, PT2 is spanned by GT2L and GT2R (and may be coincident with the RGT at  
2182 times), PT3 is spanned by GT3L and GT3R. Note that this is the actual location of the midway  
2183 point between GTs, and will be defined by the actual location of the GTs. Not: tracks, paths,  
2184 reference ground tracks, footpaths, reference pair tracks.

2185  
2186 **Pairs.** When considered together, individual strong and weak ground tracks form a pair. For  
2187 example, GT2L and GT2R form the central pair of the array. The pairs are numbered 1 through  
2188 3: Pair 1 is comprised of GT1L and GT1R, pair 2 is comprised of GT2L and GT2R, and pair 3 is  
2189 comprised of GT3L and 3R.

2190  
2191 **Along-track.** The direction of travel of the ICESat-2 observatory in the orbit frame is defined as  
2192 the along-track coordinate, and is denoted as the +x direction. The positive x direction is  
2193 therefore along the Earth-Centered Earth-Fixed velocity vector of the observatory. Each pair has  
2194 a unique coordinate system, with the +x direction aligned with the Reference Pair Tracks.

2195  
2196 **Across-track.** The across-track coordinate is y and is positive to the left, with the origins at the  
2197 Reference Pair Tracks.

2198  
2199 **Segment.** An along-track span (or aggregation) of PE data from a single ground track or other  
2200 defined track is called a segment. A segment can be measured as a time duration (e.g. from the  
2201 time of the first PE to the time of the last PE), as a distance (e.g. the distance between the  
2202 location of the first and last PEs), or as an accumulation of a desired number of photons.  
2203 Segments can be as short or as long as desired.

2204  
2205 **Signal Photon.** Any photon event that an algorithm determines to be part of the reflected pulse.

2206

2207 **Background Photon.** Any photon event that is not classified as a signal photon is classified as a  
2208 background photon. Background photons could be due to noise in the ATLAS instrument (e.g.  
2209 stray light, or detector dark counts), sunlight, or mis-classified signal photons. Not: noise  
2210 photon.

2211

2212 **h<sub>\*\*</sub>.** Signal photons will be used by higher-level products to determine height above the  
2213 WGS-84 reference ellipsoid, using a semi-major axis (equatorial radius) of 6378137m and a  
2214 flattening of 1/298.257223563. This can be abbreviated as ‘ellipsoidal height’ or ‘height above  
2215 ellipsoid’. These heights are denoted by h; the subscript \*\* will refer to the specific algorithm  
2216 used to determine that elevation (e.g. is = ice sheet algorithm, si = sea ice algorithm, etc...). Not:  
2217 elevation.

2218

2219 **Photon Cloud.** The collection of all telemetered photon time tags in a given segment is the (or  
2220 a) photon cloud. Not: point cloud.

2221

2222 **Background Count Rate.** The number of background photons in a given time span is the  
2223 background count rate. Therefore a value of the background count rate requires a segment of PEs  
2224 and an algorithm to distinguish signal and background photons. Not: Noise rate, background  
2225 rate.

2226

2227 **Noise Count Rate.** The rate at which the ATLAS instrument receives photons in the absence of  
2228 any light entering the ATLAS telescope or receiver optics. The noise count rate includes PEs  
2229 due to detector dark counts or stray light from within the instrument. Not: noise rate,  
2230 background rate, background count rate.

2231

2232 **Telemetry band.** The subset of PEs selected by the science algorithm on board ATLAS to be  
2233 telemetered to the ground is called the telemetry band. The width of the telemetry band is a  
2234 function of the signal to noise ratio of the data (calculated by the science algorithm onboard  
2235 ATLAS), the location on the earth (e.g. ocean, land, sea ice, etc...), and the roughness of the  
2236 terrain, among other parameters. The widths of telemetry bands are adjustable on-orbit. The  
2237 telemetry band width is described in Section 7 or the ATLAS Flight Science Receiver  
2238 Algorithms document. The total volume of telemetered photon events must meet the data volume  
2239 constraint (currently 577 GBits/day).

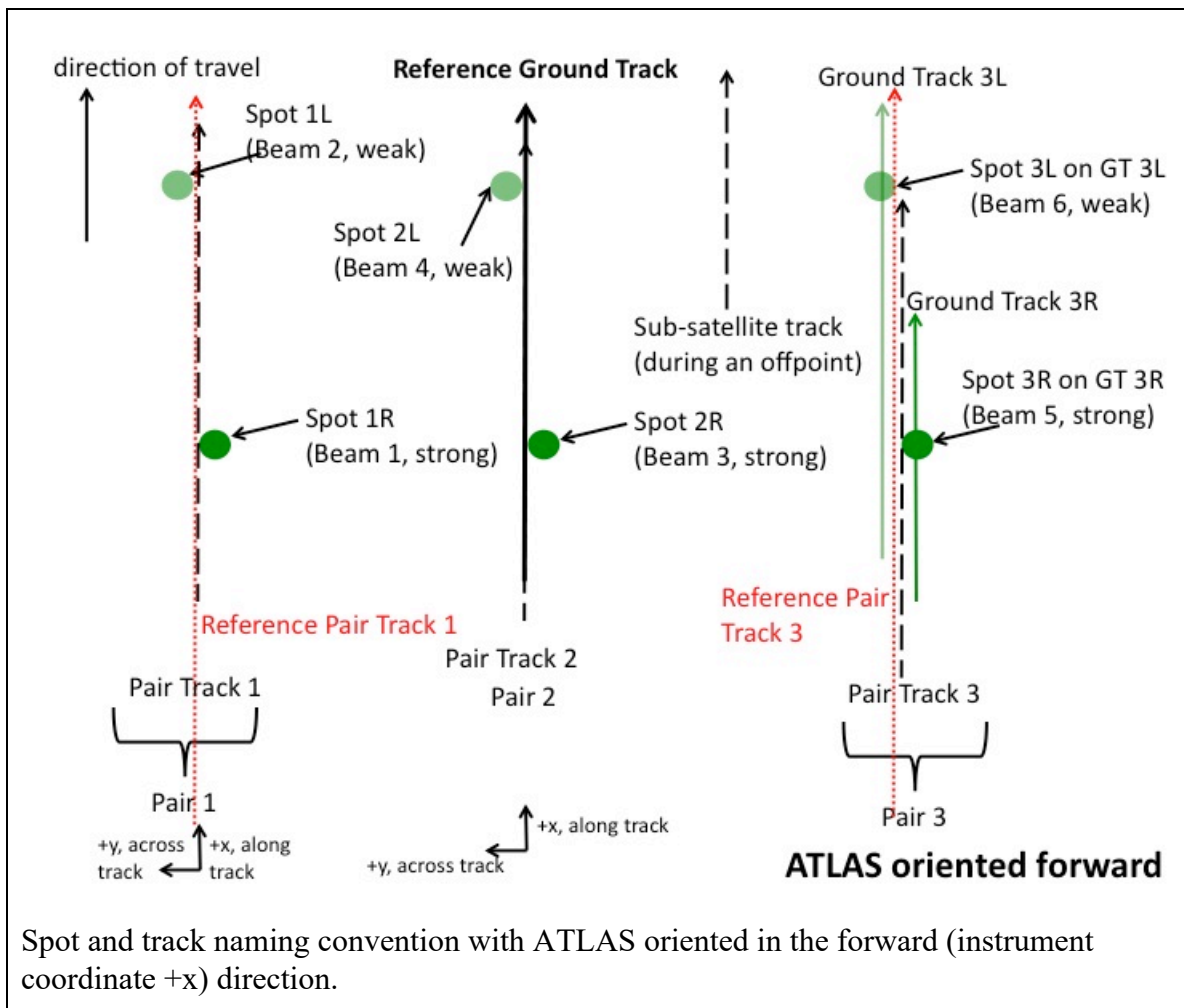
2240

2241 **Window, Window Width, Window Duration.** A subset of the telemetry band of PEs is called a  
2242 window. If the vertical extent of a window is defined in terms of distance, the window is said to

2243 have a width. If the vertical extent of a window is defined in terms of time, the window is said to  
 2244 have a duration. The window width is always less than or equal to the telemetry band.

2245

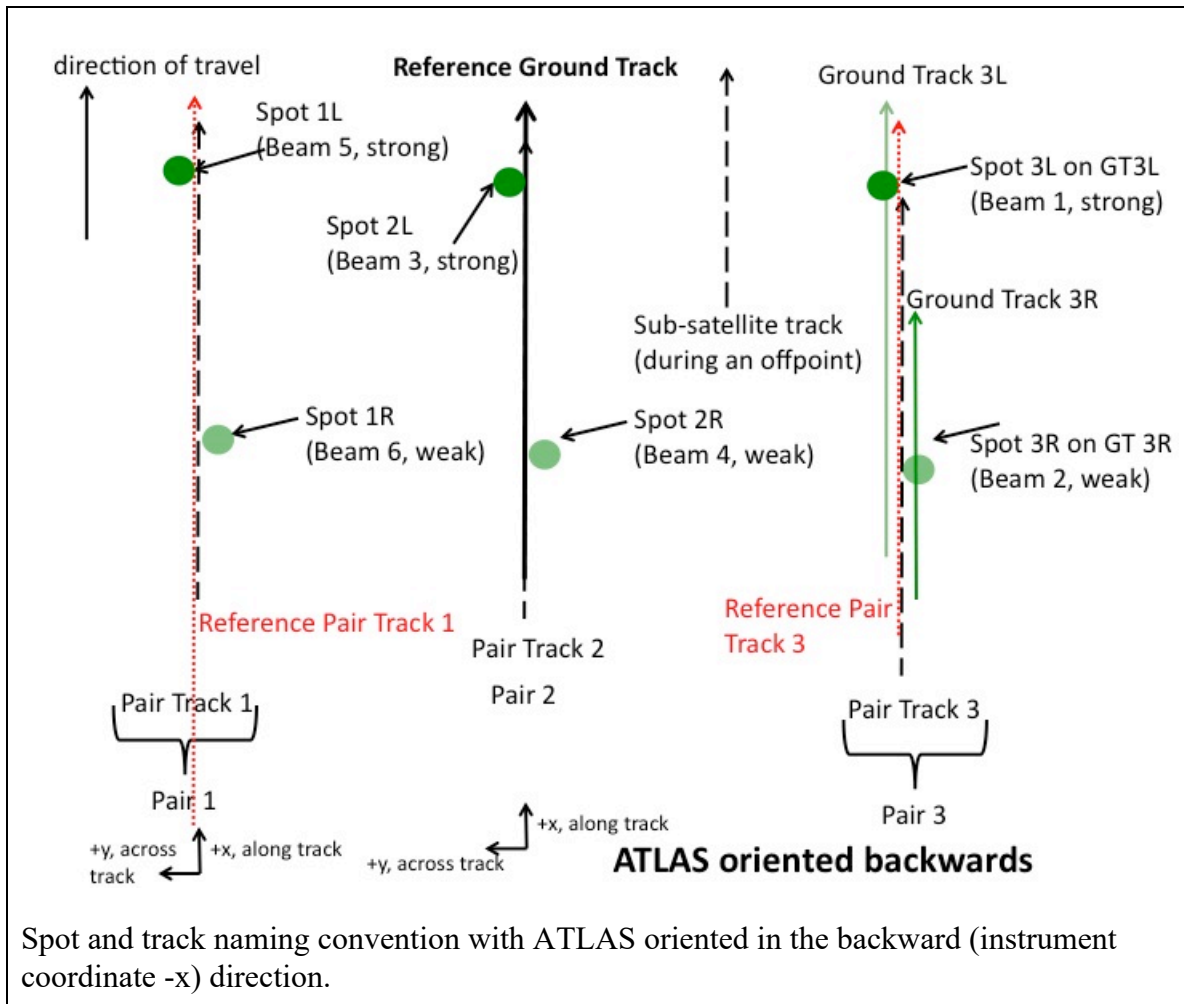
Figure 8-1. Spots and tracks, forward flight



2246

2247

Figure 8-2. Spots and tracks, forward flight



2248

2249

**Glossary/Acronyms**

ASAS	ATLAS Science Algorithm Software
ATBD	Algorithm Theoretical Basis Document
ATLAS	ATLAS Advance Topographic Laser Altimeter System
CDF	Cumulative Distribution Function
DEM	Digital Elevation Model
GSFC	Goddard Space Flight Center
GTs	Ground Tracks
ICESat-2	Ice, Cloud, and Land Elevation Satellite-2
MABEL	Multiple altimeter Beam Experimental Lidar
MIS	Management Information System
NASA	National Aeronautics and Space Administration
PE	Photon Event
POD	Precision Orbit Determination
PPD	Precision Pointing Determination
PRD	Precise Range Determination
PSO	ICESat-2 Project Science Office
PTs	Pair Tracks
RDE	Robust Dispersion Estimate
RGT	Reference Ground Track
RMS	Root Mean Square
RPTs	Reference Pair Tracks

***ICESat-2 Algorithm Theoretical Basis Document (ATBD) for Land Ice Along-Track Height  
(ATL06)***

***Release 003***

RT	Real Time
SCoRe	Signature Controlled Request
SIPS	ICESat-2 Science Investigator-led Processing System
TBD	To Be Determined
TL/DR	Too Long/Didn't Read.

2250

**References**

2251 Bamber, J.L., J.L. Gomez-Dans and J.A. Griggs 2009. A new 1 km digital elevation model of the  
2252 Antarctic derived from combined satellite radar and laser data - Part 1: Data and methods.  
2253 *Cryosphere*, **3**(1): 101-111.

2254 Menke, W. 1989. *Geophysical data analysis: discrete inverse theory*. San Diego, CA, Academic  
2255 Press.

2256 Scambos, T.A., T.M. Haran, M.A. Fahnestock, T.H. Painter and J. Bohlander 2007. MODIS-  
2257 based Mosaic of Antarctica (MOA) data sets: Continent-wide surface morphology and snow  
2258 grain size. *Remote Sensing of Environment*, **111**(2-3): 242-257.

2259 Warren, S.G., R.E. Brandt and T.C. Grenfell 2006. Visible and near-ultraviolet absorption  
2260 spectrum of ice from transmission of solar radiation into snow. *Applied Optics*, **45**(21): 5320-  
2261 5334.

2262 Yang, Y., A. Marshak, S.P. Palm, T. Varnai and W.J. Wiscombe 2011. Cloud Impact on Surface  
2263 Altimetry From a Spaceborne 532-nm Micropulse Photon-Counting Lidar: System Modeling for  
2264 Cloudy and Clear Atmospheres. *Ieee Transactions on Geoscience and Remote Sensing*, **49**(12):  
2265 4910-4919.

2266 Yang, Y., A. Marshak, S.P. Palm, Z. Wang and C. Schaaf 2013. Assessment of Cloud Screening  
2267 With Apparent Surface Reflectance in Support of the ICESat-2 Mission. *Ieee Transactions on*  
2268 *Geoscience and Remote Sensing*, **51**(2): 1037-1045.

2269 Yi, D.H. and C.R. Bentley 1999. Geoscience Laser Altimeter System waveform simulation and  
2270 its applications. *Annals of Glaciology, Vol 29, 1999*, **29**: 279-285.

2271